THESIS ON NATURAL AND EXACT SCIENCES B165

Optical Pulse Wave Signal Analysis for Determination of Early Arterial Ageing in Diabetic Patients

KRISTJAN PILT

TUT PRESS

TALLINN UNIVERSITY OF TECHNOLOGY
Technomedicum
Department of Biomedical Engineering

Dissertation was accepted for the defense of the degree of Doctor of Philosophy (in Biomedical Technology) on December 3, 2013.

Supervisor: Professor **Kalju Meigas**, PhD, Department of Biomedical Engineering, Technomedicum, Tallinn University of Technology, Estonia

Co-supervisor: Professor **Margus Viigimaa**, MD, PhD, Department of Biomedical Engineering, Technomedicum, Tallinn University of Technology, Estonia

Reviewed by: Professor Emeritus **Hiie Hinrikus**, DSc, Department of Biomedical Engineering, Technomedicum, Tallinn University of Technology, Estonia

Opponents: Professor **Göran Salerud**, PhD, Department of Biomedical Engineering, Linköping University, Sweden
Associate Professor **Miklós Illyés**, MD, PhD, Heart Institute, Faculty of Medicine, University of Pécs, Hungary

Defence of the thesis: January 24, 2014, Tallinn, Estonia

Declaration:
Hereby I declare that this doctoral thesis, my original investigation and achievement, submitted for the doctoral degree at Tallinn University of Technology has not been submitted for any academic degree.

/Kristjan Pilt/

ISSN 1406-4723
ISBN 978-9949-23-578-0 (publication)
ISBN 978-9949-23-579-7 (PDF)

LOODUS- JA TÄPPISTEADUSED B165

Optilise pulsilaine signaali analüüs arterite varase vananemise määramiseks diabeedihaigetel

KRISTJAN PILT

TTÜ KIRJASTUS

CONTENTS

List of Publications

I **Pilt K**, Meigas K, Viigimaa M, Temitski K, Kaik J (2010) "An experimental measurement complex for probable estimation of arterial stiffness", *In: Proceedings of 30th Annual International Conference of the IEEE EMBS, Buenos Aires, Argentina, August 31 – September 4*, 194-197 (DOI: 10.1109/IEMBS.2010.5627925).

II **Pilt K**, Meigas K, Ferenets R, Kaik J (2010) "Photoplethysmographic signal processing using adaptive sum comb filter for pulse delay measurement", *Estonian Journal of Engineering*, 16: 78-94 (DOI: 10.3176/eng.2010.1.08).

III **Pilt K**, Ferenets R, Meigas K, Lindberg L-G, Temitski K, Viigimaa M (2013) "New photoplethysmographic signal analysis algorithm for arterial stiffness estimation", *The Scientific World Journal*, vol. 2013, Article ID 169035, 9 pages (DOI: 10.1155/2013/169035).

IV **Pilt K**, Meigas K, Temitski K, Viigimaa M (2012) "Second derivative analysis of forehead photoplethysmographic signal in healthy volunteers and diabetes patients", *In: IFMBE Proceedings of World Congress on Medical Physics and Biomedical Engineering, Beijing, China, May 26-31*, 410-413 (DOI: 10.1007/978-3-642-29305-4_109).

V **Pilt K**, Meigas K, Ferenets R, Temitski K and Viigimaa M (2013) "Photoplethysmographic signal waveform index for detection of increased arterial stiffness", *Manuscript submitted*

Author's Contribution to the Publications

In publication I the author built the PPG and piezoelectric signal modules and compiled the devices together into one working unit. In addition, the author carried out the experiments and data analysis and developed the concept of the LabView recording program.

In publication II the author developed the algorithm of adaptive comb filter and implemented it in MATLAB. In addition, the author carried out all the experiments, simulations, and data analysis.

In publication III the author developed the SDPPG signal analysis algorithm, processed all the signals and carried out data analysis. In addition, the author participated in planning of the experiments and conducted 75% of the signal recordings from the subjects in cooperation with other members of the group.

In publication IV the author processed all the signals, carried out data analysis, and conducted 90% of the experiments in cooperation with other members of the group.

In publication V the author processed all the signals and carried out data analysis.

Approbation

- Method and device for long term variability monitoring of cardiovascular parameters based on a registered electrocardiograph and pulse wave signals; Priority number: P201100016; Priority date: 09.03.2011.
- 11th Mediterranean Conference of the Medical and Biological Engineering and Computing, Ljubljana, Slovenia, June 26-30, 2007.
- 29th Annual International Conference of the IEEE EMBS, Lyon, France, August 23-26, 2007.
- 14th Nordic-Baltic Conference on Biomedical Engineering and Medical Physics, Riga, Latvia, June 16-20, 2008.
- 30th Annual International Conference of the IEEE EMBS, Vancouver, Canada, August 20-24, 2008.
- 11th Biennial Baltic Electronics Conference, Tallinn, Estonia, October 6-8, 2008.
- 31st Annual International Conference of the IEEE EMBS, Minneapolis, USA, September 2-6, 2009.
- 11th International Congress of the Medical Physics and Biomedical Engineering, Munich, Germany, September 7-12, 2009.
- 12th Mediterranean Conference on Medical and Biological Engineering and Computing, Chalkidiki, Greece, May 27-30, 2010.
- 32nd Annual International Conference of the IEEE EMBS, Buenos Aires, Argentina, August 31 – September 4, 2010.
- 12th Biennial Baltic Electronics Conference, Tallinn, Estonia, October 4-6, 2010.
- 15th Nordic-Baltic Conference on Biomedical Engineering and Medical Physics, Aalborg, Denmark, June 14-17, 2011.
- 5th European Conference of the IFMBE, Budapest, Hungary, September 14-18, 2011.
- World Congress on Medical Physics and Biomedical Engineering, Beijing, China, May 26-31, 2012.
- 13th Biennial Baltic Electronics Conference, Tallinn, Estonia, October 3-5, 2012.
- International Symposium on Biomedical Engineering and Medical Physics, Riga, Latvia, October 10-12, 2012.
- 35th Annual International Conference of the IEEE EMBS, Osaka, Japan, July 3-7, 2013.

Introduction

Cardiovascular diseases are the leading cause of death globally according to the WHO global status report (Alwan et al 2011). The number of people who die annually due to cardiovascular diseases is the largest among the causes of death. In 2008 about 17.3 million people died due to cardiovascular diseases, which constitute 30% of all global deaths. However, most of the cardiovascular diseases can be prevented through healthy lifestyle. The major behavioral risk factors of the cardiovascular disease are smoking, immoderate use of alcohol, obesity, and physical inactivity.

The prevention and treatment of the cardiovascular disease is based on 'risk factors', which are known to cause harm to the arterial system, such as elevated blood pressure, high level of cholesterol and blood sugar, and smoking. However, a considerable number of cardiovascular events happen each year in subjects who do not qualify for treatment based on such guidelines (Herrington et al 2004). Therefore, major efforts have been placed into research to develop methods, which would enable more accurate identification of the subjects with high risk from general population. Early diagnosis and treatment of the cardiovascular disease could provide treatment benefits and reduce the cost to society (Perk et al 2012).

Diabetes is not a cardiovascular disease, but more than 75% of diabetic patients die because of the causes related to atherosclerosis. The premature increase in the stiffness of the arteries in the case of diabetes patients is often explained through accelerated arterial ageing. With early diagnosis of the atherosclerosis the disease can be decelerated through treatment and lifestyle change. Therefore, it is essential to detect the early changes in the arterial walls of diabetes patients.

The aortic PWV, which is an index of aortic stiffness, has already been entered to the guidelines for hypertension of the European Society of Hypertension as providing extra cardiovascular risk prediction besides classical risk factors (Mancia et al 2007). However, the atherosclerosis involves the whole cardiovascular system and changes in smaller arteries can arise even earlier. The assessment of peripheral arteries may enable earlier detection of atherosclerosis (Cohn 2006).

Different devices and methods have been developed to estimate arterial stiffness (Laurent et al 2006, Woodman et al 2005). Usually the measurements are time consuming, uncomfortable for a subject and a trained operator is needed. A user independent, rapid performance and inexpensive noninvasive technique is needed to estimate arterial stiffness.

The general aim of this study was to investigate the possibilities to detect the premature increase in arterial ageing using a non-invasive optical method and pulse waveform analysis. Further the aim was to compare the effectiveness of the developed method and algorithms with recognized methods used in clinical practice to differentiate between the patients with normal and higher arterial stiffness.

In the first part of the study (Publication I), the measurement complex, which includes the modules for synchronous recording of optical pulse wave signals from different segments of arteries, was compiled and tested. The synchronous recording

of the signals is essential for the PTT and PWV estimation. In addition, the measurement complex enables recording of other physiological signals, which are relevant to the cardiovascular system evaluation and arterial stiffness estimation from different segments of arteries. In publication II an algorithm was developed for motion caused noise suppression in the recorded optical signal providing significant improvement of the signal quality.

In the second part of study the waveform analysis of the recorded optical signals was carried out in order to determine the features of the signal characteristics for increased arterial stiffness and, consequently, to estimate the premature increase in arterial ageing. Publication III introduces the new pulse waveform analysis algorithm for the finger signal to differentiate between the subjects with normal and increased arterial stiffness. In publication IV the optical signal from the forehead was investigated by using the algorithm and optical waveform index developed in publication III to differentiate subjects with higher arterial stiffness. The aim of publication V was to compare the effectiveness of the developed optical waveform index and the arterial stiffness index used in commercial clinical devices to differentiate patients with increased arterial stiffness.

Acknowledgements

I am sincerely thankful to everyone who has been helping and contributing to my thesis work. I am grateful to my supervisor professor Kalju Meigas and co-supervisor professor Margus Viigimaa for their guidance and support. I wish to thank Kristina Kööts who was actively participating in the preparation and conduction of experiments in hospital, all the supervised master and bachelor students for their helpful co-operation, Dr. Anu Ambos who helped in finding and convincing the patients to participate in the study, all diabetes patients and other volunteers who agreed to participate in the experiments, Rain Ferenets for the practical advice in signal processing.

I would also like to thank my colleagues at the Department of Biomedical Engineering for providing a pleasant and inspiring work environment, Rain Kattai and Deniss Karai for fruitful discussions and competent technical advice, Jana Holmar for assistance during formal finalization of the thesis and great company in conferencing. I appreciate the time and inspiring positive support from Lars-Göran Lindberg during my semester in Linköping University.

Most importantly, I would like to thank my parents Epp and Jaan who have believed in me, supported and encouraged in all the levels of education. Special thanks to my brother Mihkel who was always willing to participate as a volunteer in all the pilot studies and experiments. Last but not least, I would like to thank my girlfriend Jelena who has been patient and kind regardless of my ups and downs in the thesis work.

The research was supported by the Estonian Science Foundation Grant no. 7506, by the Estonian targeted financing project SF0140027s07, by the European Union through the European Regional Development Fund, European Social Fund's Doctoral Studies and Internationalization Programs "DoRa" and "Kristjan Jaak".

Abbreviations

AGI – ageing index
AIx – augmentation index
ECG – electrocardiography
HDL – high-density lipoprotein
IMT – intima-media thickness
LDL – low-density lipoprotein
LED – light emitting diode
MRI – magnetic resonance imaging
NO – nitric oxide
PEP – pre-ejection period
PPG – photoplethysmography
PPGAI – PPG waveform augmentation index
PTT – pulse transit time
PWV – pulse wave velocity
SDPPG – second derivative photoplethysmography
SNR – signal to noise ratio
WHO – World Health Organization

1. Anatomy of arteries and pathogenesis of artherosclerosis

1.1. Anatomy of arteries

The structure of the arterial vessel wall is heterogeneous and can be generally divided into three layers: *tunica interna* (*intima*), *tunica media* (*media*), *tunica externa* (*externa*) (Figure 1). The thickness and the structure of the layers vary depending on the type of the artery. The inner layer contributes minimally to the total thickness of the vessel and it is in contact with blood. The innermost layer of *intima* is endothelium, which is a thin layer of cells that covers the whole surface of the cardiovascular system. The smooth surface of the endothelial cells enables efficient blood flow by reducing surface friction. In addition, it prevents the blood coagulation inside the vessel. The next layer in *intima* is the basement membrane, which consists of collagen fiber. This layer provides a physical support base for epithelial cells of endothelium. The outermost layer of the *intima* is *internal elastic lamina*, which forms a thin sheet of elastic fibers around the inner layers (Tortora and Derrickson 2011).

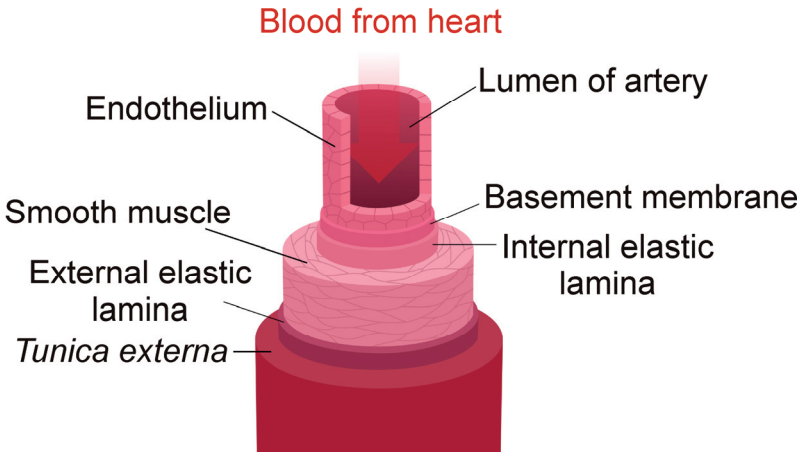

Figure 1. The anatomy of the artery [CC: By Kelvin Song, http://creativecommons.org/licenses/by/3.0/].

The structure of *tunica media* is more complex and its composition varies most among different arterial vessels. This layer is relatively thick in most vessels and it consists of smooth muscle cells, which are connected together with the net of elastin and collagen fibers (Dobrin 1999). This construction prevents damage to the wall of the arterial vessel at high transmural pressures. The main purpose of the muscular cells in the wall is to change the diameter of the vessel's lumen. Vasoconstriction (decrease in the diameter) and vasodilatation (increase in the diameter) is typically caused by parasympathetic intervention or in response to blood pressure.

The outer layer of the arterial vessel, *tunica externa*, is separated from *tunica media* by the external elastic lamina, which consists of elastin and collagen. In addition, this layer contains numerous nerves. In particular, in larger vessels this layer contains small blood vessels that supply the tissue of the vessel wall. In addition, this layer connects the vessel to the surrounding tissue (Tortora and Derrickson 2011).

Arteries have normally high compliance, which means that a small increase in the transmural pressure causes the stretch in the wall without tearing. The elasticity of the arterial vessel wall is determined by several components. The passive (without using biochemical energy) elastic components of the *tunica media* are collagen and elastin. Collagen has higher Young's modulus ($\sim 10^8$Pa) than elastin ($\sim 3 \cdot 10^5$Pa) (Nichols and O'Rourke 2005). The elastic fibers of the vessel wall enable stretching more than two times from the initial length and they dominate the wall behavior at the low strain levels. Collagen starts to dominate at the higher strain levels. In addition, the layer of smooth muscle cells enables a noticeable change in the elasticity of the arterial wall.

Largest arteries, such as aorta and branches of aorta, in the body are the most elastic. Those arteries have the largest diameter (>10mm) and a relatively thin wall (1/10 of the diameter) compared to the overall size of the vessel (Avolio 1980, Westerhof et al 1969). In these vessels the tunica media is dominated by elastic fibers. Those vessels help to propel the blood onward due to the high elasticity, while the aortic valve is closed and the ventricles are relaxing. The aorta stretches due to the blood ejection from heart into the cardiovascular system. Due to the stretch of the vessel, the elastic fibers store the mechanical energy (potential energy). It is followed by the recovery of the vessel diameter and the stored potential energy in the wall is converted into the kinetic energy of the blood.

The muscular arteries, also called as conduit arteries (e.g. brachial, femoral, radial, etc.), contain more smooth muscle and less elastic fibers than elastic arteries. The lumen diameter of the muscular artery is between 0.1 mm up to 10 mm and the wall thickness comprises about 25% of the diameter (Avolio 1980, Westerhof et al 1969). The muscular arteries are less elastic due to the reduced amount of elastic fibers. In addition, the muscle tissue is able to maintain the state of partial contraction. This reduces the elasticity or increases the stiffness of the artery.

1.2. Pathogenesis of atherosclerosis

Thickening and stiffening of the arteries is considered arteriosclerosis. The arteries stiffen with disease and healthy ageing. Atherosclerosis is the specific form of the arteriosclerosis, which is an endovascular inflammatory disease, resulting in a build up of a plaque (Cavalcante et al 2011). The disease is triggered by the chemical or physical damage of the endothelial cell layer. The damage can be caused by one or multiple of the following factors: physical damage or stress due to hypertension, turbulent blood flow in the branch points of arteries, free radicals (reactive oxygen species) in blood caused by smoking, high concentrations of LDL

in blood (hyperlipidemia), constantly high blood glucose levels in blood, high concentrations of homocysteine in blood (Libby 2002a).

In healthy arteries the blood cells in blood do not stick to the endothelial cells. Due to the above mentioned reasons the endothelial cell layer gets damaged and mostly LDL starts to pass through the endothelial cells and accumulates in the *intima*. Oxidation of LDL in the arterial wall is caused by the exposure to NO, and some enzymes. Oxidized LDL is toxic and this initiates an inflammatory process. (Libby et al 2002). The cell surface adhesion molecules (VCAM-1) are produced due to the injury of the endothelial cells and oxidative stress (Li et al 1993, Huo and Ley 2001). Monocytes respond to the inflammation process and start to stick and infiltrate through endothelium cells into media (Crowther 2005). After entering the *intima* the monocyte interact with stimuli. Through formation of macrophages and foam cells, the lipid and end products of the cells are collected between *intima* and *media* layers of the artery.

In case the process continues, the fatty streaks start to form to the artery wall and it is the first visible sign of atherosclerosis (Libby et al 2002). It can be seen in most of people by the age of 20 in the surfaces of the aorta and carotid arteries as a yellow hue (Strong et al 1992). It is part of the ageing process. In addition, smooth muscle cells migrate through the *internal elastic lamina* and accumulate, which leads to the built-up of an extracellular matrix in plaque and fatty streaks turn into fatty fibrous lesions. In the next stages fibrosis continues and sometimes with smooth cell death. This leads to fibrous cap formation over the lipid core. The fibrous cap consists largely of collagen and elastin. This represents the reaction by the body to heal the lesion. Formed fatty streaks may turn into atherosclerotic plaques or remain stable and even regress (Libby 2002a, 2002b).

Continued plaque growth caused by an accumulation of LDL within the intima causes the external elastic membrane to expand. This compensatory luminal enlargement and wall thickening, known as an arterial remodeling, allows the vessel to maintain normal or sufficient lumen area and blood flow (Boutouyrie et al 1992, Cheng et al 2002 and Zieman et al 2005).

However, as a plaque increases, the artery can no longer compensate by expanding outward and the plaque begins to foray into the lumen. Usually it occurs when plaque thickness reaches about 40% of the lumen diameter (Glagov et al 1987). Rupture of plaques may occur due to the biomechanical and hemodynamic stresses (Cloves and Berceli 2000). Plaques that contain a large lipid core and are covered by a thin fibrous cap rupture more easily (Hennerici 2004).

The lipid core comes into contact with blood when a fibrous cap ruptures. From this stage the formation of a thrombus or clot starts. The thrombus may partially or totally block an artery causing a sudden reduction in blood flow. Partial blockage of the lumen may cause the symptoms of angina. Complete blockage of the vessel lasting more than two to four hours may cause an acute event, such as myocardial infarction (Naghavi et al 2003).

Healing of the vessel may also take place. Plaque rupture with subsequent healing is believed to be the major mechanism by which atherosclerotic lesions

progress and narrow the lumen. Plaques that heal generally have a higher fibrotic composition than before making them more stable and less prone to future rupture (Waxman et al 2006).

At early ages the atherosclerotic fatty plaques are seen mainly in the carotid and femoral arteries (Tuzcu et al 2001, Stary 2003). Atherogenic inflammation may appear in any arteries, but the disease is marginal in the upper limb, renal and other muscular arteries (Stary et al 1992). However, it has been reported that atherosclerosis and increase in the stiffening of arteries are strongly associated at various locations in the vascular tree (van Popele et al 2001).

There are a number of risk factors for atherosclerosis, which include age, hypercholesterolemia, hypertension, diabetes mellitus, smoking, physical inactivity, and obesity. In addition, the biochemical risk factors of atherosclerosis are decreased HDL-cholesterol and increased LDL-cholesterol, lipoprotein, C-reactive protein, and homocystine (Smith et al 2011).

2. Premature arterial stiffness in diabetes patients and importance of its early detection

Insulin is a hormone produced by the β-cells in the pancreas. The rise in blood sugar excites the secretion of insulin to the circulation. Insulin receptors in muscle and fat cells are binding insulin, which triggers the process where the glucose from the blood stream is entered into the fat and muscle cell (Guyton and Hall 2006).

Type I diabetes results from a lack of insulin in blood. It is caused by the autoimmune process, which destroys the β-cells and due to that glucose cannot enter fat or muscle cells. This causes the glucose rise in blood, resulting over time with hyperglycemia. Type I diabetes is also called insulin-dependent diabetes (Guyton and Hall 2006).

Type II diabetes is primarily caused by the insulin resistance, which is caused by the dysfunctional interaction between insulin and its receptor. Despite sufficient levels of insulin, glucose is not entered into fat and muscle cells. Increased glucose levels in blood lead to hyperglycemia and endothelial cell dysfunction. Type II diabetes is also called non-insulin dependent diabetes (Guyton and Hall 2006).

Diabetes augments the process of atherosclerosis by a variety of mechanisms. Increased blood sugar has two effects on endothelium as part of atherosclerosis. The hyperglycemia elevates the production of free radicals, which are highly reactive molecules that cause damage and premature death of endothelial cells (Hudson et al 2005). In addition, the accumulation of advanced glycation end products in endothelial cells increases oxidative stress, which minimizes the availability of NO. Otherwise NO enables blood vessels to relax. Oxidative stress subsequently encourages the formation of fatty streaks in the artery wall (Creager et al 2003, Rask-Madsen and King 2007).

Good diet and exercise brings faster blood flow through arteries contrary to diabetes. The force along the arterial walls, which is caused by fast and steady blood flow, has been reported in recent studies to protect the arteries from

atherosclerosis. It has been found that physical force can be a key player in the function which is capable of changing biochemical processes (Woo et al 2008).

The progression of diabetes mellitus is closely connected with hypertension, renal disease and different forms of cardiovascular diseases. Diabetes is not a vascular disease, but more than 75% of diabetic patients die because of the causes related to atherosclerosis. However, about 70% of diabetic patients do not take it seriously that they are at high risk for the cardiovascular disease (Hurst and Lee 2003). However, with early diagnosis of the atherosclerosis the disease can be decelerated through treatment and lifestyle change.

Elastin and collagen ratio determines the stiffness of the artery wall. Vascular ageing through endothelial dysfunction and elastic fiber degeneration leads to progressive arterial stiffness and atherosclerosis development. Arterial stiffness has been considered one of the risk markers of an early cardiovascular disease.

It has been found that arterial stiffness is increased with diabetes mellitus type I (Llauradó et al 2012) and type II (Urbina et al 2010). Diabetic vascular disease can be explained through the accelerated ageing of the arteries. Earlier studies have reported that the calculated cardiovascular age, based on aortic stiffness changes, increases with diabetes mellitus about 8.9 years in the case of diabetes type I (Ravikumar et al 2002) and 11.1 years in diabetes type II (Cockroft and Wilkinson 2002). Higher arterial stiffness in diabetes patients through the measurement of aortic pulse wave velocity and aortic augmentation has been also confirmed in the earlier studies (Brooks et al 2001, Wilkinson et al 2000a, Cruickshank et al 2002).

Hypertension is connected to the increase of arterial stiffness and is part of development of the diabetes mellitus (Sowers et al 2001). Arteries of diabetes patients compared to the healthy arteries are more exposed to the injuries caused by high blood pressure and more often rupture or occlude occurs (Williams 1999). Due to that the damage is caused often to retina, brain and kidneys (Safar et al 2004). However, the consequences can be effectively avoided through the blood pressure reduction. In extensive studies (HOPE and LIFE) it has been shown that benefit in the reduction of cardiovascular mortality was achieved by lowering the blood pressure (Yusuf et al 2000, Dahlöf et al 2002). Thus, the rapid monitoring of blood pressure in diabetes patients is strongly recommended (Solomon 2003, Rydén et al 2013).

3. Non-invasive methods for evaluation of arterial stiffness

Several indices for the evaluation of the cardiovascular system have been developed. Generally, they are addressed to the assessment of arterial stiffness either systemically, regionally or locally (Pannier et al 2002). Due to several reasons the stiffness of the arterial wall is closely connected with the development and progression of cardiovascular diseases. Firstly, the pathogenesis mechanism of isolated systolic hypertension (increased systolic blood pressure) includes an increase in arterial stiffness (Cohen and Townsend 2011). Secondly, the stiffness of the arteries determines the ability of the vessel to accommodate ejected blood from the heart. Thus, increased arterial stiffness imposes a higher left ventricle afterload

(Chirinos and Segers 2010). Thirdly, the increased pulse pressure, which is connected to the increase of aortic stiffening, may damage the organs such as the kidney and the brain (O'Rourke and Safar 2005). Fourthly, different biologic processes are connected with arterial stiffness, which causes the cardiovascular diseases (Franklin 2008). Increase in arterial stiffness is caused by ageing and accelerated due to the propagation of the diseases, such as diabetes mellitus, hypertension, hypercholesterolemia, kidney disease, obesity, and smoking (Payne et al 2010).

Non-invasive assessment of arterial stiffness is based on the measurement of indirect and intrinsically associated parameters, which can be related to stiffness. Generally, the methodologies can be divided into three groups: 1) direct stiffness estimation using measurements of the diameter and the distending pressure (local arterial stiffness estimation), 2) pulse wave velocity and pulse transit time (regional arterial stiffness estimation), 3) analysis of the pulse waveform.

3.1. Direct arterial stiffness estimation

Stiffness, which is the rigidity of an object, can be defined through the resistance of the body to the applied deformation force. The stiffness of the arterial wall is expressed through the ration of the stress σ (mechanical stress caused by applied mechanical force on the unit area measured in N/m^2), which is applied from a given direction, and strain ε (relative deformation of the body measured in arbitrary units), which is the Young's elastic modulus (E) measured in Pascal's (Pa) (Nichols and O'Rourke 2005, Cavalcante et al 2011). Specifically, the Young's elastic modulus expresses the slope of the stress and the strain linear relationship within the Hooke's limits in case the material is linear-elastic or "Hookean". Furthermore, the slope can be calculated by using any two points within the Hooke's limit range. In this way the calculated slope is called an incremental elastic modulus (E_{inc}) (Nichols and O'Rourke 2005).

The Young's modulus is independent of the direction where the force was applied if the material is isotropic. The arterial wall is assumed to be isotropic in the calculations of most commonly used indices. However, the arterial wall is anisotropic and therefore the approximation is used for the estimation of vessel wall properties (Chirinos 2012).

The arterial wall consists of a complex structure of the components that determine the stiffness of the arterial wall. The main components are elastin, collagen fibers and smooth muscle cells. The elastin and collagen fibers are passive (without using biochemical energy) elastic components whereas smooth muscle cells are actively modulating the stiffness of the arterial wall (Bank et al 1996, Zulliger et al 2004). Furthermore, the elastic moduli of elastin and collagen fibers are different. Therefore, the arterial wall is not Hookean and the relationship between the stress and the strain is with a curved shape. The Young's modulus increases with the increasing levels of stress. This means that the elastic modulus of the artery is dependent on the distending pressure and it has to be taken into account while comparing results (Nichols and O'Rourke 2005).

It should also be noted that the relationship between the distending pressure and strain is not interchangeable with the stress and strain relationship and the law of Laplace has to be taken into account (Atlas 2008). Relatively simple formulas can be derived for the calculation of the local incremental elastic modulus of the arterial wall by using the measurement of wall thickness in diastole and two measurements of the diameters at two different pressure levels. This calculation can be done under the assumptions that the artery has a perfectly circular shape, there are no deformations in the longitudinal direction and the wall of the artery is isotropic (Laurent et al 2006). In case the pressure and diameter are measured at the same location, these measurements can be related to the wall stiffness of the artery in this location.

In addition, the parameters related to the local stiffness of the artery are estimated through the pressure-volume and pressure-area relations. However, these relationships are influenced not only by the stiffness of the artery, but also by the vessel geometry (Chirinos 2012). Furthermore, the relationships are not linear, but within relatively narrow pressure ranges can be considered as linear for larger arteries (Meinders and Hoeks 2004). In the case of smaller muscular arteries, the error can be larger (Reneman et al 2005). Thus, the measurements are carried out mainly on larger arteries.

The compliance is the ratio between the relative changes in the volume to the relative change in the pressure and in addition to the stiffness the parameter is also dependent on the diameter and the wall thickness of the artery. The reciprocal of compliance is called elastance. The compliance values for arteries with different diameters are non-comparable. Thus, the compliance is normalized with the volume of the artery and it is called distensibility (Nichols and O'Rourke 2005).

The volume of the artery is difficult to measure and in applications it is replaced by the vessel area or diameter. It has been done under assumptions that the cross-sectional vessel area is circular and the volume increase of the artery is due to the radial expansion rather than due to deformations in the longitudinal direction (Chirinos 2012).

The non-linear relationship between the pressure and the lumen diameter is compensated in the calculation of the stiffness index β (Hirai et al 1989). The stiffness index β has been used for the estimation of the mechanical properties of the artery in earlier studies (Miyaki et al 2010, O'Rourke et al 2002).

The indices described above are used to estimate local arterial stiffness in a number of different studies (O'Rourke et al 2002, Pahkala et al 2013, Ciftçi et al 2013, Oguri et al 2013). The blood pressure should be measured at the location where the mechanical changes of the artery are detected. The local blood pressure can be estimated through the registration of the pressure waveform from the location of interest by using applanation tonometry (van Bortel et al 2001) or finger cuff (Boehmer 1987) and the calibration of the pressure waveform is carried out by using the measured blood pressure of the brachial or radial artery (Verbeke et al 2005). The calibration can be carried out by different techniques, including a general transfer function method.

To determine the vessel diameter *in vivo* at the diastole and stroke changes in diameter, any bi-dimensional ultrasound system can be used. However, the ultrasound systems, which include high-resolution linear array transducers, should be used to obtain high quality ultrasound image of the artery (Currie et al 2010, Nualnim et al 2011). With advanced image analysis software the mechanical parameters of the vessel can be determined with high precision. It should be taken into account that this kind of diameter determination needs a high degree of technical expertise and the procedure takes a long time. Thus, it is not effective to use it, for example, in large screening studies. In some studies, the diameters of deep arteries, such as the aorta, have been determined also by using the MRI system (Franquet et al 2013). However, most of the pathophysiological and pharmacological studies are carried out by the ultrasound system. Despite some of the disadvantages, today the ultrasound system is the only non-invasive method, which can be used for the determination of local arterial stiffness (Young's modulus) through the determination of the diameter and the IMT of the artery (Laurent et al 2006). The IMT determination has been used in addition to the calculation of arterial stiffness as a separate parameter to monitor the inward or outward remodeling (van der Heijden-Spek et al 2000, Bussy et al 2000, Boutouyrie et al 2000) of the arterial wall and as one risk factor of cardiovascular diseases (Molinari et al 2010).

3.2. Pulse wave velocity and pulse transit time

Pulse wave velocity is the speed at which the pulse wave propagates from the heart through the arterial system to the peripheral vessels. The pulse wave propagates through the arteries with the finite speed and it is not constant for the arterial system. The PWV depends on the viscoelastic properties of the artery. It has been generally accepted that the PWV is the most simple, non-invasive, reproducible, and robust method to estimate regional arterial stiffness (Laurent et al 2006). In addition, aortic PWV, which is an index of aortic stiffness, has been included to the guidelines for hypertension of the European Society of Hypertension to provide extra cardiovascular risk prediction besides classical risk factors (Mancia et al 2007).

The pressure wave propagation without reflections along the uniform artery can be described through the transfer function. The transfer function is characterized by the propagation constant, which is a complex variable, as it has the magnitude and the phase. The magnitude is determined by the attenuation coefficient, which depends on the viscosity of the blood and mechanical properties of the arterial wall. The pulse wave propagation speed is finite and the propagation constant includes also the phase constant due to the viscoelasticity of the arteries. The pulse wave velocity varies with frequency, as the different harmonic components of the pulse wave are travelling with different speed along the artery, which is also known as harmonic dispersion (Li et al 1981, Li 2004, Callaghan et al 1984).

PWV dependency on the viscoelastic properties of the artery are expressed with the Moens-Korteweg equation (Korteweg 1878, Moens 1878), which has been corrected by Bergel (Bergel 1961) and modified by Hughes (Hughes et al 1979):

$$PWV = \sqrt{\frac{E_0 \cdot \mathrm{e}^{\xi \cdot P} \cdot h}{2 \cdot r \cdot \rho \cdot \left(1 - \sigma^2\right)}}, \quad (1)$$

where E_0 is the elastic modulus of the arterial wall at the zero intravascular pressure P (measured in mmHg), ξ is a constant that depends on the particular artery (typically between 0.016 and 0.018), h is wall thickness, r is lumen radius, ρ is blood density, and σ is the Poisson ratio. First, the Moens-Korteweg equation was derived under an assumption that the artery has a thin wall, which means that $h/(2 \cdot r)$ is small. However, in order to decrease the error of that assumption, the equation was corrected as a result of a study by Bergel (Bergel 1961) and the Poisson ratio σ was added to the relationship, which was taken equal to 0.5. Young's modulus of the artery depends non-linearly on the applied pressure. In the earlier study Hughes et al (1979) showed that the Young's modulus of the aorta increases exponentially with an increasing intravascular pressure P. Then the incremental elastic modulus E_{inc} is calculated as follows (Hughes et al 1979):

$$E_{\mathrm{inc}} = E_0 \cdot \mathrm{e}^{\xi \cdot P}. \quad (2)$$

The other relationship for the calculation of PWV was derived from the Moens-Korteweg equation by Bramwell and Hill (Bramwell and Hill 1922):

$$PWV = \sqrt{\frac{V \cdot \mathrm{d}P}{\rho \cdot \mathrm{d}V}}, \quad (3)$$

where V is the volume of an artery segment, $\mathrm{d}V$ is the volume change due to the pressure change $\mathrm{d}P$ in the artery.

Due to the difference in the Young's modulus and dimensions of the artery, the PWV is changed according to (1), while the pulse wave is propagating through the cardiovascular system. The Young's modulus is lower for proximal arteries and increases while moving towards periphery. In the case of healthy subjects, the PWV is around 4 up to 8 m/s in elastic arteries (asc. aorta, abd. aorta, carotid artery) and 8 up to 15 m/s in the muscular arteries, such as femoral, tibial and brachial artery (O'Rourke et al 2002, Nichols and O'Rourke 2005). In addition, the PWV depends on the blood pressure according to (1), which should be taken into consideration when comparing the results among the subjects and the different studies. The blood pressure should be measured as well under PWV measurements.

Although there are other methods for PWV estimation (Nichols and O'Rourke 2005, Zhang et al 2005, Khir et al 2001, Feng and Khir 2010), the technique widely used is based on the measurement of the distance between two arterial sites and the division with time it takes for the pulse wave to travel through the path length. The pulse propagation time is also called the pulse transit time - PTT. The pulse waves can be recorded by different techniques. The recorded waveform represents whether the pressure (Asmar et al 1995), the diameter (van der Heijden-Spek et al 2000), the flow velocity (Blacher et al 2003, Cruickshank et al 2002) or the volume changes (Nam et al 2013) in the artery. Those waveforms are all expressing the pulse wave, but the nature of each of them is different. However, it has been reported that the waveforms are in phase at the beginning of the cardiac cycle (Boutouyrie et al 2009a). Often the pressure signal has been recorded for the PWV estimation, although this technique may cause distortions in the waves if the pressure on the transducer is applied incorrectly (Boutouyrie et al 2009a, Pilt et al 2010a).

The distance between the recording sites of the pulse waves is measured over the skin surface. It causes a measurement error because it is not the true length of the artery (Hamilton et al 2007). The error is smaller in the case of relatively straight arterial segments. The measurement error becomes noticeably larger when the two signal recording locations are situated far away and the artery structure is more complex, such as in the case of the carotid-femoral PWV estimation (Karamanoglu 2003). It is also difficult to compare PWV measurement results between different research laboratories as the distance can be measured by different methods (Xu 2003). The systematic overestimation of the PWV can be up to 30% in case the distance measurement is carried out transcutaneously between the signal recording sites of the carotid and the femoral artery (Rajzer et al 2008, Salvi et al 2008).

To estimate the PTT, the time difference is assessed between two equiphase points on the recorded waveforms. The pulse waveform changes while propagating through the arteries. It has been explained through the influence of wave reflections appearing due to the branching of the arteries and the changes of the arterial stiffness and dimensions along the artery (Nichols and O'Rourke 2005). In addition, the arterial stiffness changes non-linearly with blood pressure, which also influences the PWV. Due to that the PWV is not constant within one cardiac cycle. The equiphase point is determined on the propagating pulse wave, which represents the velocity of the whole pulse wave. It has been found that the early region of the pulse wavefront retains its characteristics while propagating through the arterial system. Thus, it has been suggested to determine the PTT between the equiphase points on the waveforms, which are located at the “foot” of the raising front. Different algorithms are used for the equiphase point detection and PTT estimation between synchronously measured pulse waves (Chiu et al 1991, Kazanavicius et al 2005, Temitski et al 2012). The results may differ between 5 up to 15% depending on the algorithm used for the PTT estimation (Millasseau et al 2005).

The “gold standard” method for the estimation of arterial stiffness is the aortic PWV, which is assessed as the carotid to femoral PWV (Mancia et al 2007). Due to the different methodologies and techniques for the distance and PTT estimation, the

carotid to femoral PWV estimation has been standardized (Boutouyrie et al 2010). Massive epidemiological studies have been conducted in order to prove the ability of the aortic PWV to predict cardiovascular events in certain patient groups and in population at large (Laurent et al 2006).

The non-invasive estimation of the aortic PWV is difficult as the artery is hidden deep inside the body. However, the simultaneous recording of flow waves from the left subclavian artery and from the abdominal aorta just above its bifurcation by using the Doppler ultrasound enables the estimation of the aortic PWV (Lehmann et al 1998). This method needs qualified expert skills in ultra sound Doppler measurements. The alternative method is the estimation of the aortic PWV by using the pulse wave recordings from the carotid and femoral arteries, as those locations are closest to the aorta where the pressure wave registration can be carried out from the surface of skin.

There are different devices that enable the estimation of the carotid to femoral PWV. The Complior System (Artech, Les Lilas, France) enables simultaneous recording of pressure wave signals from the carotid and femoral artery using two piezoelectric transducers. The other device is the SphygmoCor system (ArtCor, Sydney, Australia) (Wilkinson et al 1998), which has been widely used in clinical studies. The pressure waves have been recorded successively from the femoral and carotid artery by using the sensitive wide band piezoelectric sensor. Separately registered pressure waves are synchronized with the ECG signal and the PWV is estimated. The third device is PulsePen (Diatecne, Milano, Italy), which is similar to the SphygmoCor system. All the devices mentioned above require trained personnel and the reproducibility of the results depends on the skills of the operator.

It should be noted that the pressure waves are travelling to the opposite direction from the heart in case the carotid to femoral PWV is estimated. Thus, for the path length calculation, the distance from the heart to the carotid artery is subtracted from the distance from the heart to the femoral artery. In addition, it has been assumed that the wave propagation speeds from the heart to the pulse wave recording sites are equal, which, however, is doubtful. The advantages and limitations of the first two devices are reviewed in Boutouyrie et al (2009b).

A method that estimates the PTT from the single pulse waveform has also been proposed (Westerhof et al 2006, Qasem and Avolio 2008). The aortic pressure waveform is decomposed into forward and backward travelling pressure waves and the time difference is measured, which corresponds to 2·PTT for the given segment of the artery. By knowing the distance from the signal recording site to the reflection site, the PWV can be calculated. However, in a recent study a problem with this methodology has been reported, as the reflection site is difficult to determine and it seems to change the location through ageing (Westerhof et al 2008).

A similar methodology has been commercialized in the Arteriograph device (TensioMed, Budapest, Hungary) (Baulmann et al 2008). It has been assumed that there is one major pressure wave reflection site in the bifurcation of the aorta. The forward and reflected waves are detected from the brachial artery by applying the

cuff around the upper-arm. The cuff is pressurized to the supra systolic pressure (systolic pressure + 35mmHg) and from the recorded waveform the time delay between the incident and the reflected waves is detected, which corresponds to 2·PTT. The distance is suggested to be measured between the jugulum (sternal notch) and the symphysis pubica (pubic symphysis), two characteristic anatomical points. Invasive validations of the Arteriograph for the aortic PWV and the AIx estimation have been conducted and relatively high correlations have been achieved (Horváth et al 2010). However, the working principle and validation is debated. Further investigations of the working principle of the Arteriograph are suggested in order to induce the medical society to bring in the device in clinical practice (Parati and De Buyzere 2010). In a number of recent clinical studies the Arteriograph was used for the aortic PWV and AIx estimation (Mulders et al 2012, Gaszner et al 2012, Ikonomidis et al 2013).

The pulse wave propagation in other branches of the arteries has been studied in addition to the carotid-femoral PWV (Naidu et al 2005). The pulse wave starts to propagate when blood is ejected from the left ventricle to the aorta. The arrival of the pressure wave is detected from the artery of the upper or the lower limb. The pressure waves in the arteries were detected by using the pressurized cuffs, which were placed around the limbs. Thus, the exact detection point of the pulse wave on the artery varied due to the cuff size. They found that all the estimated PWVs in the branches from the heart to the higher and lower limb arteries and the carotid to the femoral artery were significantly increased in the coronary artery disease patients.

Often the R-peak of the ECG signal is used for the starting point of the pulse wave propagation from the heart (Naschitz et al 2004). However, the R-peak shows only the electrical activity of the heart, not the starting point of the wave propagation. There is a short period between the heart activation and opening of the valves of the left ventricle, which is called a pre-ejection period. PEP is not constant and depends on the physical condition of the subject. The ejection of the blood to the aorta can be detected from the phonocardiographic or transthoracic impedance signal. The VaSera VS-1500N (Fukuda Denshi, Tokyo, Japan) vascular screening system registers simultaneously ECG, phonocardiographic and pressure wave signals from the limb arteries. However, the PWV values for each arterial branch are not given. Instead, the Cardio-Ankle Vascular Index (CAVI) is calculated, which is based on the PWV estimation.

The aortic PWV is of major interest as it is a cardiovascular risk marker of an advanced disease and may predict morbid events in the next five up to ten years (Mancia et al 2007). However, the aortic PWV does not offer any insight into the condition of smaller blood vessels. All the arteries are stiffening and the atherosclerotic disease involves the whole cardiovascular system. The assessment of the peripheral arteries may enable earlier detection of atherosclerosis (Cohn J N 2006). It has been noted that lower limb arteries are particularly altered by atherosclerosis (Laurent et al 2006). However, currently there is no evidence that the PWV measured from the peripheral arteries may predict the cardiovascular event (DeLoach and Townsend 2008).

3.3. Pulse waveform analysis

Pressure wave is generated by the left ventricle contraction and blood ejection into the aorta. The pressure in the aorta increases due to the blood volume increase. The pressure increase in the aorta is dependent on the capability of the arterial wall to stretch and on the blood volume decrease throughout the peripheral beds of the tissue. The blood volume change is connected to the change in the pressure through the arterial compliance. The arterial compliance is decreased due to the increase in the arterial stiffness and in the case of the same stroke volume, a larger pressure wave is generated (Avolio et al 2010).

The pulse wave propagation through the vascular tree is a complex process. The nature of wave propagation depends on the elastic properties and geometry of the arteries and blood viscosity. In addition, the pulse wave reflection appears at the location where the artery is branching. The wave reflection and reflected wave magnitude are explained through the wave transmission theory as a mismatch between the impedances of the branching arteries. The impedance is a complex quantity and it is determined by the mechanical properties of the blood and arteries. As a result, the waveform of a propagating pulse wave changes along the arterial tree. Therefore, the pressure waves at the two arterial locations with the same mean pressure can have different pulse pressure and shape (Avolio et al 2010).

The pressure waveform at the aortic root depends on the contraction of the left ventricle and the geometric and elastic properties of the arterial system. The distinctive features can be detected from one cardiac cycle long pressure waveform (Figure 2). In the ascending aorta, the peak of the flow velocity wave appears before the peak of the pressure wave, because of the stretch of the elastic artery segment. The inflection point (P_i) on the aortic pressure waveform appears about at the same time with the maximal point of the flow wave. The peak of the flow velocity wave locates at about 30% of the whole ejection duration (Westerhof et al 2006). The augmented component is described through the augmentation index (AIx) and is defined as (Murgo et al 1980):

$$AIx = \frac{P_s - P_i}{P_s - P_d} = \frac{AP}{PP}, \qquad (4)$$

where P_s is the systolic blood pressure (maximal value of the pressure waveform), P_d is the diastolic blood pressure (minimal value of the pressure waveform), AP is the augmentation pressure and PP is the pulse pressure. The AIx has been found to change through the ageing (Kelly et al 1989). The AIx calculated from the aortic pressure waveform is negative in adolescents and becomes positive for older subjects. The significant changes in the pressure wave morphology are explained through the changes in the structural components of the arterial system, which affects the pulse propagation. In addition, it has been found that the AIx is influenced by the blood pressure and the values are higher in the case of patients with type I diabetes (Wilkinson et al 2000a) and hypercholesterolemia (Wilkinson

2002), which can be explained through premature vascular ageing (Ravikumar et al 2002, Cockroft and Wilkinson 2002).

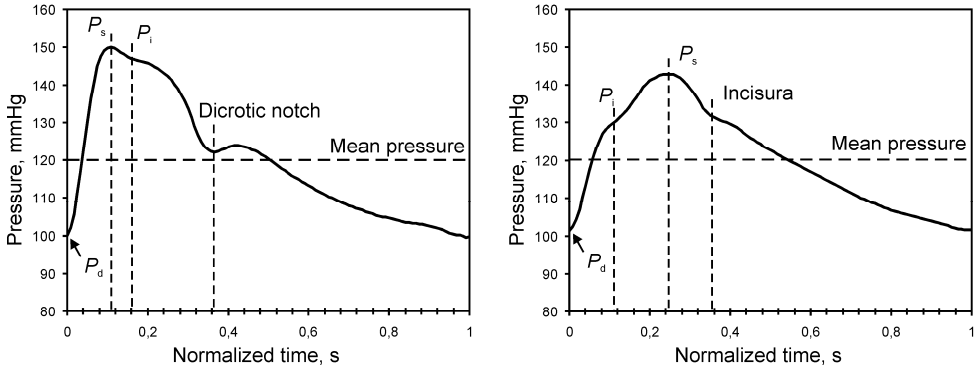

Figure 2. Averaged radial and aortic pressure waveforms normalized in time with the characteristic points (reproduced according to Avolio et al 2010).

The radial pressure waveform includes features similar to those of the aortic waveform registered from the same subject. However, the waveforms are significantly different. The minimal point of the radial artery pressure waveform corresponds to the diastolic pressure similarly to the aortic waveform. The mean pressure of the radial artery waveform is lower from the aortic waveform, but the difference is small and it can be considered equal in the case of healthy subjects. The diastolic and mean pressures measured from the radial or brachial arteries have been used as reference for the aortic waveform calibration. The maximal point in the radial artery waveform corresponds to the systolic blood pressure, but it is situated within the cardiac cycle at a different location (Avolio et al 2010). This causes also the differences between simultaneously measured invasive radial and aortic systolic pressures (Pauca et al 1992).

Usually the inflection point (P_i) appears in the radial artery pressure waveform after the first pressure peak, which in this case is the systolic pressure peak. However, due to the ageing P_i may become higher than the first peak, forming a systolic pressure peak (Kelly et al 1989). The formed systolic peak in the radial artery waveform is then also connected to the systolic peak in the aortic waveform (Takazawa et al 2007). In some cases the late systolic peak can be visible in the radial artery waveform as a separate peak with the local maximal point or it forms the convexity before the dicrotic notch, as shown in Figure 2.

The incisura, which is visible after the systolic peak in the aortic waveform, corresponds to the aortic valve closure. The local minimum after the inflection point on the radial artery waveform is called the dicrotic notch (Avolio et al 2010). The timing of incisura on the aortic waveform correlates with the dicrotic notch in the radial artery waveform and thus the ejection duration can be obtained (Gallagher et al 2004).

Often the composition of the pulse waveform has been explained through the forward and backward travelling wave. The forward travelling wave is caused by the left ventricle ejection. The backward travelling wave is mainly caused due to the reflection of the forward travelling wave from the branch points of the arteries. It has been reported that the single reflection site is difficult to determine (Westerhof et al 2008). There are many reflection sites in the arterial system and the reflected waves can summate and act as one wave arising from a single reflection point (Nichols and O'Rourke 2005).

According to the theory, the stiffness of the arteries is only one variable that determines the AIx. In addition, the aortic pressure waveform depends on the wave characteristics of the left ventricle ejection profile, magnitude and timing of the reflected waves (Kingwell and Gatzka 2002, Nichols and O'Rourke 2005). The pulse waveform analysis allows the detection of changes in the waveforms and attempts have been made to interpret it through the changes in the mechanical properties of the arteries (Hamilton et al 2007).

The increase in the aortic augmentation pressure is related to the increase in the arterial stiffness. Due to the higher arterial stiffness the reflected wave propagates with higher velocity and arrives faster back to the aorta from the reflection sites by augmenting the pressure wave and increasing the central systolic blood pressure. The reflected wave arrives back during the systolic phase by increasing the left ventricle afterload (Chirinos and Segers 2010). The earlier arrival of the reflected wave also causes the decrease in the diastolic pressure, which results in the reduction of the coronary artery perfusion pressure (Nichols and O'Rourke 2005). As the pressure waveform changes while travelling through the arterial system, it is important to record the central pressure waveform in order to define the effects on the left ventricle and coronary artery.

The direct recording of the aortic pressure wave is invasive. The aortic pressure waveform can be analyzed non-invasively by using the SphygmoCor system. The pressure wave can be registered from the carotid artery by using applanation tonometry. As the carotid artery situates close to the aorta, the waveforms are similar and no transfer function is needed for the analysis. However, the recording of the pressure wave from the carotid artery needs a highly trained person, as the vessel is not supported. In addition, the recording of the pressure wave is difficult in the case of subjects with obesity and carotid stenosis (Rhee et al 2008).

The other widely used technique, which is also applied on the SphygmoCor system, involves the pressure wave registration from the radial artery and the aortic waveform is derived by using a generalized transfer function (Pauca et al 2001). The pressure wave recording from the radial artery is preferred as it is supported by bone and the applied pressure by tonometry is easier to handle. The AIx is determined from the derived aortic waveform and it has been used widely as an indicator of aortic stiffness (Rhee et al 2008). Nevertheless, issues regarding the precision of the generalized transfer function have been raised (Hamilton et al 2007). Transfer functions are generally constructed from the data of healthy subjects. It has been found that this approach may cause errors in the case of type II

diabetes patients and the AIx is overestimated (Hope et al 2004). In addition, it has been suggested that there is no need to use the transfer function for the aortic AIx estimation. The AIx estimated from the radial artery and the AIx estimated from the derived aortic waveform are highly correlated r=0.96 (Millasseau et al 2003). This approach has been applied in the Arteriograph where the aortic AIx is estimated from the brachial artery pressure waveform without using the generalized transfer function (Horváth et al 2010).

It has been found that the aortic AIx depends on the heart rate (Wilkinson et al 2000b). Therefore, the AIx value in the SphygmoCor system has been normalized for the heart rate of 75bpm and noted as AIx@75.

4. Photoplethysmographic signal and waveform analysis

PPG is a non-invasive optical technique, which can be used to monitor the circulatory changes in the cardiovascular tissue bed. For the PPG signal recording the light source is placed towards the skin surface and light is emitted to the examined tissue. The light is absorbed and scattered in the tissue. Just a small fraction of emitted light intensity can be detected with the photodetector, which is placed on the skin adjacent to the light source (reflection mode) or opposite the measured volume (transmission mode). In the PPG probes, the LEDs and photodiodes or phototransistors are often used, which makes the technology relatively cheap and reproducible. In PPG probes the LEDs are usually in the red or infrared wavelength range. However, the other wavelength ranges are used as well and it is application dependent (Allen 2007).

The PPG signal registered from the finger or forehead generally consists of DC and AC components and noise. The amplitude of the AC component can be ten times smaller than the DC component. The DC component depends on the total blood volume in the observed tissue and it varies slowly in time. The AC component of the PPG signal is synchronous with the cardiac cycle and depends on the blood volume and flow changes, blood vessel wall movement, pulsatile pressure and the orientation of red blood cells (Kamal et al 1989, Lindberg and Öberg 1993, Allen 2007). Though origins of the AC component waveform mechanism of the PPG signal have been studied, the phenomenon is still not fully understood (Allen 2007). Generally, it has been accepted that the AC component of the PPG signal can contain valuable information about the cardiovascular system and it corresponds to the heart generated pulse wave. AC and DC components of the PPG signal are affected by respiration and factors that influence local perfusion, such as vasomotion and sympathetic nervous system activity (Johansson and Öberg 1999, Nitzan et al 1998).

PPG technology is widely used in the pulse oximeters, however other clinically important physiological parameters such as the breathing and heart rate, can be monitored as well. In addition, the PPG technology has been used for the PTT measurements in order to estimate the vascular ageing (Allen and Murray 2002). Furthermore, the PTT measurement is widely used for the estimation of beat-to-beat blood pressure without cuff. This technique would enable monitoring the blood

pressure changes over long periods (e.g. 24 hours) (Zheng et al 2013) and providing clinically important dynamical changes, which are predictors of cardiovascular events (Fagard et al 2008, Dolan et al 2005).

The PPG waveform is affected by the changes in the mechanical properties of the arteries as the AC component of the signal corresponds to the pulse wave. Therefore, this simple technique may also have a potential for the identification of premature increase in the stiffness of the arteries and may be of considerable value in the prevention of the cardiovascular disease. In all those applications the AC component carries essential information. Therefore, in the subsequent text the term "PPG signal" corresponds to the AC component of the PPG signal.

Noise in the PPG signal can be originated from different sources (Sukor et al 2011). The power line interference causes the 50Hz or 60Hz noise. The ambient light may cause the blinding of the photodetector or modulate the signal. Often the PPG signals are affected by the motion caused noise, which is related to the movement of the sensor or the limb of the subject, where the signal is obtained. In addition, the pulsating volume in the examined tissue is diminished due to the poor perfusion state and therefore the amplitude of the PPG signal is decreased. Consequently, the SNR of the signal is decreased.

Similarly to the pressure wave, the foot of the PPG signal has been detected for the PTT estimation (Nitzan et al 2002). Nevertheless, 50% of the raising front level detection has also been used for the PTT measurement, which has been found comparable with the foot detection and it is more appropriate if there is a high probability for motion artifacts in the signal (Lass et al 2004). Often the time delay between the R-peak of the ECG signal and the raising front of the PPG signal is detected for the PTT estimation (Naschitz et al 2004). In addition, the R-peak of the ECG signal has been used for the wave front detection in order to align the recurrences of the PPG signal for the waveform analysis (Allen and Murray 2003). High correlations between the blood pressure and the PTT have been found in the case of physical exercise (Marcinkevics et al 2009). Furthermore, advanced models are proposed for the blood pressure estimation from the PTT measurement and 24-hour monitoring (Poon and Zhang 2005). In addition, for more accurate blood pressure estimation, the PTT is measured without the PEP. For that purpose the time delay is measured between the opening of the aortic valve and the PPG signal raising front (Solà et al 2011). The opening of the aortic valve is detected from the phonocardiographic or transthoracic impedance signals. In the mentioned applications the raising front of the PPG signal must be able to detect accurately, which can be complicated in the case of noise.

Different methods have been used to suppress the noise in the PPG signal. The simple FIR bandpass filter can be used in order to limit the unwanted high and low frequency components. However, the gross movement, coughing and breathing patterns, such as deep gasp or yawn, may cause the noise in the PPG signal, which shares the same frequency components, where the harmonic components of the PPG signal are situated. One possibility is to detect the noisy recurrences of the PPG signal and leave them out from the further analysis (Couceiro et al 2012). The

other approach is to remove the noise by using different signal processing algorithms. Techniques based on wavelet transform (Lee and Zhang 2003) and independent component analysis (Stetson 2004, Kim and Yoo 2006) have been applied. Though, the studies have shown that these methods fail in certain situations (Foo 2006, Yao and Warren 2005). The motion artifacts can be removed from the PPG signals using the Fourier series analysis on cycle by cycle basis (Reddy et al 2008). However, this approach is computationally complex. In addition, the adaptive filters have been used to suppress the noise caused by motion under an assumption that the expected PPG signal is statistically independent of the artifacts. Additional acceleration sensors have to be used with the PPG probe for that purpose (Foo and Wilson 2006, Wood and Asada 2007, Comtois et al 2007).

The PPG signal has a slowly changing nature and most of the power of the PPG signal is concentrated into the first 10 harmonic components. The PPG waveform has characteristics similar to those of the pressure waveform and the systolic phase and diastolic phase are separated with the dicrotic notch (Chan et al 2007). The front of the PPG signal is the fastest changing part during one cardiac cycle.

The waveform analysis of the PPG signal has been carried out since 1941. Dillon and Hertzman firstly described the PPG waveform through the crest time and the height of the dicrotic notch (Dillon and Hertzman 1941). It was found that the height of the dicrotic notch from the baseline depends on the vasoconstriction and vasodilatation effects. In addition, there is an increase in the crest time and disappearance of the dicrotic notch in the subjects with hypertension and arteriosclerosis.

The PPG signal waveform depends on the location where the signal is obtained (Allen and Murray 2003). The recorded PPG signal waveform from the finger is almost identical to the pressure waveform recorded from the radial artery. The relationship can be represented by a single transfer function (Millasseau et al 2000). Thus, the mechanical properties of the arteries that are determining the waveform of the radial artery are similarly affecting the waveform of the finger PPG signal. The cardiovascular ageing has a noticeable influence on the PPG signal waveform through the mechanical changes in the arterial system. This change is visible in the PPG waveforms, which are recorded from different locations of the body (Allen and Murray 2003). The increase in the age of the subject and the consequent vascular ageing results in the triangulation of the curvy finger PPG waveform (Hlimonenko et al 2003). These changes are similar to the radial artery (Kelly et al 1989).

In the recent studies the PPG waveform has been decomposed by using the Gaussian or log-normal functions in order to separate direct and reflected waves for the cardiovascular system assessment (Rubins 2008, Huotari et al 2009). In addition, the PPG waveform has been analyzed on the frequency domain and the decrease of power in the harmonics is indicated due to the increase in age. This has been suggested as the useful non-invasive measure of ageing and vascular disease (Sherebrin and Sherebrin 1990).

A number of parameters can be used to determine the waveform of the pulse wave on the time domain, which can be applied as well for the PPG waveform

(Korpas et al 2009). On the time domain, the proportions of the pulse wave can be measured, such as the crest time of the pulse wave front, time from the foot of the pulse wave until the maximal point of the diastolic wave, total pulse duration, systolic and diastolic peak amplitude. From the previously mentioned proportions, parameters related to arterial stiffness can be calculated (Millasseau et al 2002, Millasseau et al 2006).

In the systolic phase of the PPG waveform similarly to the radial artery pressure waveform, initial wave peak, inflection point, late systolic peak, and dicrotic notch can be seen. Through triangulation of the waveform the distinctive points are difficult to distinguish. The derivatives of the PPG signal can be used for the detection of the mentioned characteristic points on the waveform.

The SDPPG signal analysis was first introduced by the Takazawa group to evaluate ageing and increase of arterial stiffness (Takazawa et al 1998). However, the detection of the distinctive points from the PPG waveform is out of scope of this analysis. Instead, the five distinctive wave peaks 'a', 'b', 'c', 'd', and 'e' from the SDPPG signal are detected and amplitudes of each wave are estimated. The amplitudes are normalized with wave 'a' as follows: b/a, c/a, d/a, e/a. It was found that with the increase of age, the value of b/a (r=0.75; P<0.001) increased and c/a (r=-0.67; P<0.001), d/a (r=-0.72; P<0.001), and e/a (r=-0.25; P<0.001) decreased. According to the results, the ageing index was proposed as follows (Takazawa et al 1998):

$$AGI = \frac{b - c - d - e}{a}. \qquad (5)$$

It was found that the average AGI was elevated in case the subject had any of the following diseases: diabetes mellitus, hypertension, ischemic heart disease, and hypercholesterolemia. The average AGI for 474 healthy subjects was -0.22±0.36 and 126 subjects with the history of a disease had an average AGI -0.06±0.41.

It was followed by the studies where the correlation relationship between the SDPPG normalized amplitudes and other physiological parameters was analyzed in more detail. The changes in the amplitudes of the SDPPG waves were analyzed in children and young people by Iketani et al (2000). They found that ageing decreased the b/a ratio and the AGI and increased the c/a and e/a ratios. Overall, the AGI decreased with age between 3 and 18 years and then increased, forming a parabolic relationship.

In the study by Bortolotto, the SDPPG amplitude ratios of the finger were compared with the Complior measured carotid-femoral PWV regarding the influencing factors of atherosclerosis and age, in a large hypertensive population (Bortolotto et al 2000). It was found that the average values of the PWV, the AIx of the PPG waveform and the AGI were elevated in the case of hypertensives with atherosclerotic alterations.

The relationship between the wave amplitudes of the SDPPG and various cardiovascular risk factors among middle-aged men were analyzed by Otsuka et al

(2007). They found that the *b*/*a* ratio increased with age, hypertension, dyslipidemia, impaired fasting glucose/diabetes mellitus, and lack of regular exercise. Similarly, the *d*/*a* ratio decreased with age, hypertension, and alcohol intake 6 up to 7 days per week. In addition, from the femoral artery, the registered PPG signal has been used for the regional and local arterial stiffness estimation by the SDPPG analysis (Grabovskis et al 2011). It was found that the *b*/*a* ratio correlated (r=0.729; P<0.0001) with Young's modulus of the femoral artery, which is a measure of arterial stiffness.

In addition to the SDPPG parameters, the AIx of the invasive aortic pressure and the finger PPG waveform were compared in the study by the Takazawa group (Takazawa et al 1998). The AIx was estimated as a ratio between the amplitudes of the late and early systolic component. They found high correlation between the two measures of the AIx (r=0.86; P<0.001). This shows the possibility to use the finger PPG signal waveform to estimate the changes in the aortic pressure wave. However, in the later studies, the ratio between the amplitudes of the PPG signal and the diastolic wave peak has been used to estimate arterial stiffness and it is called the reflection index. However, this measure differs from the AIx.

The PPG signal has to be twice differentiated for the SDPPG analysis. The differentiator works as a high-pass filter and as a result, higher frequency components are amplified (Proakis and Manolakis 2006). The amplified higher frequency components have to be suppressed, because it consists of unwanted noise.

It has been noted that in the case of the PPG waveform analysis it is important to apply appropriate filtering and it is principally essential when using the second derivative analysis (Millasseau et al 2003). In the same study, more detailed information about the band limiting filter of the PPG signal has been given, where the Parks-McClellan digital low-pass filter (aka Remez filter) was used with the following parameters: edge-frequency of 10 Hz, transition-band of 2Hz, pass-band ripple of 0.05 dB, stop-band attenuation of 100 dB. The edge-frequency of the pass band is the highest frequency of interest in the PPG signal. According to Millasseau et al (2003), the parameters of the filter were claimed to be chosen by unpublished observations, where the filter with the given edge-frequency produced no loss of information. However, the suppression of the higher frequency components has to be enough in order to detect the distinct wave peaks from the SDPPG signal.

The band limiting filter for the SDPPG analysis, similar to that of Millasseau et al (2003), has commonly not been described in detail including Takazawa et al (1998), Iketani et al (2000), and Otsuka et al (2007). The cut-off frequency of the low-pass filter has been used between 10 up to 10.6 Hz in many studies. In addition, the transition band of the filter, which plays an important role in the processing of the signal, has not been given in most of the studies (Bortolotto et al 2000, Hashimoto et al 2005, Otsuka et al 2006).

5. Experimental studies

5.1. Experimental measurement complex (Publication I)

A measurement complex for synchronous recording of pulse wave signals from different locations of arterial and peripheral sites as well as other physiological signals registered by different devices was developed (Publication I). The complex provides simultaneous estimation of the PWV and pulse waveform parameters related to the arterial stiffness. The experiments were carried out in the North Estonia Medical Centre. The study was conducted in accordance with the Declaration of Helsinki and formally approved by the Tallinn Ethics Committee on Medical Research.

Two reference devices, a SphygmoCor and an Arteriograph, were used in the measurement complex for the aortic AIx and PWV estimation. As those devices are widely used in the clinical studies a possibility was open to compare the PWVs from other segments of the arteries and pulse waveform analysis results.

The PWVs were measured from the segments of upper and lower limb arteries in addition to the aortic PWV. In publication I the pulse wave signals were recorded from the elbow, wrist, index finger, forehead, neck, earlobe, knee, and the big toe. However, after the pilot studies some of the locations were changed. After corrections the pulse waves were recorded from the index finger, wrist (radial artery), elbow (brachial artery), forehead, knee (popliteal artery), femoral artery, and the big toes.

The pulse waves were registered from the index finger, big toe and forehead by using the PPG technique. The PPG signals were obtained from the finger and the big toe using the commercially available Envitec F-3222-12 clip sensors. The Masimo LNOP TF-I reflectance sensor was used to record the forehead PPG signal. The distance between the LED and the photodetector was 7mm. In both sensors the infrared LED was used, which has peak at 880 nm. The PPG sensors were connected to the lab-built modules, which drives the LED and transforms the photoelectric current from the photodiode into the voltage signal. LED was working in the pulsed mode, which enables the noise from ambient light to be cancelled. In addition, the current of the LED can be adjusted manually from the module and be optimized for the recording. Four PPG modules were built by the author of this thesis.

It is difficult to obtain the pulse wave signal from the arteries by using the commercially available PPG sensors. The arteries are situated under other types of tissues and the intensity of diffused light from the deeper layers of the tissue can be low. For that purpose, location specific reflectance sensors should be developed. The piezoelectric transducers were used for the pulse wave recording from the radial, brachial, femoral and popliteal artery. Commercially available piezoelectric transducers MP100 (ADInstruments, USA) were used for the registration of mechanical pulsations of the arteries. The piezoelectric transducers were placed above the artery and the additional pressure was applied with elastic bandage. It was ensured that the applied pressure was not affecting the signal quality (Pilt et al

2010a, Pilt et al 2010b). Two piezoelectric modules with two input channels were built by the author of this thesis in order to amplify the signals and convert them suitable for an analog-to-digital converter.

In addition to the pulse waves the following signals were recorded simultaneously: phonocardiographic, ECG, peripheral pressure wave. For the PWV estimation in the arterial segments from the heart to the lower and upper limb arteries, the phonocardiographic signals were recorded using the ADInstruments cardiomicrophone. From the phonocardiographic signal it is possible to detect the opening of the left ventricle aortic valve and to leave out the PEP in the estimation of the PTT. In addition, the ECG signal was recorded simultaneously and used as a reference signal for the signal processing. ECG signal is stable and less sensitive to motion caused noise. In addition, it is easy to detect the beginning of heart contraction from the R-peak of the ECG signal. The ECG signal was recorded with a commercially available ADInstruments PowerLab 4/20T device in order to ensure the safety of the patient. In addition, the device enables to recording of the phonocardiographic signal. The ECG and phonocardiographic signals were digitized with the sampling rate of 1 kHz.

Beat-to-beat blood pressure wave was monitored from the right hand index finger by using the Finapres system. The device enables analogue output from where the calibrated pressure wave can be obtained. The outputs of the Finapres system, the PPG and piezoelectric modules were connected to the National Instruments PCI MIO-16-E1 data acquisition card. The card digitizes the analogue signals with a resolution of 12-bit and sampling rate of 1 kHz.

The synchronization between two analog-to-digital converters was needed. It was carried out by using an additional synchro signal connection between the two devices. The synchronous recording of the signals was tested by the generated sine wave with the frequency of 5 Hz. The signal from the generator output was fed to the inputs of the PowerLab and the data acquisition card. After the analysis it was found that two systems are recording the signals synchronously.

In addition, the pilot study was carried out on four subjects in order to test the applicability of the measurement complex. Firstly, the measurements were carried out with reference devices, while the subject was in supine position. Next, all the signals were recorded synchronously with the measurement complex. The signals were processed in MATLAB and PWVs were calculated for the limb arterial segments and compared with the Arteriograph estimated aortic PWV. All the measured PWVs were below 9 m/s. In addition, the PWVs were lower than the aortic PWV in the segments from the elbow to the index finger and from the knee to the big toe. Similar results were also achieved in the earlier study (Hlimonenko et al 2008).

In addition, after the pilot studies the ultrasound system was included to the measurement complex in order to obtain the thickness of the arterial wall and the diameter of the vessel lumen. This enables us to estimate the Young's elastic modulus of the artery, which is the measure of stiffness.

5.2. Noise suppression in photoplethysmographic signal for PTT estimation (Publication II)

The registered pulse wave signals can be noisy in case the examined subject has to deal with some kind of physical activity or has unintentional movements during the recordings. Motion caused noise can overlap the frequency components of the pulse wave signal. In publication II the algorithm for the suppression of motion caused noise from the PPG signal was developed and tested on the simulated and recorded PPG signals from the subject. In addition, the averaging effect of the algorithm on the PTT calculation was analyzed.

Comb filter has frequency response where the main lobes are regularly spaced over the frequency domain. All the frequency components situated between the main lobes are suppressed. In case the frequency response of the filter is adjusted according to the harmonic components of the desired signal, the noise components between the main lobes are suppressed. In the case of discrete periodic signals $x[k]$, the comb filter is described as follows:

$$y[k] = \frac{x[k] + x[k - D]}{2}, \qquad (6)$$

where $y[k]$ is the output signal of the filter, k is an integer and refers to the sample number in the signal, and D is the coefficient, which determines the frequency response of the filter. The output of the filter is averaging the two consecutive periods in case the filter is adjusted for the periodic signal frequency. The filter can be modified in order to average more than two consecutive periods.

The biosignals are recurring but not periodic. Therefore, the comb filter has to be adapted for each recurrence of the PPG signal. In publication II the filter was adapted based on the pulse frequency, which was calculated from the ECG signal. Generally, in MATLAB the developed adaptive comb filter interpolates the r consecutive recurrences of the PPG signal to the same length and calculates the average waveform. The attenuation between the main lobes is increased by enlarging the number of averaged recurrences r. However, using more than four (first side lobe attenuation 11.4dB) or five (first side lobe attenuation 12.1dB) recurrences will not lead to considerable advantage, as with ten recurrences the first side lobe attenuation is 13.1dB.

The adaptive comb filters were tested on 24s long simulated PPG and ECG R-peak signals, the frequency of which varied from 1 Hz up to 2 Hz. The white noise was added to the signal. It was found that the adaptive comb filter with r=3, r=4, r=5 attenuated noise 24 dB, 32 dB, and 39 dB, respectively.

In addition, the adaptive comb filter was tested on the PPG signals, which were recorded from the forehead. The ECG signal was recorded synchronously. The subject was asked to make squat downs in order to decrease the SNR of the signal. The recorded PPG signal was filtered with high- and low-pass filters with cut-off frequencies of 0.3Hz and 30Hz, respectively. Next, the adaptive comb filter was

applied. By comparing the frequency spectrums before and after comb filtering it was visible that the frequency components were suppressed between the harmonic components of the PPG signal. Furthermore, the fronts of the PPG signal were able to visually detect after the comb filtering.

The adaptive comb filter has an averaging effect on the signal waveform and due to that its influence on the PTT estimation was analyzed by using simulated PPG and ECG R-peak signals. In the first simulated test signal the PTT varied between 0.25 and 0.35 s. The PTT was estimated by using a raw and a comb filtered PPG signal. The comb filter used six recurrences r=6 for the output signal calculation. It was found that the PTTs estimated using the comb filtered signal are delayed about three periods from that of the raw generated PPG signal. Furthermore, in the second simulated test signal the PTT value was changed sharply from 0.35 to 0.25 s. Six-period long reaction time was found in case the adaptive comb filter used six recurrences for output signal calculation.

In addition, the PTT delay effect was analyzed in the case of the forehead recorded PPG signal. The change in the PTT was obtained with the Valsalva maneuver. The similar PTT delay effect was visible in case the comb filtered PPG signal was used. However, the typical PTT changes of the Valsalva maneuver were mostly visible in case the four recurrences were used for the filter output signal calculation.

The developed adaptive comb filter is a simple method for the suppression of the motion caused noise in the PPG signal. However, the output signal of the filter depends on the previous recurrences and due to that the small characteristic changes were reduced. The balance between noise suppression and allowable signal averaging effect was considered in the applications of the filter.

5.3. Second derivative photoplethysmographic signal analysis algorithm (Publication III)

The AGI derived from the analysis of the finger SDPPG waveform can be a potential parameter for the estimation of the arterial stiffness and the evaluation of cardiovascular ageing. In publication III the SDPPG analysis algorithm was improved in order to achieve the minimal standard deviation of the AGI. Lower standard deviation of the AGI gives more effective differentiation between the levels of cardiovascular ageing.

It is shown in publication III that in the case of a healthy subject the AGI value may differ between the consecutive recurrences by using the SDPPG analysis algorithm (Millasseau et al 2003). Although the subject was in the supine position and it was assumed that the cardiovascular system was not changing during short periods of time, the difference between the minimal and maximal values of the AGI constituted about 39% from the whole scale of the AGI. It was visible that the detected peaks of the SDPPG waveform were situated in the two consecutive recurrences of the PPG signal at the different phases of the cardiac cycle. The different detection of wave peaks in the consecutive recurrences is due to the

insufficient suppression of noise and higher harmonic components of the PPG signal.

The differentiator works as a high-pass filter and it amplifies the noise located at higher frequency components. It has to be suppressed with a low-pass filter. The low-pass filter with a static cut-off frequency suppresses the frequency components of two consecutive recurrences differently, as the frequency components of the PPG signal are dependent on the heart rate. The new SDPPG signal analysis algorithm limits equally the number of harmonic components in each of the recurrence. The analysis algorithm was implemented in MATLAB.

For that purpose, the raw SDPPG signal was resampled to ensure that one of the selected recurrence lengths is 1 s long. Next, the Parks-McClellan low-pass filter with a 1 Hz wide transmission band was applied. The copy of the selected recurrence from the filtered SDPPG signal was placed to the waveform matrix. Then the next recurrence was selected from the raw SDPPG signal and the resampling, filtering and copying process was carried out. The selected recurrence was placed to the next row in the waveform matrix. The described processing loop was carried out for all of the recurrences in the SDPPG signal. In addition, parallel with the SDPPG signal processing, the PPG and the fourth derivative of the PPG signal were processed in the same way. As a result, the three waveform matrices were constructed.

All the waveforms in the matrices were aligned according to the 50% level point of the PPG signal raising front. Next, the distinct wave peaks ‘a’, ‘b’, ‘c’, ‘d’, and ‘e’ in the SDPPG waveforms were found between the zero crossing points of the fourth derivative of the PPG signal waveform and the amplitude ratios b/a, c/a, d/a, e/a and AGI were calculated.

The optimal edge frequency was found for the Parks-McClellan low-pass filter in order to achieve the lowest standard deviation of the SDPPG wave amplitudes, which in the end minimizes the standard deviation of the AGI. Furthermore, the variation in the placement of detected waves on the time domain has to be minimal throughout all the recurrences for a subject. For that purpose, the 1-minute long PPG signals from the index finger were obtained using the measurement complex described in the publication I. The temperature of the room was controlled and kept at 23±1 degrees Celsius. The PPG signals were recorded from 21 healthy and physically active subjects aged from 21 to 66 years. The subjects were grouped by the age as follows: 20-30, 30-40, 40-50, 50-60, 60-70. Each age group from 20 to 50 years comprised 5 subjects. The other two groups comprised three subjects. The recorded PPG signals were processed with the new SDPPG algorithm and the edge frequency of the Parks-McClellan filter was changed between 4 to 14 Hz with a step of 1 Hz. For comparison, the same signals were processed with the algorithm by the research group of Millasseau (Millasseau et al 2003).

It was found that the minimal standard deviation of the amplitude ratios and minimal variations in the placement of the detected waves on the time domain achieved in the case of the edge frequency of the low pass filter was 6 Hz. This edge frequency has been considered optimal for the finger PPG signals. Compared

to the previous algorithm, the average standard deviation of the AGI was twice lower, which constitutes 5% of the whole scale of the AGI (Takazawa et al 1998). A relatively high correlation (r=0.91) was found between the age and the AGI, which is in agreement with the previously published results (r=0.80) by the Takazawa group (Takazawa et al 1998).

The algorithm was also tested on the signals from the diabetes patient group. The diabetes patients may have an increase in the cardiovascular age and elevation in the arterial stiffness due to the sclerotic processes. The diabetes patient group included 20 subjects.

The linear regression model was constructed in order to estimate the relation between the age and the AGI. The regression model was constructed based on the results of healthy subjects. The AGI values found were relatively high for the diabetes patients as compared of those of the healthy subjects. However, some of the diabetes patients had AGI values similar to the healthy subjects. It can be caused by the effective treatment of diabetes mellitus and active lifestyle of the subject, which has stopped the premature stiffening of arteries. It was seen from the Bland-Altman plot that the average difference of the diabetes patient group from the regression line was 0.36. In addition, a significant difference between the two groups was found ($P<0.0005$).

Based on these results, the improved SDPPG algorithm can be used for the estimation of cardiovascular ageing and the subjects with probable increase in arterial stiffness can be differentiated.

5.4. Forehead photoplethysmographic waveform indices for cardiovascular ageing estimation (Publications IV)

In publication IV the forehead PPG signal was analyzed by using the SDPPG analysis algorithm introduced in publication III. The aim was to investigate the cardiovascular ageing effect on the forehead PPG signal and to find SDPPG indices for the differentiation of the subjects with increased arterial stiffness. In this study the forehead PPG signals were recorded from 22 supposedly healthy subjects aged from 21 to 50 years and from two diabetes patients at the age of 33 and 27. As the finger and forehead PPG signal recordings were carried out simultaneously, almost half of the recordings were used from the study described in publication III.

In this study the aortic PWV was estimated as a reference for the evaluation of the cardiovascular system. The estimated PWV is related to the stiffness of the aorta through the Moens-Korteweg equation. Elevated PWV indicates the increase in the stiffness of the aorta and it is assumed that the stiffness of blood vessels in the forehead has also increased due to the sclerotic processes. The PWV in the aorta was estimated by the TensioMed Arteriograph.

It was found that the diabetes patients had the PWV above 10 m/s, which indicates the increase in the stiffness of the aorta. Furthermore, one healthy subject had the PWV of 15.4 m/s. All the other subjects had the PWV below 9 m/s. However, compared to an earlier study (Ohmori et al 2000), no relationship between the aortic PWV and the age was found.

In this study the optimal low-pass filter edge frequency was found at 6 Hz, which is similar to the study in publication III. The PPG signals were processed and the SDPPG signal amplitude ratios were estimated. It was found that the extracted amplitude ratios *b*/*a* (*r*=0.60), *c*/*a* (*r*=-0.24), *d*/*a* (*r*=-0.59), and *e*/*a* (*r*=-0.50) are dependent on the age. Furthermore, the changes in the amplitude ratios were in the same direction as the finger signal amplitude ratios (Takazawa et al 1998). This means that the changes similar to those of the finger waveform can be seen in the forehead signal, although the waveforms are not identical. In addition, the absolute values of the amplitude ratios from the forehead and the finger signal are different due to the waveform differences.

The values of amplitude ratios *b*/*a* and *d*/*a* form the diabetes patients and from one healthy subject with elevated PWV were noticeably different from healthy subjects. At the amplitude ratio *b*/*a*, the values were elevated and at the amplitude ratio *d*/*a*, the values were lowered.

The changes in the forehead PPG waveform caused by the cardiovascular ageing can be characterized using the SDPPG amplitude ratios. Based on the results it can be assumed that the premature increase in cardiovascular ageing is more evident at the amplitude ratios of *b*/*a* and *d*/*a*.

5.5. Finger photoplethysmographic waveform index for discrimination of subjects with higher arterial stiffness (Publications V)

In publication V the finger PPG waveform index was compared with the SphygmoCor derived aortic AIx to show that the PPGAI can be used for the detection of premature cardiovascular ageing. The PPGAI was obtained using the SDPPG analysis algorithm described in publication III. The amplitudes of the PPG waveform were obtained at the locations of wave peaks ‘b’ and ‘d’. The named amplitudes were normalized with the amplitude of the PPG waveform and denoted as *PPGb* and *PPGd*. The PPGAI was calculated as follows:

$$PPGAI = \frac{PPGd}{PPGb} . \quad (7)$$

In this study the subject groups and participated subjects were the same as in the study of publication III. Furthermore, in this study the recorded signals for publication III were used. During the experiments the pressure waves were obtained from the left hand radial artery with SphygmoCor prior to the PPG signal recordings. The aortic pressure waveform was derived from the radial artery waveform by using the transfer function. The AIx@75 was estimated from the aortic pressure waveform.

The strong linear correlation relationship was found between the SphygmoCor derived aortic AIx@75 and the PPGAI (*r*=0.85). All the data points from healthy subjects and diabetes patients were used in the correlation coefficient calculation. Similarly, a high correlation relation (*r*=0.86) between the invasive aortic AIx@75

and the PPG AIx was found by the Takazawa group (Takazawa et al 1998). In addition, the regression model was constructed for the aortic AIx@75 estimation from the PPGAI.

The linear relationships between the aortic AIx@75, the PPGAI and the age were investigated by using the data points from healthy subjects. Relatively high correlation relationship was found between the age and the PPGAI (r=0.75) and the regression model was constructed. The data points from healthy subjects were situated close to the regression line. However, the PPGAI values from diabetes patients were noticeably higher from the regression line, which indicates the premature cardiovascular ageing and increase in the arterial stiffness. Similarly, the positive correlation relationship (r=0.58) was found between the age and the aortic AIx@75. The data points were more dispersed around the regression line as compared to the PPGAI. However, the values of the AIx@75 were higher than the regression model line, which is similar to the PPGAI.

The data point differences from the regression lines were calculated for the aortic AIx@75 and the PPGAI. For both indices, significant differences between the healthy subject and diabetes patient groups were found. The average difference of diabetes patients from the regression line was 0.26 and the regression model standard deviation was found 0.10 in the case of the PPGAI. Similarly, the average group difference from the regression line was 14.4% and the regression model standard deviation was 12.11%. It was found that the sensitivity, detectability (specificity) and accuracy were equally 75% in the case of PPGAI. The same values for AIx@75 were 55%, 57% and 56%, respectively. Based on the results, the PPGAI provides better discrimination of the subjects with higher arterial stiffness than the aortic AIx@75. It has been shown that the relatively cheap PPG technology and the developed SDPPG analysis algorithm can be applied to discriminate the subjects with premature increase in the arterial stiffness from the healthy subjects.

Conclusions

The results of this study confirm the possibility to detect premature increase in arterial ageing using an inexpensive and non-invasive optical method based on the novel algorithm of the SDPPG waveform analysis. The measurement complex provides synchronous recording of the pulse wave parameters in different sites and other physiological signals required for the investigations. The adaptive comb filter was developed and tested for the motion caused noise suppression to increase the SNR of the PPG signal.

The main results of the current study are as follows:

- The adaptive comb filter attenuated the white noise in the PPG signal by 24 dB, 32 dB, and 39 dB in the case of the filter used for output calculation 3, 4, and 5 recurrences, respectively. In addition, it was possible to increase the PPG signal SNR for the PTT calculation in case the signal was recorded from the forehead and affected by motion caused noise. However, the filter has an averaging effect on the output signal waveform and the PTT calculation. This effect must be considered in the applications of the filter.
- Compared to the former algorithm, the standard deviation of the *AGI* was twice lower using the new SDPPG algorithm for the finger PPG waveform analysis. This gives more effective differentiation between the levels of arterial ageing. Furthermore, the diabetes patients had elevated AGI values, which can be explained through increased arterial ageing. A significant difference was found between the groups of healthy subjects and diabetes patients.
- Changes caused by the arterial ageing in the forehead PPG signal can be characterized using the developed SDPPG signal analysis algorithm. Furthermore, the subjects with increased arterial stiffness had noticeable increase in the SDPPG signal amplitude ratio of *b*/*a* and a decrease in the amplitude ratio of *d*/*a*, which indicated the premature arterial ageing. In addition, it was found that the changes caused by the arterial ageing in the forehead waveform are of the same direction as the finger waveform.
- Strong linear relationship was found between the aortic AIx@75 and the PPGAI. The AIx@75 and PPGAI values were elevated in the diabetes patient group. The PPGAI enables better discrimination between healthy subjects and patients with higher arterial stiffness.

References

Allen J 2007 Photoplethysmography and its applications in clinical physiological measurement *Physiol Meas* **28** R1-R39

Allen J and Murray A 2002 Age-related changes in peripheral pulse timing characteristics at the ears, fingers and toes *J Hum Hypertens* **16** 711–7

Allen J and Murray A 2003 Age-related changes in peripheral pulse shape characteristics at various body sites *Physiol Meas* **24** 297–307

Alwan A et al 2011 Global status report on noncommunicable disaeses 2010. Geneva, World Health Organization

Asmar R, Benetos A, Topouchian J, Laurent P, Pannier B, Brisac A M, Target R and Levy B 1995 Assessment of arterial distensibility by automatic pulse wave velocity measurement. Validation and clinical application studies *Hypertension* **26** 485–90

Atlas G M 2008 Development and application of a logistic-based systolic model for hemodynamic measurements using the esophageal Doppler monitor *Cardiovasc Eng* **8** 159-73

Avolio A P 1980 Multi-branched model of the human arterial system *Med Biol Eng Comput* **18** 709-18

Avolio A P, Butlin M and Walsh A 2010 Arterial blood pressure measurement and pulse wave analysis - their role in enhancing cardiovascular assessment *Physiol Meas* **31** R1-47

Bank A J, Wang H, Holte J E, Mullen K, Shammas R and Kubo S H 1996 Contribution of collagen, elastin, and smooth muscle to in vivo human brachial artery wall stress and elastic modulus *Circulation* **94** 3263–70

Baulmann J, Schillings U, Rickert S, Uen S, Düsing R, Illyes M, Cziraki A, Nickering G and Mengden T 2008 A new oscillometric method for assessment of arterial stiffness: comparison with tonometric and piezo-electronic methods *J Hypertens* **26** 523-8

Bergel D H 1961 The dynamic elastic properties of the arterial wall *J Physiol* **156** 458–69

Blacher J, Safar M E, Guerin A P, Pannier B, Marchais S J and London G M 2003 Aortic pulse wave velocity index and mortality in end-stage renal disease *Kidney Int* **63** 1852-60

Boehmer R D 1987 Continuous, real-time, noninvasive monitor of blood pressure: Penaz methodology applied to the finger *J Clin Monit* **3** 282-7

Bortolotto L A, Blacher J, Kondo T, Takazawa K and Safar M E 2000 Assessment of vascular aging and atherosclerosis in hypertensive subjects: second derivative of photoplethysmogram versus pulse wave velocity *Am J Hypertens* **13** 165-71

Boutouyrie P, Laurent S, Benetos A, Girerd X J, Hoeks A P and Safar M E 1992 Opposing effects of ageing on distal and proximal large arteries in hypertensives *Journal of Hypertension Supplement* **10** S87-91

Boutouyrie P, Bussy C, Hayoz D, Hengstler J, Dartois N, Laloux B, Brunner H and Laurent S 2000 Local pulse pressure and regression of arterial wall hypertrophy during long term antihypertensive treatment *Circulation* **101** 2601–6

Boutouyrie P, Briet M, Collin C, Vermeersch S and Pannier B 2009a Assessment of pulse wave velocity *Artery Research* **3** 3-8

Boutouyrie P, Revera M and Parati G 2009b Obtaining arterial stiffness indices from simple arm cuff measurements: the holy grail? *J Hypertens* **27** 2159-61

Boutouyrie P et al 2010 Determinants of pulse wave velocity in healthy people and in the presence of cardiovascular risk factors: 'establishing normal and reference values' *Eur Heart J* **31** 2338-50

Bramwell J and Hill A 1922 The velocity of the pulse wave in man *Proc R Soc Lond* **93** 298-306

Brooks B A, Molyneaux L M and Yue D K 2001 Augmentation of central arterial pressure in Type 2 diabetes *Diabet Med* 2001 **18** 374-80

Bussy C, Boutouyrie P, Lacolley P, Challande P and Laurent S 2000 Intrinsic stiffness of the carotid artery wall material in essential hypertensives *Hypertension* **35** 1049–54

Callaghan F J, Babbs C F, Bourland J D and Geddes L A 1984 The relationship between arterial pulse-wave velocity and pulse frequency at different pressures *J Med Eng Technol* **8** 15-8

Cavalcante J L, Lima J A, Redheuil A and Al-Mallah M H 2011 Aortic stiffness: current understanding and future directions *Journal of the American College of Cardiology* **57** 1511-22

Chan G S H, Middleton P M, Branko G C, Wang L and Lovell N H 2007 Automatic detection of left ventricular ejection time from a finger photoplethysmographic pulse oximetry waveform: comparison with Doppler aortic measurement *Physiol Meas* **28** 439–52

Cheng K S, Baker C R, Hamilton G, Hoeks A P and Seifalian A M 2002 Arterial elastic properties and cardiovascular risk/event *European Journal of Vascular and Endovascular Surgery* **24** 383-97

Chirinos J A 2012 Arterial stiffness: basic concepts and measurement techniques *J Cardiovasc Transl Res* **5** 243-55

Chirinos J A and Segers P 2010 Noninvasive evaluation of left ventricular afterload: Part 1: Pressure and flow measurements and basic principles of wave conduction and reflection *Hypertension* **56** 555–62

Ciftçi O, Günday M, Calişkan M, Güllü H, Güven A and Müderrisoğlu H 2013 Light cigarette smoking and vascular function *Acta Cardiol* **68** 255-61

Chiu Y C, Arand P W, Schroff S G, Feldman T and Carroll J D 1991 Determination of pulse wave velocities with computerised algorithms *American Heart Journal* **121** 1460-9

Clowes A W and Berceli S A 2000 Mechanisms of vascular atrophy and fibrous cap disruption *Annals of the New York Academy of Sciences* **902** 153-61

Cockcroft J R and Wilkinson I B 2002 Arterial stiffness and pulse contour analysis: an age old concept revisited *Clin Sci (Lond)* **103** 379-80

Cohen D L and Townsend R R 2011 Update on pathophysiology and treatment of hypertension in the elderly *Current Hypertension Reports* **13** 330–7

Cohn J N 2006 Arterial stiffness, vascular disease, and risk of cardiovascular events *Circulation* **113** 601–3

Comtois G, Mendelson Y and Ramuka P A 2007 Comparative evaluation of adaptive noise cancellation algorithms for minimizing motion artifacts in a forehead mounted wearable pulse oximeter *In Conf Proc IEEE Eng Med Biol Soc* **2007** 1528-31

Couceiro R, Carvalho P, Paiva R P, Henriques J and Muehlsteff J 2012 Detection of motion artifacts in photoplethysmographic signals based on time and period domain analysis *In Conf Proc IEEE Eng Med Biol Soc* **2012** 2603-6

Creager M A, Lüscher T F, Cosentino F and Beckman J A 2003 Diabetes and vascular disease: pathophysiology, clinical consequences, and medical therapy: Part I *Circulation* **108** 1527-32

Crowther M A 2005 Pathogenesis of atherosclerosis *Hematology Am Soc Hematol Educ Program.* **2005** 436-41

Cruickshank K, Riste L, Anderson S G, Wright J S, Dunn G and Gosling R G 2002 Aortic pulse-wave velocity and its relationship to mortality in diabetes and glucose intolerance: an integrated index of vascular function? *Circulation* **106** 2085-90

Currie K D, Proudfoot N A, Timmons B W and MacDonald M J 2010 Noninvasive measures of vascular health are reliable in preschool-aged children *Appl Physiol Nutr Metab* **35** 512-7

Dahlöf B, Devereux R B, Kjeldsen S E et al 2002 Cardiovascular morbidity and mortality in the Losartan Intervention For Endpoint reduction in hypertension study (LIFE): a randomised trial against atenolol *Lancet* **359** 995-1003

DeLoach S S and Townsend R R 2008 Vascular stiffness: its measurement and significance for epidemiologic and outcome studies *Clin J Am Soc Nephrol* **3** 184-92

Dillon J B and Hertzman A B 1941 The form of the volume pulse in the finger pad in health, arteriosclerosis, and hypertension *Am Heart J* **21** 172–90

Dobrin P B 1999 Distribution of lamellar deformations: implications for properties of the arterial media *Hypertension* **33** 806-10

Dolan E, Stanton A, Thijs L, Hinedi K, Atkins N, McClory S, Den Hond E, McCormack P, Staessen J A and O'Brien E 2005 Superiority of ambulatory over clinic blood pressure measurement in predicting mortality: the Dublin outcome study *Hypertension* **46** 156-61

Fagard R H, Celis H, Thijs L, Staessen J A, Clement D L, De Buyzere M L and De Bacquer D A 2008 Daytime and nighttime blood pressure as predictors of death and cause-specific cardiovascular events in hypertension *Hypertension* **51** 55-61

Feng J and Khir A W 2010 Determination of wave speed and wave separation in the arteries using diameter and velocity *Journal of Biomechanics* **43** 455-62

Foo J Y A 2006 Comparison of wavelet transformation and adaptive filtering in restoring artifact-induced time-related measurement *Biomedical signal processing and control* **1** 93-8

Foo J and Wilson S 2006 A computational system to optimise noise rejection in photoplethysmography signals during motion or poor perfusion states *Medical and Biological Engineering and Computing* **44** 140-5

Franklin S S 2008 Beyond blood pressure: Arterial stiffness as a new biomarker of cardiovascular disease *Journal of the American Society of Hypertension: JASH*, **2** 140–51

Franquet A, Avril S, Le Riche R, Badel P, Schneider F C, Boissier C and Favre J P 2013 Identification of the in vivo elastic properties of common carotid arteries from MRI: a study on subjects with and without atherosclerosis *J Mech Behav Biomed Mater* **27** 184-203

Grabovskis A, Marcinkevics Z, Lukstina Z et al 2011 Usability of photoplethysmography method in estimation of conduit artery stiffness *In Proc of SPIE-OSA Biomedical Optics* **8090** 80900X1-7

Gallagher D, Adji A and O'Rourke M F 2004 Validation of the transfer function technique for generating central from peripheral upper limb pressure waveform *Am J Hypertens* **17** 1059–67

Gaszner B, Lenkey Z, Illyés M, Sárszegi Z, Horváth I G, Magyari B, Molnár F, Kónyi A and Cziráki A 2012 Comparison of aortic and carotid arterial stiffness parameters in patients with verified coronary artery disease *Clin Cardiol* **35** 26-31

Glagov S, Weisenberg E, Zarins C K, Stankunavicius R and Kolettis G J 1987 Compensatory enlargement of human atherosclerotic coronary arteries *N Engl J Med* **316** 1371-5

Guyton A C and Hall J E 2006 Textbook of Medical Physiology, 11th edition. Elsevier Saunders

Hamilton P K, Lockhart C J, Quinn C E and McVeigh G E 2007 Arterial stiffness: clinical relevance, measurement and treatment *Clin Sci (Lond)* **113** 157-70

Hashimoto J, Watabe D, Kimura A, Takahashi H, Ohkubo T, Totsune K and Imai Y 2005 Determinants of the second derivative of the finger photoplethysmogram and brachial-ankle pulse-wave velocity: the Ohasama study *Am J Hypertens* **184** 477–85

Hennerici M G 2004 The unstable plaque *Cerebrovasc Dis* **17** (Suppl 3) 17-22

Herrington D M, Brown W V, Mosca L et al 2004 Relationship between arterial stiffness and subclinical aortic atherosclerosis *Circulation* **110** 432–7

Hirai T, Sasayama S, Kawasaki T and Yagi S 1989 Stiffness of systemic arteries in patients with myocardial infarction. A noninvasive method to predict severity of coronary atherosclerosis *Circulation* **80** 78-86

Hlimonenko I, Meigas K and Vahisalu R 2003 Waveform analysis of peripheral pulse wave detected in the fingertip with photoplethysmograph *Measure Sci Rev* **3** 49–52

Hlimonenko I, Meigas K, Viigimaa M and Temitski K 2008 Aortic and arterial pulse wave velocity in patients with coronary heart disease of different severity *Estonian J Eng* **14** 167-76

Hope S A, Tay D B, Meredith I T and Cameron J D 2004 Use of arterial transfer functions for the derivation of central aortic waveform characteristics in subjects with type 2 diabetes and cardiovascular disease *Diabetes Care* **27** 746-51

Horváth I G, Németh A, Lenkey Z, Alessandri N, Tufano F, Kis P, Gaszner B and Cziráki 2010 A Invasive validation of a new oscillometric device (Arteriograph) for measuring augmentation index, central blood pressure and aortic pulse wave velocity *J Hypertens* **28** 2068-75

Hudson B I, Wendt T, Bucciarelli L G, Rong L L, Naka Y, Yan S F and Schmidt A M 2005 Diabetic vascular disease: it's all the RAGE *Antioxid Redox Signal* **7** 1588–600

Hughes D J, Babbs C F, Geddes L A and Bourland J D 1979 Measurements of Young's modulus of elasticity of the canine aorta with ultrasound *Ultrason Imaging* **1** 356-67

Hurst R T and Lee R W 2003 Increased incidence of coronary atherosclerosis in type 2 diabetes mellitus: mechanisms and management *Ann Intern Med* **139** 824-34

Huo Y and Ley K 2001 Adhesion molecules and atherogenesis *Acta Physiologica Scandinavica* **173** 35-43

Huotari M, Yliaska N, Lantto V, Määttä K and Kostamovaara J 2009 Aortic and arterial stiffness determination by photoplethysmographic technique *Procedia Chemistry* **1** 1243-6

Iketani Y, Iketani T, Takazawa K and Murata M 2000 Second derivative of photoplethysmogram in children and young people *Jpn Circ J* **64** 110-6

Ikonomidis I, Ntai K, Kadoglou N P et al 2013 The evaluation of pulse wave velocity using Arteriograph and Complior apparatus across multiple cohorts of cardiovascular-related diseases *Int J Cardiol* **168** 4890-2

Johansson A and Öberg P Å 1999 Estimation of respiratory volumes from the photoplethysmographic signal. Part I: experimental results *Med Biol Eng Comput* **37** 42–7

Kamal A A R, Harness J B, Irving G and Mearns A J 1989 Skin photoplethysmography – a review *Comput Methods Programs Biomed* **28** 257-69

Karamanoglu M 2003 Errors in estimating propagation distances in pulse wave velocity *Hypertension* **41** E8

Kazanavicius E, Gircys R and Vrubliauskas A 2005 Mathematical methods for determining the foot point of the arterial pulse wave and evaluation of proposed methods *Information Technology and Control* **34** 29-36

Kelly R, Hayward C, Avolio A and O'Rourke M 1989 Noninvasive determination of age-related changes in the human arterial pulse *Circulation* **80** 1652–9

Khir A W, O'Brien A, Gibbs J S R and Parker K H 2001 Determination of wave speed and wave separation in the arteries *Journal of Biomechanics* **34** 1145-55

Kim B S and Yoo S K 2006 Motion artifact reduction in photoplethysmography using independent component analysis *IEEE Trans Biomed Eng* **53** 566-8

Kingwell B A and Gatzka C D 2002 Arterial stiffness and prediction of cardiovascular risk *J Hypertens* **20** 2337-40

Korpas D, Hálek J and Dolezal L 2009 Parameters describing the pulse wave *Physiol Res* **58** 473-9

Korteweg D J 1878 Ueber die Fortpflanzungsgeschwindigkeit des Schalles in elastischen Röhren *Annalen der Physik* **241** 525-42

Lass J, Meigas K, Kattai R, Karai D, Kaik J and Rosmann M 2004 Optical and electrical methods for pulse wave transit time measurement and its correlation with arterial blood pressure *Proc Estonian Acad Sci Eng* **10** 123-36

Laurent S, Cockcroft J, Van Bortel L et al 2006 Expert consensus document on arterial stiffness: methodological issues and clinical applications *Eur Heart J* **27** 2588-605

Lee C M and Zhang Y T 2003 Reduction of motion artifacts from photoplethysmographic recordings using a wavelet denoising approach *In Proc IEEE EMBS Asian-Pacific Conf on Biomed Eng* **2003** 194-5

Lehmann E D, Hopkins K D, Rawesh A, Joseph R C, Kongola K, Coppack S W, Gosling R G 1998 Relation between number of cardiovascular risk factors/events and noninvasive Doppler ultrasound assessments of aortic compliance Hypertension 32 565-9

Li H, Cybulsky M I, Gimbrone M A Jr and Libby P 1993 An atherogenic diet rapidly induces VCAM-1, a cytokine-regulatable mononuclear leukocyte adhesion molecule, in rabbit aortic endothelium *Arterioscler Thromb* **13** 197-204

Li J K-J, Melbin J, Riffle R A and Noordergraaf A 1981 Pulse wave propagation *Circ Res* **49** 442-52

Li J K-J 2004 Dynamics of the Vascular System (Series on Bioengineering & Biomedical Engineering - Vol. 1). World Scientific Pub Co Inc

Libby P 2002a Inflammation in atherosclerosis *Nature* **420** 868-74

Libby P 2002b Atherosclerosis: a new view *Scientific American* **286** 46-55

Libby P, Ridker P M and Maseri A 2002 Inflammation and Atherosclerosis *Circulation* **105** 1135-43

Lindberg L-G and Öberg P Å 1993 Optical properties of blood in motion *Opt Eng* **32** 253-7

Llauradó G, Ceperuelo-Mallafré V, Vilardell C, Simó R, Freixenet N, Vendrell J and González-Clemente J M 2012 Arterial stiffness is increased in patients with type 1 diabetes without cardiovascular disease: a potential role of low-grade inflammation *Diabetes Care* **35** 1083-9

Mancia G, De Backer G, Dominiczak A et al. 2007 ESH-ESC practice guidelines for the management of arterial hypertension: ESH-ESC Task Force on the management of arterial hypertension *J. Hypertens* **25** 1751–62

Marcinkevics Z, Greve M, Aivars J I, Erts R and Zehtabi A H 2009 Relationship between arterial pressure and pulse wave velocity using photoplethysmography during the post-exercise recovery period *Biology* **753** 59–68

Meinders J M and Hoeks A P 2004 Simultaneous assessment of diameter and pressure waveforms in the carotid artery *Ultrasound Med Biol* **30** 147-54

Miyaki A, Maeda S, Yoshizawa M, Misono M, Sasai H, Shimojo N, Tanaka K and Ajisaka R 2010 Is pentraxin 3 involved in obesity-induced decrease in arterial distensibility? *Journal of Atherosclerosis and Thrombosis* **17** 278-84

Millasseau S C, Guigui F G, Kelly R P, Prasad K, Cockcroft J R, Ritter J M and Chowienczyk P J 2000 Noninvasive assessment of the digital volume pulse. Comparison with the peripheral pressure pulse *Hypertension* **36** 952-6

Millasseau S C, Kelly R P, Ritter J M and Chowienczyk P J 2002 Determination of age-related increases in large artery stiffness by digital pulse contour analysis *Clin Sci (Lond)* **103** 371-7

Millasseau S C, Patel S J, Redwood S R, Ritter J M and Chowienczyk P J 2003 Pressure wave reflection assessed from the peripheral pulse. Is a transfer function necessary? *Hypertension* **41** 1016–20

Millasseau S C, Stewart A D, Patel S J, Redwood S R and Chowienczyk P J 2005 Evaluation of carotid-femoral pulse wave velocity: influence of timing algorithm and heart rate *Hypertension* **45** 222-6

Millasseau S C, Ritter J M, Takazawa K and Chowienczyk P J 2006 Contour analysis of the photoplethysmographic pulse measured at the finger *J Hypertens* **24** 1449-56

Moens A I 1878 Die Pulskurve. Leiden

Molinari F, Zeng G and Suri J S 2010 A state of the art review on intima-media thickness (IMT) measurement and wall segmentation techniques for carotid ultrasound *Computer Methods and Programs in Biomedicine* **100** 201-21

Mulders T A, van den Bogaard B, Bakker A, Trip M D, Stroes E S, van den Born B J and Pinto-Sietsma S J 2012 Arterial stiffness is increased in families with premature coronary artery disease *Heart* **98** 490-4

Murgo J P, Westerhof N, Giolma J P and Altobelli S A 1980 Aortic input impedance in normal man: relationship to pressure wave forms *Circulation* **62** 105-16

Naghavi M, Libby P, Falk E, et al 2003 From vulnerable plaque to vulnerable patient: a call for new definitions and risk assessment strategies: Part I *Circulation* **108** 1664-78

Naidu M U R, Reddy B M, Yashmaina S, Patnaik A N and Rani P U 2005 Validity and reproducibility of arterial pulse wave velocity measurement using new device with oscillometric technique: A pilot study *Biomed Eng Online* **4** 49

Nam D-H, Lee W-B, Hong Y-S and Lee S-S 2013 Measurement of spatial pulse wave velocity by using a clip-type pulsimeter equipped with a hall sensor and photoplethysmography *Sensors* **13** 4714-23

Naschitz J E, Bezobchuk S, Mussafia-Priselac R et al 2004 Pulse transit time by R-wave-gated infrared photoplethysmography: review of the literature and personal experience *J Clin Monit Comput* **18** 333-42

Nichols W W and O'Rourke M F 2005 Mcdonald's blood flow in arteries. Theoretical, experimental and clinical principles. Oxford University Press

Nitzan M, Babchenko A, Khanokh B and Landau D 1998 The variability of the photoplethysmographic signal – a potential method for the evaluation of the autonomic nervous system *Physiol Meas* **19** 93-102

Nitzan M, Khanokh B and Slovik Y 2002 The difference in pulse transit time to the toe and finger measured by photoplethysmography *Physiol Meas* **23** 85-93

Nualnim N, Barnes J N, Tarumi T, Renzi C P and Tanaka H 2011 Comparison of central artery elasticity in swimmers, runners, and the sedentary *Am J Cardiol* **107** 783-7

Oguri M, Nakamura T, Tamanuki K, Akita C, Kitaoka C, Saikawa Y and Takahashi M 2013 Subclinical arterial stiffness in young children after Kawasaki disease *Cardiol Young* **6** 1-8

Ohmori K, Emura S and Takashima T 2000 Risk factors of atherosclerosis and aortic pulse wave velocity *Angiology* **51** 53-60

O'Rourke M F, Staessen J A, Vlachopoulos C, Duprez D and Plante G E 2002 Clinical applications of arterial stiffness; definitions and reference values *Am J Hypertens* **15** 426-44

O'Rourke M F and Safar M E 2005 Relationship between aortic stiffening and microvascular disease in brain and kidney: Cause and logic of therapy *Hypertension* **46** 200–4

Otsuka T, Kawada T, Katsumata M, Ibuki C and Kusama Y 2007 Independent determinants of second derivative of the finger photoplethysmogram among various cardiovascular risk factors in middle-aged men *Hypertens Res* **30** 1211-18

Pahkala K, Laitinen TT, Heinonen OJ et al 2013 Association of fitness with vascular intima-media thickness and elasticity in adolescence *Pediatrics* **132** e77-84

Pannier B, Avolio A P, Hoeks A, Mancia G and Takazawa K 2002 Methods and devices for measuring arterial compliance in humans *Am J Hypertens* **15** 743–53

Parati G and De Buyzere M 2010 Evaluating aortic stiffness through an arm cuff oscillometric device: is validation against invasive measurements enough? *J Hypertens* **28** 2003-6

Pauca A L, Wallenhaupt S L, Kon N D and Tucker W Y 1992 Does radial artery pressure accurately reflect aortic pressure? *Chest* **102** 1193–8

Pauca A L, O'Rourke M F and Kon N D 2001 Prospective evaluation of a method for estimating ascending aortic pressure from the radial artery pressure waveform *Hypertension* **38** 932–7

Payne R A, Wilkinson I B, and Webb D J 2010 Arterial stiffness and hypertension: Emerging concepts *Hypertension* **55** 9–14

Perk J et al 2012 European Guidelines on cardiovascular disease prevention in clinical practice *European Heart Journal* **33** 1635–701

Pilt K, Meigas K, Viigimaa M, Kaik J, Kattai R and Karai D 2010a Arterial pulse transit time dependence on applied pressure *In: IFMBE Proceedings of the 12th Mediterranean Conference on Medical and Biological Engineering and Computing, Thessaloniki, Greece, May 27-30*, 406-9

Pilt K, Meigas K, Viigimaa M, Kaik J, Kattai R and Karai D 2010b Arterial pulse waveform dependence on applied pressure *In: Proceedings of 2010*

International Biennial Baltic Electronics Conference, Tallinn, Estonia, October 4-6, 277-80

Poon C C and Zhang Y T 2005 Cuff-less and noninvasive measurements of arterial blood pressure by pulse transit time *In Conf Proc IEEE Eng Med Biol Soc* **6** 5877-80

Proakis J G and Manolakis D K 2006 Digital signal processing 4th edn. Pearson Prentice Hall

Qasem A and Avolio A 2008 Determination of aortic pulse wave velocity from waveform decomposition of the central aortic pressure pulse *Hypertension* **51** 188-95

Rajzer M W, Wojciechowska W, Klocek M, Palka I, Brzozowska-Kiszka M and Kawecka-Jaszcz K 2008 Comparison of aortic pulse wave velocity measured by three techniques: Complior, SphygmoCor and Arteriograph *J Hypertens* **26** 2001-7

Rask-Madsen C and King G L 2007 Mechanisms of Disease: endothelial dysfunction in insulin resistance and diabetes *Nat Clin Pract Endocrinol Metab* **3** 46–56

Ravikumar R, Deepa R, Shanthirani C and Mohan V 2002 Comparison of carotid intima-media thickness, arterial stiffness, and brachial artery flow mediated dilatation in diabetic and nondiabetic subjects (The Chennai Urban Population Study [CUPS-9]) *Am J Cardiol* **90** 702-7

Reddy K A, George B and Jagadeesh Kumar V 2008 Motion Artifact Reduction and Data Compression of Photoplethysmo-graphic Signals utilizing Cycle by Cycle Fourier Series Analysis *In Conf Proc of Instrumentation and Measurement Technology IEEE* **2008** 176-9

Reneman R S, Meinders J M and Hoeks A P 2005 Non-invasive ultrasound in arterial wall dynamics in humans: what have we learned and what remains to be solved *Eur Heart J* **26** 960-6

Rhee M-Y, Lee H-Y and Park J B 2008 Measurements of Arterial Stiffness: Methodological Aspects *Korean Circ J* **38** 343-50

Rubins U 2008 Finger and ear photoplethysmogram waveform analysis by fitting with Gaussians *Med Biol Eng Comput* **46** 1271-6

Rydén L, Grant P J et al 2013 ESC Guidelines on diabetes, pre-diabetes, and cardiovascular diseases developed in collaboration with the EASD: The Task Force on diabetes, pre-diabetes, and cardiovascular diseases of the European Society of Cardiology (ESC) and developed in collaboration with the European Association for the Study of Diabetes (EASD) *Eur Heart J* **34** 3035-87

Safar M E, London G M and Plante G E 2004 Arterial stiffness and kidney function *Hypertension* **43** 163-8

Salvi P, Magnani E, Valbusa F, Agnoletti D, Alecu C, Joly L and Benetos A 2008 Comparative study of methodologies for pulse wave velocity estimation *J Hum Hypertens* **22** 669-77

Sherebrin M H and Sherebrin R Z 1990 Frequency Analysis of the Peripheral Pulse Wave Detected in the Finger with a Photoplethysmograph *IEEE Trans Biomed Eng* **37** 313-7

Smith S C Jr, Benjamin E J, Bonow R O, Braun L T, Creager M A et al 2011 AHA/ACCF Secondary Prevention and Risk Reduction Therapy for Patients with Coronary and other Atherosclerotic Vascular Disease: 2011 update: a guideline from the American Heart Association and American College of Cardiology Foundation *Circulation* **124** 2458-73

Solà J, Chételat O, Sartori C, Allemann Y and Rimoldi S F 2011 Chest pulse-wave velocity: a novel approach to assess arterial stiffness *IEEE Trans Biomed Eng* **58** 215-23

Solomon C G 2003 Reducing cardiovascular risk in type 2 diabetes *N Engl J Med* **348** 457-9

Sowers J R, Epstein M and Frohlich E D 2001 Diabetes, hypertension, and cardiovascular disease: an update *Hypertension* **37** 1053-9

Stetson P F 2004 Independent component analysis of pulse oximetry signals *Conf Proc IEEE Eng Med Biol Soc* **1** 231-4

Strong J P, Malcom G T, Newman W P 3rd and Oalmann M C 1992 Early lesions of atherosclerosis in childhood and youth: natural history and risk factors *J Am Coll Nutr* **11** 51S-54S

Stary H C, Blankenhorn D H, Chandler A B et al 1992 A definition of the intima of human arteries and of its atherosclerosis-prone regions. A report from the Committee on Vascular Lesions of the Council on Arteriosclerosis, American Heart Association *Circulation* **85** 391-405

Stary H C 2003 Atlas of atherosclerosis: progression and regression, 2nd edition. Parthenon Publishing

Sukor J A, Redmond S J and Lovell N H 2011 Signal quality measures for pulse oximetry through waveform morphology analysis *Physiol Meas* **32** 369-84

Takazawa K, Tanaka N, Fujita M, Matsuoka O, Saiki T, Aikawa M, Tamura S and Ibukiyama C 1998 Assessment of vasoactive agents and vascular aging by the second derivative of photoplethysmogram waveform *Hypertension* **32** 365-70

Takazawa K, Kobayashi H, Shindo N, Tanaka N and Yamashina A 2007 Relationship between radial and central arterial pulse wave and evaluation of central aortic pressure using the radial arterial pulse wave *Hypertens Res* **30** 219–28

Temitski K, Lauri J, Pilt K and Meigas K 2012 Assessment of algorithms for detecting an arterial pulse pressure wave equiphase point *In: Proceedings of 2012 International Biennial Baltic Electronics Conference, Tallinn, Estonia, October 3-5*, 191-4

Tortora G J and Derrickson B 2011 Principles of anatomy and Physiology, 13th edition. John Wiley & Sons

Tuzcu E M, Kapadia S R and Tutar E 2001 High prevalence of coronary atherosclerosis in asymptomatic teenagers and young adults: evidence from intravascular ultrasound *Circulation* **103** 2705-10

Urbina E M, Kimball T R, Khoury P R, Daniels S R and Dolan L M 2010 Increased arterial stiffness is found in adolescents with obesity or obesity-related type 2 diabetes mellitus *J Hypertens* **28** 1692-8

van Bortel L M, Balkestein E J, van der Heijden-Spek J J et al 2001 Non-invasive assessment of local arterial pulse pressure: comparison of applanation tonometry and echo-tracking *J Hypertens* **19** 1037-44

van der Heijden-Spek J J, Staessen J A, Fagard R H, Hoeks A P, Boudier H A and van Bortel L M 2000 Effect of age on brachial artery wall properties differs from the aorta and is gender dependent: a population study *Hypertension* **35** 637–42

van Popele N M, Grobbee D E, Bots M L, Asmar R, Topouchian J, Reneman R S, Hoeks A P, van der Kuip D A, Hofman A and Witteman J C 2001 Association between arterial stiffness and atherosclerosis: the Rotterdam Study *Stroke* **32** 454-60

Verbeke F, Segers P, Heireman S, Vanholder R, Verdonck and Van Bortel L 2005 Noninvasive assessment of local pulse pressure. Importance of brachial-to-radial pressure amplification *Hypertension* **46** 244–8

Waxman S, Ishibashi F and Muller J E 2006 Detection and treatment of vulnerable plaques and vulnerable patients: novel approaches to prevention of coronary events. *Circulation* **114** 2390-411

Westerhof N, Bosman F, De Vries C J and Noordergraaf A 1969 Analog studies of the human systemic arterial tree *J Biomech* **2** 121-43

Westerhof B E, Guelen I, Westerhof N, Karemaker J M and Avolio A 2006 Quantification of wave reflection in the human aorta from pressure alone: a proof of principle *Hypertension* **48** 595-601

Westerhof B E, van den Wijngaard J P, Murgo J P and Westerhof N 2008 Location of a reflection site is elusive: consequences for the calculation of aortic pulse wave velocity *Hypertension* **52** 478-83

Wilkinson I B, Fuchs S A, Jansen I M, Spratt J C, Murray G D, Cockcroft J R and Webb D J 1998 Reproducibility of pulse wave velocity and augmentation index measured by pulse wave analysis *J Hypertens* **16** 2079-84

Wilkinson I B, MacCallum H, Rooijmans D F, Murray G D, Cockcroft J R, McKnight J A and Webb D J 2000a Increased augmentation index and systolic stress in type 1 diabetes mellitus *QJM* **93** 441-8

Wilkinson I B, MacCallum H, Flint L, Cockcroft J R, Newby D E and Webb D J 2000b The influence of heart rate on augmentation index and central arterial pressure in humans *J Physiol* **525** 263–70

Wilkinson I B, Prasad K, Hall I R, Thomas A, MacCallum H, Webb D J, Frenneaux M P and Cockcroft J R 2002 Increased central pulse pressure and augmentation index in subjects with hypercholesterolemia *J Am Coll Cardiol* **39** 1005-11

Williams B 1999 The unique vulnerability of diabetic subjects to hypertensive injury *J Hum Hypertens* **13** S3-8

Woo C H, Shishido T, McClain C, Lim J H, Li J D, Yang J, Yan C and Abe J 2008 Extracellular signal-regulated kinase 5 SUMOylation antagonizes shear stress-induced antiinflammatory response and endothelial nitric oxide synthase expression in endothelial cells *Circulation research* **102** 538-45

Wood L B and Asada H 2007 Low Variance Adaptive Filter for Cancelling Motion Artifact in Wearable Photoplethysmogram Sensor Signals *In Conf Proc IEEE Eng Med Biol Soc* **2007** 652-5

Woodman R J, Kingwell B A, Beilin L J, Hamilton S E, Dart A M and Watts G F 2005 Assessment of central and peripheral arterial stiffness: studies indicating the need to use a combination of techniques *Am J Hypertens* **18** 249–60

Xu J 2003 Do we need a better approach for measuring pulse-wave velocity? *Ultrasound Med Biol* **29** 1373–4

Yao J and Warren S 2005 A short study to assess the potential of independent component analysis for motion artifact separation in wearable pulse oximeter signals *In Conf Proc IEEE Eng Med Biol Soc* **4** 3585-8

Yusuf S, Sleight P, Pogue J et al 2000 Effects of an Angiotensin-Converting–Enzyme Inhibitor, Ramipril, on Cardiovascular Events in High-Risk Patients *N Engl J Med* **342** 145-53

Zhang X, Kinnick RR, Fatemi M and Greenleaf J F 2005 Noninvasive method for estimation of complex elastic modulus of arterial vessels *IEEE Trans Ultrason Ferroelectr Freq Control* **52** 642-52

Zheng Y, Yan B P, Zhang Y, Yu C M and Poon C C 2013 Wearable cuff-less PTT-based system for overnight blood pressure monitoring *In Conf Proc IEEE Eng Med Biol Soc* **2013** 6103-6

Zieman S J, Melenovsky V and Kass D A 2005 Mechanisms, pathophysiology, and therapy of arterial stiffness *Arteriosclerosis, Thrombosis, and Vascular Biology* **25** 932-43

Zulliger M A, Rachev A, and Stergiopulos N 2004 A constitutive formulation of arterial mechanics including vascular smooth muscle tone *American Journal of Physiology - Heart and Circulatory Physiology* **287** H1335–43

Author's publications

Pilt K, Meigas K, Lass J, Rosmann M (2007) "Signal Processing methods for PPG Module to Increase Signal Quality", *In: IFMBE proceedings of 11th Mediterranean Conference on Medical and Biomedical Engineering and Computing, Ljubljana, Slovenia, June 26-30*, vol. 16, 434-437 (DOI: 10.1007/978-3-540-73044-6_111).

Pilt K, Meigas K, Lass J, Rosmann M, Kaik J (2007) "Analogue step-by-step DC component eliminator for 24-hour PPG signal monitoring", *In: Proceedings of the 29th Annual International Conference of the IEEE EMBS, Lyon, France, August 23-26*, 1006-1009 (DOI: 10.1109/IEMBS.2007.4352464).

Pilt K, Meigas K, Rosmann M, Lass J, Kaik J (2008) "An Experimental Study of PPG Probe Efficiency Coefficient Determination on Human Body", *In: IFMBE Proceedings of 14th Nordic-Baltic Conference on Biomedical Engineering and Medical Physics, Latvia, Riga, June 16–20*, vol. 20, 311-314 (DOI: 10.1007/978-3-540-69367-3_83).

Pilt K, Meigas K, Lass J, Rosmann M, Kaik J (2008) "Adaptive impulse correlated filter (AICF) improvement for photoplethysmographic signals", *In: Proceedings of the 30th Annual International Conference of the IEEE EMBS, Vancouver, Canada, August 20-25*, 273-276 (DOI: 10.1109/IEMBS.2008.4649143).

Pilt K, Meigas K, Lass J, Rosmann M, Kaik J (2008) "Adaptive sum comb filter for PPG signals by using ECG signal as reference", *In: Proceedings of 2008 International Biennial Baltic Electronics Conference, Tallinn, Estonia, October 6-8,* 317-320 (DOI: 10.1109/BEC.2008.4657544).

Pilt K, Meigas K, Ferenets R, Kaik J (2009) "Adjustment of adaptive sum comb filter for PPG signals", In: *Proceedings of the 31st Annual International Conference of the IEEE EMBS, Minneapolis, USA, September 2-26*, 5693-5696 (DOI: 10.1109/IEMBS.2009.5333539).

Pilt K, Meigas K, Karai D, Kaik J (2009) "PPG signal processing for pulse delay computing by using adaptive comb filter", *In: IFMBE Proceedings of the 11th International Congress of the Medical Physics and Biomedical Engineering, Munich, Germany, September 7-12,* 1653-1656 (DOI: 10.1007/978-3-642-03882-2_438).

(Publication II) Pilt K, Meigas K, Ferenets R, Kaik J (2010) "Photoplethysmographic signal processing using adaptive sum comb filter for pulse

delay measurement", *Estonian Journal of Engineering*, 16: 78-94 (DOI: 10.3176/eng.2010.1.08).

Pilt K, Meigas K, Viigimaa M, Kaik J, Kattai R, Karai D (2010) "Arterial pulse transit time dependence on applied pressure", *In: IFMBE Proceedings of the 12th Mediterranean Conference on Medical and Biological Engineering and Computing, Thessaloniki, Greece, May 27-30,* 406-409 (DOI: 10.1007/978-3-642-13039-7_102).

(Publication I) Pilt K, Meigas K, Viigimaa M, Temitski K, Kaik J (2010) "An experimental measurement complex for probable estimation of arterial stiffness", *In: Proceedings of the 30th Annual International Conference of the IEEE EMBS, Buenos Aires, Argentina, August 31 – September 4*, 194-197 (DOI: 10.1109/IEMBS.2010.5627925).

Pilt K, Meigas K, Viigimaa M, Kaik J, Kattai R, Karai D (2010) "Arterial pulse waveform dependence on applied pressure", *In: Proceedings of 2010 International Biennial Baltic Electronics Conference, Tallinn, Estonia, October 4-6,* 277-280 (DOI: 10.1109/BEC.2010.5630888).

Pilt K, Meigas K, M. Viigimaa, K. Temitski (2011) "Possibility to use finapres signal for augmentation index estimation", *In: IFMBE Proceedings of the 15th Nordic-Baltic Conference on Biomedical Engineering and Medical Physics, Aalborg, Denmark, June 14-17*, vol. 34, 25-28 (DOI: 10.1007/978-3-642-21683-1_6).

Pilt K, Meigas K, Viigimaa M, Temitski K (2011) "Possibility to Use Finapres Signal for the Estimation of Aortic Pulse Wave Velocity", *In: IFMBE Proceedings of 5th European Conference of the International Federation for Medical and Biological Engineering, Budapest, Hyngary, September 14-18*, vol. 37, 524-527 (DOI: 10.1007/978-3-642-23508-5_136).

(Publication IV) Pilt K, Meigas K, Temitski K, Viigimaa M (2012) "Second derivative analysis of forehead photoplethysmographic signal in healthy volunteers and diabetes patients", *In: IFMBE Proceedings of World Congress on Medical Physics and Biomedical Engineering, Beijing, China, May 26-31*, vol. 39, 410-413 (10.1007/978-3-642-29305-4_109).

Temitski K, Lauri J, **Pilt K**, Meigas K (2012) "Assessment of algorithms for detecting an arterial pulse pressure wave equiphase point", *In: Proceedings of 2012 International Biennial Baltic Electronics Conference, Tallinn, Estonia, October 3-5*, 191-194 (DOI: 10.1109/BEC.2012.6376849).

Pilt K, Meigas K, Temitski K, Viigimaa M (2013) "The analysis of finger photoplethysmographic waveform in healthy volunteers and diabetes patients" *In: IFMBE Proceedings of International Symposium on Biomedical Engineering and Medical Physics, Riga, Latvia, October 10-12, 2012*, vol. 38, 55-58 (DOI: 10.1007/978-3-642-34197-7_14).

(Publication III) Pilt K, Ferenets R, Meigas K, Lindberg L-G, Temitski K, Viigimaa M (2013) "New photoplethysmographic signal analysis algorithm for arterial stiffness estimation", *The Scientific World Journal*, vol. 2013, Article ID 169035, 9 pages (DOI: 10.1155/2013/169035).

Pilt K, Meigas K, Temitski K, Viigimaa M (2013) "The effect of local cold and warm exposure on index finger photoplethysmographic signal waveform", *In: Proceedings of the 35th Annual International Conference of the IEEE EMBS, Osaka, Japan, July 3–7*, 2300-2003 (DOI: 10.1109/EMBC.2013.6609997).

(Publication V) Pilt K, Meigas K, Ferenets R, Temitski K and Viigimaa M (2013) "Photoplethysmographic signal waveform index for detection of increased arterial stiffness", *Manuscript submitted*

Kokkuvõte

Optilise pulsilaine signaali analüüs arterite varase vananemise määramiseks diabeedihaigetel

Südame-veresoonkonna haigused on üheks peamiseks surmapõhjuseks maailmas. Vananedes arteri endoteel kulub ja kahjustub ning põhjustab ateroskleroosi ja naastude teket veresoone seinale. Erinevate haiguste korral, seal hulgas diabeedi puhul, on arterite vananemise protsess kiirenenud. Arterite lupjumise tulemusena suureneb nende jäikus, mis põhjustab südame koormuse tõusu, sest veresoonte poolt avaldatud suurema takistuse tõttu on verd raskem läbi soonte pumbata. See põhjustab omakorda erinevaid veresoonkonnaga seotud haiguseid nagu näiteks hüpertensiooni, südame isheemiatõve jne. Veresoonkonna seisundi muutuste varajase avastamise ning selle tulemusena rakendatud õige ravi korral on võimalik edasine haiguse süvenemine ära hoida.

Arterite jäikuse hindamiseks töötatakse välja ning võetakse kasutusele üha enam mitteinvasiivseid meetodeid. Enamus meetodeid on suhteliselt keerukad ja kallid ning protseduuride läbiviimiseks on vaja selleks spetsiaalse väljaõppe saanud operaatorit. Arterite seisundi hindamiseks oleks vaja meetodit, mis oleks mitteinvasiivne, odav ning lihtsalt teostatav. Uute ja mitteinvasiivsete meetodite esiletõusuga on hakatud aina tihedamini kasutama pulsilaine levikiirust ja pulsilaine kuju analüüsi.

Antud töö eesmärgiks oli uurida optilise meetodi abil salvestatud pulsilaine kuju ja leviaja analüüsi võimalusi varajase arterite jäikuse suurenemise ning sellest tuleneva veresoonkonna vanuse määramiseks. Selleks koostati uurimiskompleks pulsilainete ja teiste füsioloogiliste signaalide mitteinvasiivseks sünkroonseks salvestamiseks. Signaalide salvestused ning muud vajalikud protseduurid viidi läbi Põhja-Eesti Regionaalhaiglas tervetel ning diabeedihaigetel. Töö käigus uuriti ning koostati algoritm liikumisest tingitud mürade vähendamiseks salvestatud optilises pulsilaine signaalis. Arterite jäikuse erinevuste uurimiseks töötati välja optilise pulsilaine signaali kuju analüüsi algoritm, mis põhineb teise tuletise meetodil. Lisaks võrreldi väljatöötatud meetodi ning algoritmi efektiivsust kliinilises praktikas kasutatavate meetoditega, mis võimaldaks eristada normaalse ning suurenenud arterite jäikusega uuritavaid.

Töö tulemusena leiti järgmist:

- Koostatud uurimiskompleks võimaldab sünkroonselt salvestada pulsilaine ja teisi füsioloogilisi signaale.
- Koostatud algoritm eemaldab optilisest signaalist liikumisest tingitud müra, mille tulemusena on võimalik pulsilaine leviaega edukalt määrata.
- Väljatöötatud optilise pulsilaine signaali kuju analüüsi algoritm võimaldab eristada arterite jäikust ning seeläbi veresoonkonna vanust tervete ja diabeedihaigete grupi vahel.

Abstract

Optical pulse wave signal analysis for determination of early arterial ageing in diabetic patients

Cardiovascular diseases are one of the leading causes of death in the world. Through ageing the endothelium of the artery abrase and get damaged, which causes the atherosclerosis and generation of plaques to the vessel wall. Due to different diseases and diabetes mellitus, the ageing process of the arteries is accelerated. The stiffness of the arteries is increased as a result of calcification, which causes the increase in the load of the heart, because it is more difficult to pump the blood throught the vessels with increased resistance. This in turn causes different diseases connected to the cardiovascular system, for example, hypertension, ischemia etc. Further propagation of the disease can be prevented with premature detection of the changes in the cardiovascular system condition and with applied correct treatment.

Different non-invasive methods have been developed lately and applied to estimate the arterial stiffness. However, most of the methods are relatively complex and expensive, furthermore the trained operator is needed for the measurements. There is a need for methods that are non-invasive, inexpensive and easy to perform. The PWV and pulse wave analysis methods have been used more often in the novel non-invasive devices for the arterial stiffness estimation.

The aim of the current work was to investigate the possibilities to detect the premature increase in the arterial stiffness and the consequent increase in the cardiovascular ageing using the pulse waveform and the transit time analysis on an optically recorded signal. The measurement complex was built for the non-invasive syncrhronous recording of the pulse wave and other physiological signals. The recording of the signals and other necessary procedures were carried out on healthy subjects and diabetes patients in the North Estonia Medical Centre. During the study the algorithm was investigated and developed for the supression of the motion caused noise in the recorded optical signal. The optical pulse waveform analysis algorithm was developed, based on the second derivative method. In addition, the effectiveness of the developed method was compared with recognized methods used in clinical practice to differentiate the subjects with normal and higher arterial stiffness.

This thesis research has resulted in the following findings:

- The measurement complex compiled enables synchronous recording of the pulse wave and other physiological signals.
- Constructed algorithm suppresses the motion caused noise from the optical signal and as a result it is possible to estimate successfully the pulse transit time.

- The algorithm developed for the analysis of the optical pulse wave signal enables differentiation of the arterial stiffness and the consequent cardiovascular system age between the healthy and diabetes patient groups.

APPENDIX 1

PUBLICATIONS

Publication I

Pilt K, Meigas K, Viigimaa M, Temitski K, Kaik J (2010) "An experimental measurement complex for probable estimation of arterial stiffness", *In: Proceedings of 30th Annual International Conference of the IEEE EMBS, Buenos Aires, Argentina, August 31 – September 4*, 194-197 (DOI: 10.1109/IEMBS.2010.5627925).

32nd Annual International Conference of the IEEE EMBS
Buenos Aires, Argentina, August 31 - September 4, 2010

An Experimental Measurement Complex for Probable Estimation of Arterial Stiffness

Kristjan Pilt, Kalju Meigas, Margus Viigimaa, Kristina Temitski and Jüri Kaik

Abstract— **Current work is a part of long term research, which aim is to study the possibilities to diagnose the atherosclerosis in early stadium by using pulse wave velocity and its waveform analysis. The mobile experimental measurement complex is built and technically tested for the long term study in hospital. Measurement complex consists of ten physiological signal recording channels and reference devices: Sphygmocor, Arteriograph, Finapres. The measurements with this complex are planned to carry out during six month on patients with different severity of coronary disease and diabetes.**

I. Introduction

Atherosclerosis is pathology, which causes the most of the early deaths in Europe. In case the atherosclerosis is diagnosed in early stadium, the pathogenesis can be stopped with right treatment. Before the fats are buildup on walls of artery, the first changes are taking place in the walls of blood vessels. The walls become stiffer and thicker. In this stadium the pathogenesis of atherosclerosis can be stopped.

Numerous methods and devices have been developed to assess the stiffness of the arteries, including pulse wave velocity (PWV) measurements and pulse waveform analysis. Arterial stiffness rise causes the PWV increase [1-2]. The stiffness of arteries can be estimated easily and non-invasively with recognized devices as Sphygmocor and Arteriograph. With both devices it is possible to estimate the PWV in aorta.

Our study aim is to analyze the physiological parameters, which can be used for the early diagnosis of atherosclerosis. In our previous research there have been studied the relationships between PWV and the depth of atherosclerosis on patients with the coronary heart disease. It showed that patients with coronary heart disease had increased PWV in aorta, leg and arm arteries compared with healthy subjects.

In following wider research the PWV is planned to measure from different arteries simultaneously and to investigate the changes in parameters of pulse waveform, which are caused by the arterial stiffness. In addition the other physiological signals and parameters are measured from subject, which describes the cardiovascular system, such as electrocardiographic (ECG) signal, blood pressure, etc. The experiments are planned to carry out on larger number of patients with coronary disease and diabetes.

For the synchronous measurement of the physiological signals, which are originated from different devices, the measurement complex is needed built. As the experiments are carried out in hospital, the system needs to be mobile, compact and easy to use. The types of sensors should be selected according to body location, where the pulse waveform is registered.

II. Methods

During the experiment different physiological signals are recorded with measurement complex from subject (Figure 1). Pulse wave signals are registered from index finger, wrist, elbow, neck, earlobe, temple of the head, knee and the big toe. Enumerated pulse wave signal registration locations are on arteries and also in periphery. In addition to pulse wave signals the electrocardiographic, phonocardiographic and peripheral blood pressure signals are registered synchronously.

The pulse waves from index finger, earlobe, temple of the head and neck are registered by using photo-plethysmographic (PPG) method. PPG is a non-invasive optical technique for measuring changes in a blood circulation and has been used mainly for monitoring blood perfusion in skin [3]. The pulsating AC component of the registered PPG signal corresponds to pulse wave.

There are two main PPG sensor design modes: the reflection and the transmission mode. In the reflection mode, a photodiode is placed adjacent to the LED and directed towards the skin. The photodiode measures the reflected and scattered light intensity from the skin surface. In the transmission mode, the photodiode and the light source are placed on opposite sides of the measured volume. The photodiode measures the transmitted light intensity. The transmission sensor measurement sites are limited, because of geometrics, whereas a reflection mode sensor can be placed at any point on the skin surface.

The PPG signal is registered from index finger and from earlobe by using commercially available transmission sensors. Due to the clip type of construction the sensors can

Manuscript received April 23, 2010. This study was supported by the Estonian Science Foundation (grant No. 7506), by the Estonian targeted financing project SF0140027s07, and by the European Union through the European Regional Development Fund.

Kristjan Pilt is with the Department of Biomedical Engineering, Tallinn University of Technology, Tallinn, 19086 Estonia (phone: +372 6202200; fax: +372 6202201; e-mail: kristjan.pilt@cb.ttu.ee).

Kalju Meigas, Margus Viigimaa, Kristina Temitski, Jüri Kaik and Deniss Karai are with the Department of Biomedical Engineering, Tallinn University of Technology, Tallinn, 19086 Estonia (e-mail: kalju@cb.ttu.ee, margus@cb.ttu.ee, kristina@cb.ttu.ee, jyri@cb.ttu.ee, deniss@cb.ttu.ee).

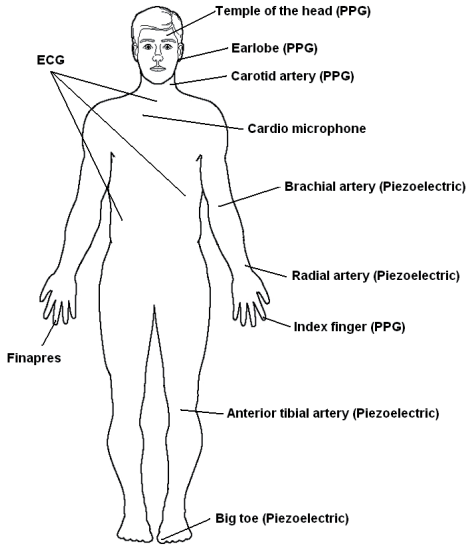

Fig. 1. The locations of the sensors on human body.

be easily fixed to measurement location. For temple of the head and neck the reflection mode sensors are used. In this research have been used Nellcor Max-Fast reflectance sensors and Nellcor finger and ear clip transmission mode sensors. The registration of PPG signal may be difficult during poor perfusion. Before the signal recording process the blood circulation can be stimulated in those locations.

PPG signals are easily obtained from previously described peripheries. PPG signal registration is difficult from wrist, elbow, knee, because the arteries are hidden under other type of tissues. Also the big toe may have poor perfusion and the signal is hard to obtain with high signal-to-noise ration (SNR). For those locations the piezoelectric method is used.

With piezoelectric sensor it is possible to register mechanical pulsation of arteries. It is relatively simple method for the detection of the pulse wave. By placing the piezoelectric sensor above the artery and applying the additional pressure on it, the pulse wave signal can be obtained. On the same time the applied pressure can affect the pulse wave velocity and its waveform. Still under the critical pressure level the influence is not noticeable [4]. In this research have been used ADInstruments MP100 transducers.

Besides the pulse wave signals the ECG and phonocardiography signals are registered synchronously during the whole experiment. ECG signal describes the electrical activity of the heart. In addition it is easy to determine the beginning of heart contraction period from the R-peak of the signal. As the ECG signal is more stable and less influenced by movements of subject, than registered pulse wave signals are, it can be used as reference for the

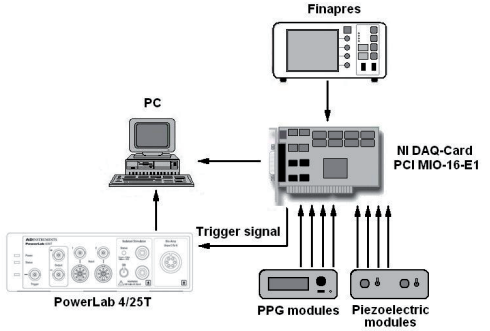

Fig. 2. Experimental measurement complex block diagram with data flow directions.

offline signal processing. For example to remove the motion caused noises from the PPG signal, which is registered from neck [5].

Phonocardiographic signal characterizes the heart related processes, which are measurable through acoustic signals. In frequency spectrum from 70 up to 300Hz are situated the frequencies, which are describing the movement of aortic valve [6]. By using ECG and phonocardiographic signals it is possible to measure directly the pre-ejection period and ejection duration during the heart cycle. It is also possible to measure the PWVs starting from opening of the aortic valve.

To measure in online the blood pressure changes the Finapres is used as reference device. It is possible to get the estimation of blood pressure during the whole experiment. On the same time it has to be taken account that Finapress gives the information about blood pressure in periphery. It can be assumed, that similar changes in blood pressure are also taking place in arteries, while the subject is lying down.

In addition to Finapres the Arteriograph and Sphygmocor are used as reference devices to estimate the arterial stiffness. By using Sphygmocor the pressure wave is registered from radial artery with tonometer. Arteriograph closes with cuff the blood flow in brachial artery and the pressure waves on different pressures are registered. With both devices the registered pressure wave shape is analyzed and the two main parameters are estimated: augmentation index and PWV in aorta; which characterize the stiffness of arteries. The measurements with Sphygmocor and Arteriograph are carried out separately from general synchronous signal recording process.

On Figure 2 the block diagram of measurement complex is given. The raw PPG signals are registered with lab-built modules. The current of the PPG sensor LED and registered PPG signal gain can be set manually from the module. This way the PPG module is adjusted for the patient skin parameters and the signal is registered with high SNR. Similarly the raw piezoelectric signals are registered with lab-built amplifier, which has adjustable gain.

The output signals from modules are digitalized with

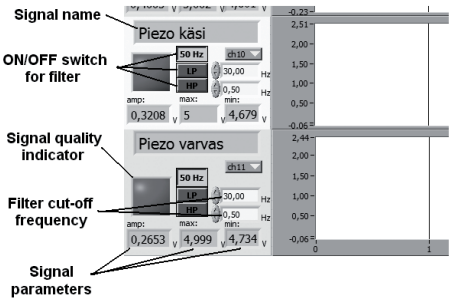

Fig. 3. LabVIEW program outline for signal monitoring and recording. For easier monitoring every signal tracks has adjustable filters, signal quality parameters and signal quality indicator.

National Instruments PCI MIO-16-E1 data acquisition card with sampling frequency 1kHz. Similarly the Finapres analogue output was connected to data acquisition card to register the peripheral blood pressure wave.

The PPG, piezoelectric and Finapres signals are monitored in online and recorded through program, which is written in LabVIEW environment. On Figure 3 is given program outline for two signal tracks. For better monitoring all the signals are displayed on the screen during experiment. All the signals are recorded raw without using any additional filter or algorithm. Still for monitoring every signal can be filtered with low and high pass filters, which cut-off frequency can be set manually. In addition the power line interference can be eliminated with 50Hz notch filter. For the recorded data validation the maximal, minimal and amplitude of the signal are displayed online for every five seconds. Every track of the signal has quality indicator, which turns into red in case the signal is out of range, with too low or too high amplitude. As there are 11 signals to monitor the indicator helps operator to get fast overview the quality of the signals.

The raw ECG and phonocardiographic signals are obtained and digitalized with ADInstruments PowerLab 4/20T device. This device has optically isolated ECG amplifier, which ensures the patient safety. As the PowerLab 4/20T has data communication only through USB port then the signals are recorded with Chart Software. The signals are digitized similarly to data acquisition card with sampling frequency 1kHz.

As the ECG and phonocardiographic signals are recorded with different software from LabVIEW environment the synchronization has to be ensured between two recording programs. In this measurement complex the PowerLab 4/20T is triggered by the LabVIEW program. When the record process is started in LabView recording interface, the trigger signal is sent to PowerLab 4/20T trigger input via DAQ Card. The trigger signal starts the recording in Chart Software.

Fig. 4. Built experimental measurement complex.

For the hospital environment the measurement complex is fixed on cart, which enables to carry it easily from one patient to another. On Figure 4 is given built measurement complex.

III. Results

The measurement complex was firstly tested with sine wave to ensure that the two monitoring programs are working synchronously. Inputs of PowerLab 4/20T and piezoelectric signal modules were connected to the sine wave generator output. The generated signal frequency was 5Hz. The recording process was started in LabVIEW program,

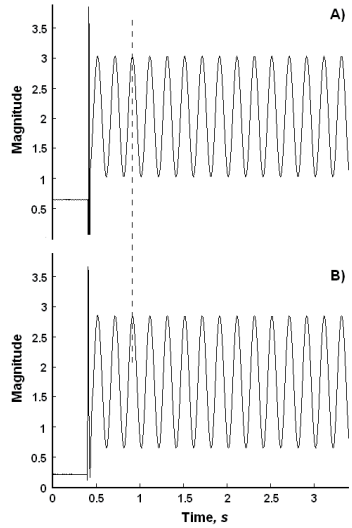

Fig. 5. Experimental results for synchronous test. A) Sine wave, which is recorded with Chart Software. B) Sine wave, which is recorded with LabVIEW program.

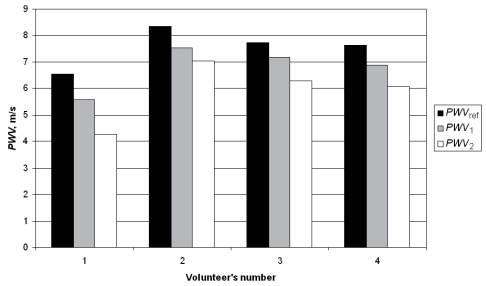

Fig. 6. Experiment results for four voulnteers. PWV_{ref} is obtained with Arteriograph. PWV_1 and PWV_2 are calculated from the recorded signals, which are obtained with measurement complex.

which also started the recording process in Chart Software through trigger signal. As follows the signal generator was switched on. After recording the signals were monitored offline in MATLAB. On Figure 5 is given the results of this test. The dotted line is put through sine wave maximal point, which is recorded with Chart Software. The dotted line also goes through sine wave maximal point, which is recorded with LabVIEW program. It is visible, that recorded signals are aligned and the systems are synchronous with each other.

The first experiments were carried out on four volunteers to test the measurement complex. The subject was lying down and the signals were registered for about 60 seconds. In addition the reference measurements were carried out with Arteriograph to obtain the PWV in aorta.

The signals were post-processed in MATLAB and the average PWVs were calculated. On Figure 6 are given results. For every volunteer are given three PWVs. The PWV_{ref} is measured by using Arteriograph. The PWV_1 was calculated as the ratio of the distance travelled by the pulse wave from elbow to index finger and the time delay between the two pulse waves. The PWV_2 is calculated similarly to PWV_1 by using distance between knee and big toe and the time delay between pulse waves. On Figure 6 is visible that PVWs, which are calculated for the hand and leg arteries (PWV_1 and PWV_2), are comparable with reference device measured PWV (PWV_{ref}). In case the PWV_{ref} is higher, also the PWV_1 and PWV_2 are increased. It corresponds to the results, which were presented also in our previous research [2].

IV. Conclusions

The experimental measurement complex for physiological signals registration was built and tested to study the possibilities to diagnose the atherosclerosis in early stadium. The experimental complex enables to register the signals from different locations of body including pulse waves from periphery and arteries. In addition the physiological signals, which are originating from different devices, are recorded synchronously. The measurement complex was technically tested on volunteers. The results were similar with our previous study outcome, which ensures that our experimental complex can be used for experiments with larger group of patients. The complex is planned to use in hospital, where the patients with coronary heart disease and diabetes are examined.

Acknowledgment

This work was supported by the Estonian Science Foundation Grant no. 7506, by the Estonian targeted financing project SF0140027s07, and by the European Union through the European Regional Development Fund.

References

[1] R. P. Smith, J. Argod, J. L. Pepin, P. A. Levy, “Pulse transit time: An appraisal of potential clinical applications”, *Thorax*, vol. 54, pp. 452-457, 1998.

[2] I. Hlimonenko, K. Meigas, M. Viigimaa, K. Temitski, “Aortic and Arterial Pulse Wave Velocity in Patients with Coronary Heart Disease of Different Severity”, *Estonian J. Eng.*, vol. 14, no. 2, pp. 167-176, 2008.

[3] J. Allen, “Photoplethysmography and its applications in the clinical physiological measurement”, *Physiol. Meas.,* vol. 28, pp. R1-R39, 2007.

[4] K. Pilt, K. Meigas, M. Viigimaa, J. Kaik, R. Kattai, D. Karai, “Arterial Pulse Transit Time Dependence on Applied Pressure”, *IFMBE Proc. Mediterranean Conf. on Med. Biol. Eng. Comput.*, vol. 29, pp. 406-409, 2010.

[5] K. Pilt, K. Meigas, R. Ferenets, J. Kaik, “Photoplethysmographic Signal Processing Using Electrocardiogram Reference Adaptive Sum Comb Filter for Pulse Delay Measurement”, *Estonian J. Eng.*, vol 16, no. 1, pp. 78-94, 2010.

[6] A. K. Abbas, R. Bassam, *Phonocardiography Signal Processing*, Morgan & Claypool, 2009.

PUBLICATIONS

Publication II

Pilt K, Meigas K, Ferenets R, Kaik J (2010) "Photoplethysmographic signal processing using adaptive sum comb filter for pulse delay measurement", *Estonian Journal of Engineering*, 16: 78-94 (DOI: 10.3176/eng.2010.1.08).

Estonian Journal of Engineering, 2010, **16**, 1, 78–94 doi: 10.3176/eng.2010.1.08

Photoplethysmographic signal processing using adaptive sum comb filter for pulse delay measurement

Kristjan Pilt, Kalju Meigas, Rain Ferenets and Jüri Kaik

Department of Biomedical Engineering, Technomedicum, Tallinn University of Technology, Akadeemia tee 21, 12618 Tallinn, Estonia; {kristjan.pilt, kalju, rafe, jyri}@cb.ttu.ee

Received 28 October 2009, in revised form 19 January 2010

Abstract. Pulse transit time, which correlates with blood pressure, is measured between the electrocardiogram R-wave peak and 50% raising front level of a photoplethysmographic (PPG) signal. Registered PPG signal bandwidth may be shared by noise and therefore the signal raising front is undetectable. Electrocardiogram reference adaptive sum comb filter was used to extract the harmonic components of the PPG signal and suppress the noises between them. Averaging effect of the filter on the PPG signal was studied and adjustments were made. The influence of the comb filtered PPG signal on the measurement of pulse transit time was analysed.

Key words: photoplethysmography, electrocardiography, pulse transit time, adaptive comb filter.

1. INTRODUCTION

Pulse transit time (PTT) is the time of a pulse wave to travel between two arterial sites. It has been shown that PPT is inversely proportional to systolic blood pressure [1]. Different methods have been used to measure the PTT, such as Doppler ultrasound, piesoelectrical pressure sensors, PPG [2,3]. The interval between the peak of the R-wave on the ECG and the raising front of the PPG signal can serve for PTT measurement [4]. In the literature this method is also called "R-wave-gated photoplethysmography" (RWPP).

ECG signals characterize the electrical activity of the heart. Electrical waves can be measured at selectively placed electrodes on the skin. Electrodes on different sides of the heart measure the activity of different parts of the heart muscle. ECG signal shape varies depending on the placement of the electrodes. In a standard solution, the ECG is measured with 10 electrodes, out of which 12 different signals are combined. To measure RWPP, three electrodes are used to

compose one ECG signal. Electrodes should be placed so that the QRS complex with a sharp R-peak can be detected.

PPG is a non-invasive optical technique for measuring changes in blood circulation, mainly used for monitoring blood perfusion in skin. The optical radiation from the light source is emitted to the skin, where the blood volume and its changes are measured. The incident light, which is often red or infrared, is absorbed, reflected and scattered in the tissue and blood. Only a small fraction of light intensity changes are received by the photodetector. Changes in the intensity of the received light are related to the blood flow in the underlying tissue [5].

There are two main ways to measure a PPG signal: the reflection and the transmission mode. In the reflection mode, a photodetector is placed adjacent to the light source and directed toward skin. Only a small fraction of the reflected and scattered light is received by the photodetector. The photodetector measures the reflected and scattered light intensity from the skin surface. In the transmission mode, the photodetector and the light source are placed on opposite sides of the measured volume. The photodetector measures the transmitted light intensity.

Measured PPG signals can be divided into two components: the DC and the AC component. The DC component of the signal varies slowly and reflects variations in the total blood volume of the examined tissue. The AC component is synchronous with the heart rate and depends on the changes in the pulsatile pressure and pulsatile blood volume. The amplitude of the AC component can be over ten times smaller than that of the DC component.

PPG signal shape is slowly varying and its starting point is difficult to determine. Raising front is the sharpest part of the PPG signal where the derivative is maximal. According to previous research, the pulse delay (PD) that is measured similarly to RWPP is suggested to be measured between 50% of the PPG signal raising front and ECG signal R-peak [2]. In this article we denote this delay as PD50.

In 24-hour PPG signal monitoring devices [6], the PPG signal can be with low signal-to-noise ratio (SNR) because of poor perfusion state and different noises (e.g., power line interference) and motion artifacts. Different methods have been applied to remove the unwanted noises. By using a band-pass filter it is possible to remove the DC component and higher frequency noises, including power line interference. Still this filtering does not remove noises caused by the PPG sensor movement, which are in the band pass region. Recent research has also shown that noises caused by motion can be successfully removed by using additional acceleration sensors and an adaptive filter [7,8]. The first input of the adaptive filter is the PPG signal with noise and the second input is unwanted noise from acceleration sensors. Motion-caused noises are removed by using the LMS algorithm.

Comb filter is an alternative method to remove noises, which are sharing the same bandwidth with the PPG signal. The AC component of the PPG signal can be described by its harmonic components. Fundamental harmonic is related to the heart pulsation frequency. All the other components are at the frequency multiples of the fundamental frequency. By using a comb filter, it extracts the

PPG signal harmonic components and suppresses the noises between them. As the PPG signal periods are not of constant length, the comb filter frequency response needs to be calculated for every period. ECG signal can be used as the reference to determine the fundamental frequency of a comb filter. This article proposes an ECG-referenced comb filter design for PPG signals and analyses its influence on the measurement of PD50.

2. METHODS

2.1. Sum comb filter design for PPG signals

In this article it is assumed that all signals are discrete, if it is not otherwise stated. The discrete signal, $x[k]$, consists of periodically taken samples of the analogue signal, $x(t)$, where k is integer and refers to sample number in the sequence and t is time in seconds.

Comb filter frequency response consists of a series of regularly spaced spikes. A sum FIR comb filter is expressed as [9]

$$y[k] = \frac{x[k] + x[k - D]}{2}, \tag{1}$$

where $x[k]$ is the filter input signal, $y[k]$ is the filter output signal and D is an integer. Depending on the value of D, the comb filter sums up two samples from the signal and calculates the average; D also determines the comb filter frequency response. On the z-plane [10] a comb filter is formed with the number of D poles at the origin and the number of D zeros, z, evenly spaced unit circle at [9]:

$$z = \exp\left[\frac{j(2l+1)\pi}{D}\right], \tag{2}$$

where l is an integer $(l = 0, 1, \ldots, D-1)$. By substituting $z = e^{j\omega T}$ in Eq. (2), the comb filter frequency response can be expressed as [9]:

$$H(j\omega T) = \exp\left(-j\frac{D\omega T}{2}\right)\cos\left(\frac{D\omega T}{2}\right), \tag{3}$$

where ω is the normalized frequency, T is the sampling interval and H is the frequency response. Figure 1a shows the frequency response for the sum comb filter with $D = 10$ zeros and Fig. 1b demonstrates the respective z-plane plot. As seen from the frequency response plot, this filter does not remove the DC component because of the lowest lobe centered to zero frequency. The filter frequency response exhibits peaks at multiples of the fundamental frequency f_1:

$$f_1 = \frac{f_s}{D}, \tag{4}$$

where f_s is the sample frequency.

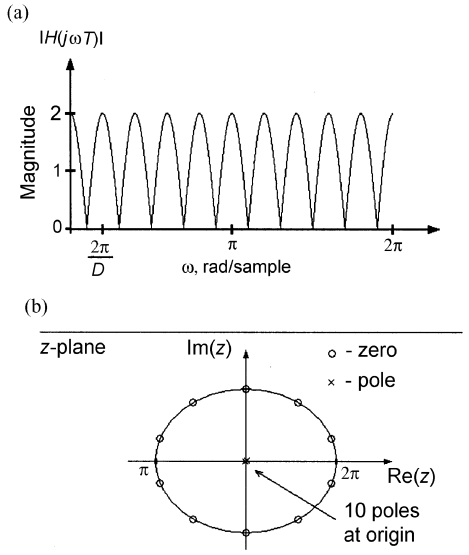

Fig. 1. (a) Comb filter magnitude response with $D = 10$ zeros; (b) respective zeroes and poles plot on the z-plane.

To select D, it is required that the fundamental frequency of the comb filter matches the fundamental frequency of the PPG signal. In this case D should be equal to the length of the PPG signal period. As a result, according to Eq. (1), the comb filter averages sample by sample two consecutive PPG signal periods. In practice, the biosignals, e.g. PPG and ECG, which are related to the heart, are recurring but not periodic. Because two consecutive recurrences are of different length, they should be equalized during the comb filter averaging process.

The process of equalization can be explained as follows (Fig. 2). Let the two consecutive recurrences $R_1(m = 1, \ldots, M)$ and $R_2(k = 1, \ldots, K)$ of the signal have different lengths M and K, respectively, $(K \neq M)$, where m and k are sample numbers within recurrences. The equalization is based on the R_2 recurrence length currently being processed. In the previous recurrence R_1, each sample number responds to the sample number of the recurrence R_2 through the following relation:

$$m = \frac{kK}{M}. \tag{5}$$

As the sample numbers must be integers, m is rounded to the closest integer. Starting points for each PPG signal recurrence are determined from synchronously measured ECG signals. Each QRS complex marks the starting point of the next recurrence.

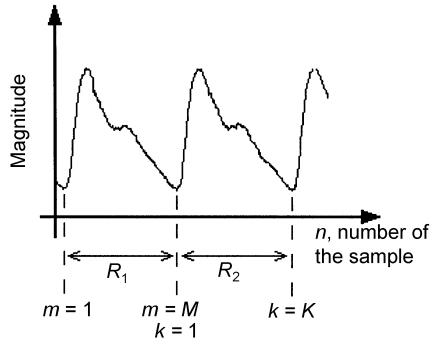

Fig. 2. Two consecutive signal recurrences R_1 and R_2 with different durations M and K, respectively.

Samples average calculations by the comb filter can be expanded over a larger number of signal recurrences. It allows for higher noise attenuation to be obtained. Assume that in a general calculation $(r-1)$ recurrences are used with $r \geq 2$, where r is integer number of recurrences. Then the modified comb filter is given by the equation

$$y[k] = x[k-D] + x[k-2D] + \ldots + x[k-(r-1)D]. \tag{6}$$

On the z-plane, the filter zeroes, z, are located as follows [9]:

$$z = \exp\left(j\frac{2m\pi}{Dr}\right), \quad m = 0, 1, 2, \ldots, (Dr-1) \tag{7}$$

and the cancelling poles, p, are as follows [9]:

$$p = \exp\left(j\frac{2n\pi}{D}\right), \quad n = 0, 1, 2, \ldots, (D-1). \tag{8}$$

A pole-zero plot, drawn for $D = 10$ and $r = 4$, is shown in Fig. 3b. The filter pass-band centres are at frequencies where the poles and zeroes are cancelling each other. Similarly to Eq. (3), the frequency response is given by [9]

$$H(j\omega T) = \exp\left[\frac{-j(Dr-D)\omega T}{2}\right]\frac{\sin\left(\frac{Dr\omega T}{2}\right)}{\sin\left(\frac{D\omega T}{2}\right)} \tag{9}$$

as plotted in Fig. 3a.

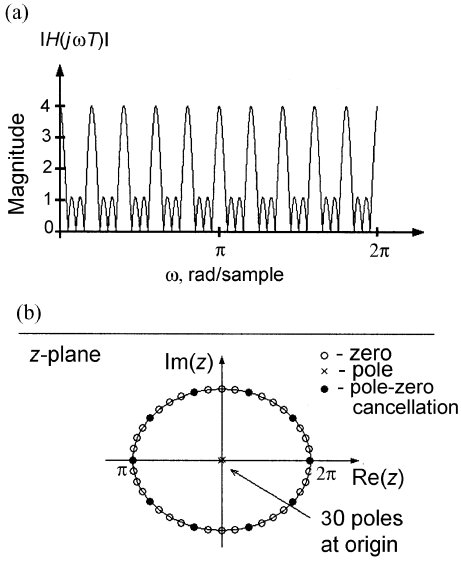

Fig. 3. (a) Response of the modified comb filter magnitude with $D = 10$ and $r = 4$; (b) plot of respective zeroes and poles on the z-plane.

By enlarging the number of recurrences, r, in the filter output calculation it is possible to minimize the noise between the main lobes of the filter more effectively. Table 1 shows the relationship between the number of recurrences used in the filter output calculation and the attenuation of the first side lobe of the stop-band. The first side lobe attenuations are calculated by using Eq. (9), where D is kept constant and r is changed according to Table 1. It is clear from Table 1 that using more than four or five recurrences will not lead to a considerable advantage, as with ten recurrences the attenuation is only 13.1 dB.

Table 1. Relationship between the first side lobe attenuation of the comb filter stop-band and the number of filter averaged recurrences r

r	Attenuation, dB
2	0.0
3	9.5
4	11.4
5	12.1
6	12.6
10	13.1

2.2. Comb filter adjustment

Averaging behaviour of a comb filter causes a decrease in signal shape differences between the beats. From Eqs. (1) and (6) it follows that every recurrence has the same weight in the filter output calculation. The filter weights can be adjusted so that the filter uses less information from a larger number of passed recurrences [11]. The sum comb filter, described by Eq. (6), can be rewritten as

$$y[k] = \frac{x[n] + \sum_{n=2}^{r} a_{n-1} \cdot x[k-(n-1)D]}{1 + \sum_{n=2}^{r} a_{n-1}}, \tag{10}$$

where a_n is the weight of the recurrence. By using discrete Fourier transform on Eq. (10), the corresponding frequency response, similarly to Eq. (9), is obtained:

$$H(j\omega T) = \frac{1 + \sum_{n=2}^{r} a_{n-1} e^{-(n-1)j\omega D}}{1 + \sum_{n=2}^{r} a_{n-1}}. \tag{11}$$

Each weight, a_n, describes the amount of information, which is taken from the previous recurrence for the filter output calculation. In Eq. (6), all the weights are equal to one.

The changes of weights cause the changes in the filter frequency response shape. Here the comb filter weights are adjusted according to the following criteria:

a) all weights should be as small as possible and $a_1 > a_2 > \ldots > a_{r-1}$; at the same time the adjusted filter frequency response should be as close to the filter frequency response as possible, as described by Eq. (9);
b) the whole stop-band magnitude of the adjusted filter should be at least as low as the first side lobe magnitude of the non-adjusted filter.

Filter weights a_n $(0 < n < r,$ where n and r are integers) are calculated numerically. The frequency response for the adjusted filter is calculated from Eq. (11) for all weights by changing a_n from 0 to 1 with step s. The magnitude of the adjusted filter in the place of the first side lobe maximum of the non-adjusted filter and the stop-band maximum are calculated and separated into square matrices **L** and **M**, respectively. The dimensions of **M** and **L** equal to $r-1,$ if $r > 2.$ In the case $r = 3,$ **M** and **L** are $1/s \times 1/s$ matrices.

First, all the values in the **M** matrix, exceeding the allowed maximum, are eliminated. In the next step, the matrix is scanned through. Scanning is explained here for the case $r = 4,$ which means that **M** is a 3D matrix.

Matrix **M** elements are m_{ijk}. It must be noted that $is = a_1,$ $js = a_2$ and $ks = a_3$. Scanning starts when $i = j = k = 0.$ The value of k is changed until the end of the matrix row. In the next step $i = 0,$ $j = 1$ and again the k value is

changed until the end of the matrix row. The previously explained scanning sequence is processed until the first existing matrix value is found, which was not eliminated before, and it should correspond to the condition $i > j > k$. Weights for the adjusted filter are found and scanning is finished if the **L** matrix value, in place of i, j and k, is lower than the allowed maximum. Otherwise scanning is continued until the weights are found.

Numerical calculations of the weights were made in MATLAB. Weights were changed from 0 to 1 with a step of $s = 0.04$. Table 2 shows weights for adjusted filters. The plot for respective frequency responses for adjusted filters is given in Fig. 4.

Table 2. Calculated weights for the adjusted comb filter

r	a_1	a_2	a_3	a_4
3	0.64	0.20	–	–
4	0.72	0.44	0.12	–
5	0.68	0.60	0.36	0.12

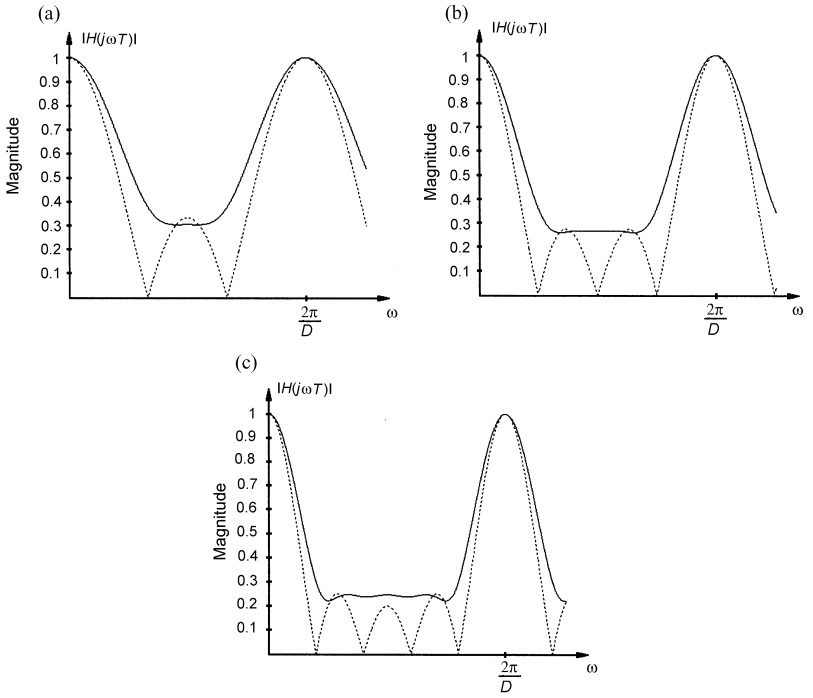

Fig. 4. Adjusted (solid line) and non-adjusted (dashed line) sum comb filter frequency responses in the case $D = 8$: (a) frequency response in case $r = 3$; (b) $r = 4$; (c) $r = 5$.

2.3. Influence of the comb filter on the pulse delay measurement

As explained above, PD50 is measured between the ECG signal R-peak and the 50% PPG signal raising front level. As the PPG signal has slow behaviour, it is difficult to determine the starting point of the recurrence. In previous studies the starting point of the PPG signal recurrence was detected from its maximum or minimum point, but it is not sufficiently accurate [2]. The raising front is the fastest changing part in the PPG signal. In case the calculated 50% level is between two samples, it is possible to interpolate the signal as the front rises linearly. It allows for a more precise determination of PD50. The 50% level is calculated for each recurrence separately. Within one recurrence, the maximum and minimum points of the PPG signal are detected and the 50% level is calculated.

Comb filter output can also be taken also as a product of the moving window average [12]. Therefore the output signal is delayed for half of the number of periods used in the filter calculation.

Let the comb filter output be calculated from two consecutive recurrences. It is expected that PD50 is an average of the two consecutive recurrences PD50. The PD50 mean value is calculated as

$$\mathrm{PD50}_2(n) = \frac{\mathrm{PD50}(n-1) + \mathrm{PD50}(n)}{2}, \tag{12}$$

where n is the number of recurrence in the PPG signal. $\mathrm{PD50}_2$ index 2 means the number of recurrences used in the filter output calculation. A generalization of Eq. (12) can be written as:

$$\mathrm{PD50}_r(n) = \frac{1}{r} \sum_{m=n-r+1}^{n} \mathrm{PD50}(m). \tag{13}$$

Equation (13) can be interpreted as the moving average window method with the window length r. The output of the moving average window is delayed regarding to input by half the window length, which is similar to the filter output calculation. It means that the PD50, measured from the comb filtered signal, is an average over r recurrences and delayed by half of the r recurrences.

In addition to the procedure described, test signals were generated in MATLAB to analyse the influence of the comb filter on the PD50 measurement. The first input of the signal generator is the unit impulse train, related to the ECG signal (Fig. 5c). Each unit impulse marks the ECG signal R-peak.

Impulses appeared at constant frequency 1 Hz. The second generator input is PD50 that determines the PPG signal raising front delay from the R-peak for each generated recurrence (Fig. 5b). In the middle of the generated signal, the PD50 varies between 0.25 and 0.35 s. One period from a raw PPG signal was taken as a template. The PPG signal template was stretched and compressed through rescaling it for every generated recurrence to achieve the given PD50 (Fig. 5a).

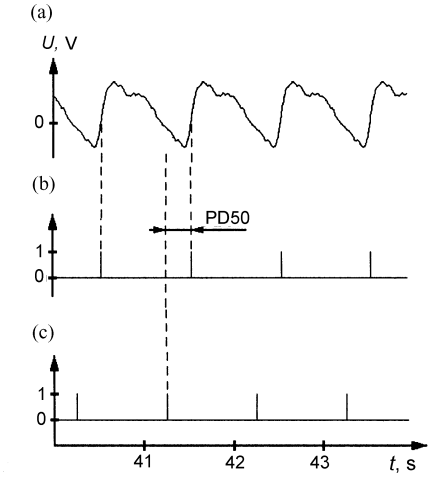

Fig. 5. (a) Part of the generated signal; (b) impulses, which are marking the detection of PPG signal raising front 50% level; (c) first PPG signal generator input signal (impulse train, which is related to the ECG signal R-peak).

In the next step, the PD50 was measured by using a raw generated signal and PPG signals filtered with comb filters. Two and six recurrence averaging comb filters were used. Results are shown in Fig. 6. It can be seen that the PD50, measured by using the raw generated PPG signal, differs from that of the filtered

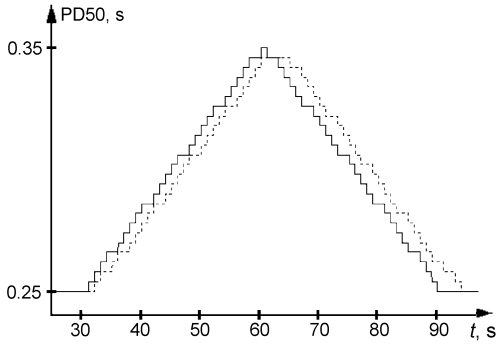

Fig. 6. Measured PD50 values while using raw generated PPG signal (solid line); generated signal, which is preprocessed with six recurrences averaging comb filter (dotted line); PD50 values varied linearly over the given range.

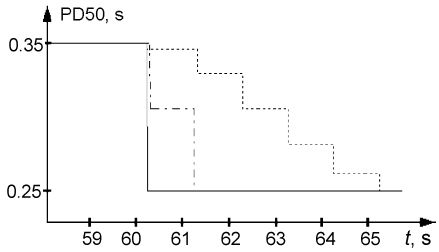

Fig. 7. Measured PD50 values while using raw generated PPG signal (solid line); generated PPG signal, which is preprocessed with two recurrences averaging comb filter (dash dotted line); generated PPG signal, which is preprocessed with six recurrences averaging comb filter (dotted line); PD50 value was changed in the middle of generated signal from 0.35 to 0.25 s.

signals. As discussed above, the comb filtered signal PD50 is shifted from the raw signal PD50. To illustrate, how a comb filter influences fast changes in the PD50, a test signal was generated. In the middle of the generated PPG signal, the PD50 changed sharply from 0.35 to 0.25 s. Figure 7 shows the results of the PD50 measurement in the case of a raw PPG signal and the comb filtered signals using two and six recurrences for the filter output calculation.

In the case of a sharp PD50 change, the reaction time for the adaptive comb filter with six recurrences averaging is longer than for the adaptive comb filter with recurrences averaging, as it was discussed above. For fast changes in registered signals, similar behaviours are expected.

3. EXPERIMENTS AND RESULTS

Experiments concentrated on the analysis of the adaptive comb filter with real signals. The raw PPG and ECG signals were registered from forehead by using a laboratory built circuit. Signals were recorded synchronously using the LabView environment and National Instruments DAQCard 6036. The analogue-to-digital conversion was made with 250 Hz sampling rate and 16-bit resolution. Digital signal processing was carried out in MATLAB. To show how filters act at low SNR signals the subject was doing squat downs during the recording process.

Firstly, the PPG signal was filtered with the band-pass filter composed of a separated high- and a low-pass filter. FIR high-pass and low-pass filters, designed by using the rectangular window method, have the cut-off frequencies at 0.3 and 30 Hz with orders of 850 and 200, respectively. After band-pass filtering, the signals were processed with the ECG referenced adjusted adaptive comb filter, which uses four recurrences for the output calculation.

The results are shown in Fig. 8. The raw PPG signal shows a noticeably high noise rate because of squat downs (Fig. 8a). After high- and low-pass filtering, the signal DC component and high frequency noises are eliminated (Fig. 8b). Still visually it is almost impossible to detect a pulsatile PPG signal. The

respective signal segment spectrum is shown in Fig. 8d. Higher magnitude peaks appear at frequencies 1, 2 and around 4 Hz.

The signal after the adaptive comb filter is given in Fig. 8c. The pulsatile shape of the PPG signal is visible and detectable. The respective signal segment spectrum is shown in Fig. 8e. The higher magnitude peak around 1 Hz appears

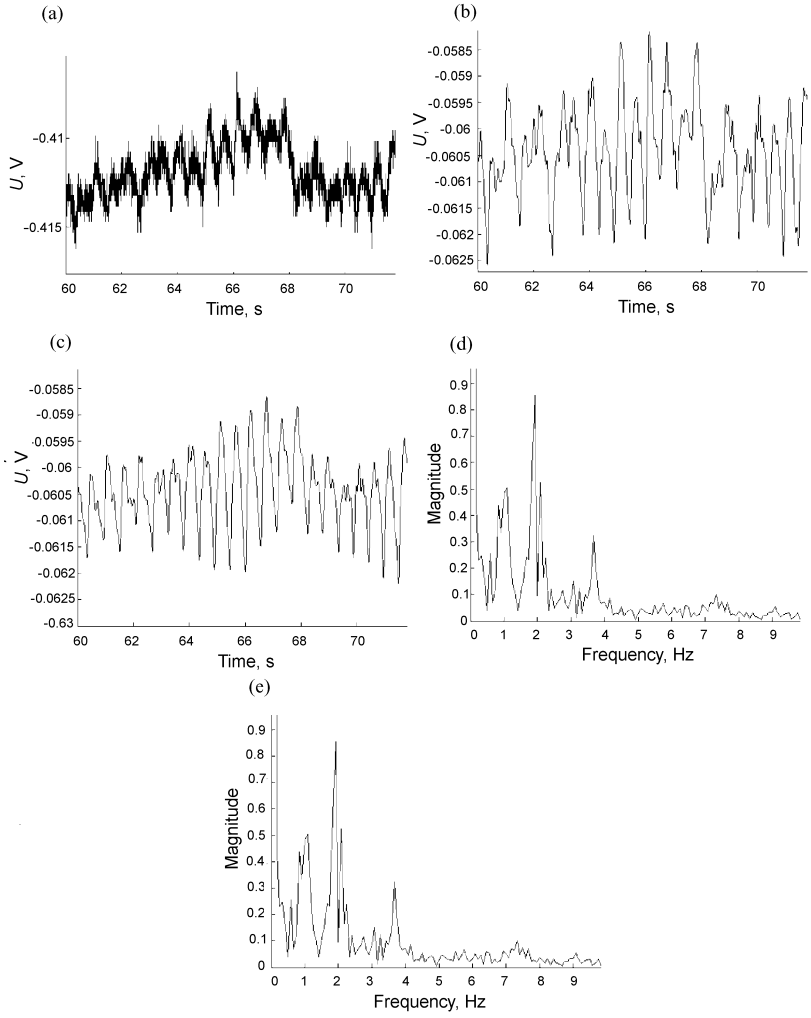

Fig. 8. (a) Raw PPG signal recorded from the forehead; (b) PPG signal after high- and low-pass filters; (c) PPG signal after adaptive comb filter; (d) signal spectrum after high- and low-pass filter; (e) signal spectrum after adaptive comb filter.

reduced, which might correspond to a noise, caused by motion. Also, at higher frequencies, between the PPG signal harmonics, noise reduction is visible.

To show influence of the comb filter on the PD50 measurement, the PPG and ECG signals were recorded while the subject was carrying out the Valsalva maneuver [13]. The PPG signal in this experiment was registered from forehead. During the Valsalva maneuver, the subject's blood pressure and heart rate changed. Recorded signals were with high SNR, as the subject was sitting during the experiment. Comparison was made between two PD50 measurements. The first PD50 measurement was made by using raw PPG signal and the second one by using the comb filtered PPG signal.

After the recording session, the PPG and ECG signals were processed offline. The PPG signal was filtered with high- and low-pass filters as described in the previous experiment above. In the next step, the PD50 was measured between the ECG signal R peaks and the PPG signal raising fronts. Subsequently the PPG signal was filtered with two comb filters, which used two and four recurrences for the output calculation. Both of the filtered PPG signals were used to measure PD50.

The results are shown in Fig. 9. Typical heart rate rise at the Valsalva maneuver can be seen at 105 s in Fig. 9d. Figures 9a–c show the calculated inverse values of PD50, by using different preprocessed PPG signals and the synchronous ECG signal. Inverse PD50 should be taken as relative blood pressure. It is not equal to certain blood pressure estimations.

Figure 9c shows that at the beginning of the Valsalva maneuver (95 s), the typical blood pressure changes, which is not so clearly seen in other signals. Also, the inverse PD50 shift is visible between the signals in Figs. 9b and 4c. The PD50 that is determined from the four recurrence averaging comb filter has a smoother shape than the other two signals, caused by the averaging property of the comb filter.

The small fluctuations in the signal in Fig. 9a may be caused by imprecise 50% raising front detection or directly related to blood pressure changes. On the one hand, by using a large number of recurrences for averaging the signal, more noise is suppressed. The detection of the PPG signal front is more precise. On the other hand, because of averaging the small changes in the signal may be lost. It is necessary to find a balance for the number of recurrences.

In our experiments we compared adjusted and non-adjusted comb filters that use a different number of recurrences r. The PPG signal was generated in MATLAB. The PPG signal was generated by using a one-period length template. In addition, a reference signal was generated, composed of unit impulses, whereas each impulse marked the beginning of the PPG signal period.

Generated PPG signal heart rate frequency was varied from 1 to 2 Hz during 24 s. The noise was generated by using the MATLAB random number generator and added to the PPG signal. Four PPG signals with different SNR were generated. Generated signals were filtered with three adjusted and three non-adjusted adaptive comb filters. Adjusted filters were using weights given in Table 2. After filtering, the signal SNR was measured and noise attenuation was calculated.

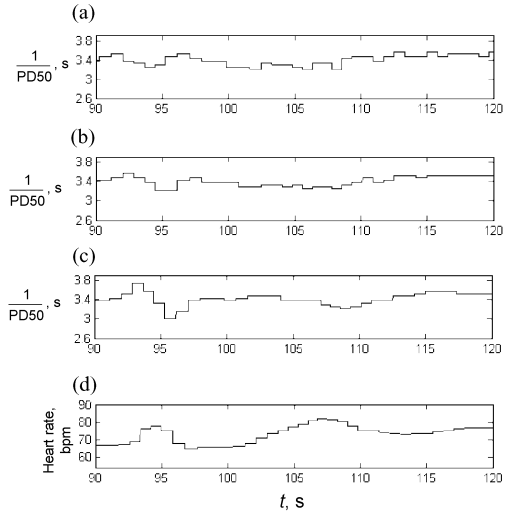

Fig. 9. Signals are starting from the beginning of the Valsalva maneuver: (a) calculated inverse value of PD50 by using ECG and only a high-pass filtered PPG signal; (b) calculated inverse value of PD50 by using ECG and comb filtered PPG signal, where comb filter used two recurrences for averaging; (c) calculated inverse value of PD50 by using ECG and the comb filtered PPG signal, where the comb filter used four recurrences for averaging; (d) heart rate.

Table 3 shows the results and Fig. 10 illustrates the use of information. The aim of the comb filter adjustment was to decrease the effect of the filter on the signal shape averaging by using less information from previous recurrences. The amount of information that filters are using from previous recurrences is given in Table 2; 100% corresponds to the situation when samples of one recurrence are involved to the filter output calculation with weight 1. It can be seen that the amount of information is reduced twice. At the same time, less information is taken from past recurrences.

Table 3. Non-adjusted and adjusted comb filter noise attenuation and use of information for output calculation

r	3	4	5
Adjusted comb filter			
Amount of information, %	184	228	276
Noise attenuation, dB	18	24	32
Non-adjusted comb filter			
Amount of information, %	300	400	500
Noise attenuation, dB	24	32	39

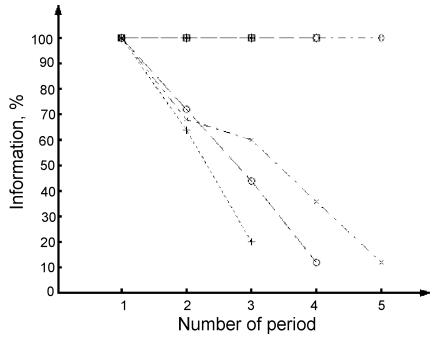

Fig. 10. Amount of information that is used for adjusted and non-adjusted comb filter output calculation; dotted line with "+": adjusted comb filter uses 3 recurrences; dashed line with "o": adjusted comb filter uses 4 recurrences; dash dotted line with "x": adjusted comb filter uses 5 recurrences.

The drawback of the adjusted filter is a decrease in noise attenuation. For every filter, the average SNR was calculated. It can be seen in Table 3 that the noise attenuation of the adjusted filters is about 7 dB better than of the non-adjusted filters by using the same number of recurrences for filter output calculation. It should be pointed out that noise attenuation is equal for the adjusted filter with r and the non-adjusted filter with $r - 1$.

4. CONCLUSIONS

An ECG reference adaptive comb filter has been proposed to filter out the noises that share the same bandwidth with the signal to measure the PD50. The comb filter was customized for non-periodic biosignals such as the PPG signal by equalizing the lengths of consecutive recurrences. The filter averages the signal over determined previous recurrences. Enlarging the averaging over the number of periods enables the noise attenuation to be improved. Still, it was found that using more than four or five recurrences for averaging do not give significant advantages.

The adaptive comb filter decreases differences between the beats because it calculates the average over the recurrences. Adaptive sum comb filter adjustment was performed numerically to minimize the influence of past recurrences on an ongoing processed recurrence. At the same time, the frequency response properties of the filter were kept as similar as possible to those of the non-adjusted filter. The adjustment method was explained and new weight values were calculated.

Adjusted and non-adjusted comb filter noise attenuations were compared by generating a noisy PPG signal. The adjusted filter was found to have lower noise

attenuation than a non-adjusted filter by using the same number of recurrences. By expanding the calculation of the non-adjusted filter output over one more recurrence, in contrast to the non-adjusted filter, the noise attenuations were equal. At the same time, the adjusted filter used almost twice less information from previous recurrences than the non-adjusted filter did.

Filtered PPG and ECG signals were used to measure the PD50. The influence of the adaptive comb filter on the PD50 was analysed. The comb filter eliminates noises that share the same band width with the PPG signal and the raising fronts are detectable. The PPG signal as well as the PD50 measurement is affected by the comb filter averaging mechanism. Averaging and a PD50 shift were analysed with test signals as well as with recorded signals from the subject by the Valsalva maneuver. The averaging effect of the comb filter should be taken into account by PD50 measurements.

ACKNOWLEDGEMENTS

This study was supported by the Estonian Science Foundation (grant No. 7506), by the Estonian targeted financing project SF0140027s07, and by the European Union through the European Regional Development Fund.

REFERENCES

1. Lass, J., Meigas, K., Karai, D., Kattai, R., Kaik, J. and Rosmann, M. Continuous blood pressure monitoring during exercise using pulse wave transit time measurement. In *Proc. 26th Annual International Conference of the IEEE Eng. Med. Biol. Sci.* San Francisco, 2004, 2239–2242.
2. Lass, J., Meigas, K., Kattai, R., Karai, D., Kaik, J. and Rosmann, M. Optical and electrical methods for pulse wave transit time measurement and its correlation with arterial blood pressure. *Proc. Estonian Acad. Sci. Eng.*, 2004, **10**, 123–136.
3. Asmar, R., Benetos, A., Topouchian, J., Laurent, P., Pannier, B., Brisac, A. M., Target, R. and Levy, B. I. Assessment of arterial distensibility by automatic pulse wave velocity measurement. Validation and clinical application studies. *Hypertension*, 1995, **26**, 485–490.
4. Naschitz, J. E., Bezobchuk, D., Mussafia-Priselac, R., Sundick, S., Dreyfuss, D., Khorshidi, I., Karidis, A., Manor, H., Nagar, M. et al. Pulse transit time by R-wave-gated infrared photoplethysmography: Review of the literature and personal experience. *J. Clin. Monit. Comput.*, 2005, **18**, 333–342.
5. Kamal, A., Harness, J., Irving, G. and Mearns, A. Skin photoplethysmography – a review. *Comput. Methods Progr. Biomed.*, 1989, **28**, 257–269.
6. Pilt, K., Meigas, K., Lass, J., Rosmann, M. and Kaik, J. Analogue step-by-step DC component eliminator for 24-hour PPG signal monitoring. In *Proc. IEEE Eng. Med. Biol. Soc. Conference*. Lion, 2007, 1006–1009.
7. Wood, L. B. and Asada, H. Low variance adaptive filter for cancelling motion artifact in wearable photoplethysmogram sensor signals. In *Proc. IEEE Eng. Med. Biol. Soc. Conference*, 2007, 652–655.
8. Comtois, G., Mendelson, Y. and Ramuka, P. A comparative evaluation of adaptive noise cancellation algorithms for minimizing motion artifacts in a forehead mounted wearable pulse oximeter. In *Proc. IEEE Eng. Med. Biol. Soc. Conference*, 2007, 1528–1531.
9. Cunningham, E. P. *Digital Filtering: An Introduction*. J. Wiley, New York, 1995.

10. Oppenheim, A. V., Schafer, R. W. and Buck, J. R. *Discrete-time Signal Processing, 2nd Ed*. Prentice Hall, 1999.
11. Pilt, K., Meigas, K., Ferenets, R. and Kaik, J. Adjustment of adaptive sum comb filter for PPG signals. In *Proc. IEEE Eng. Med. Biol. Soc. Conference.* Minneapolis, 2009, vol. 1, 5693–5696.
12. Pilt, K., Meigas, K., Karai, D. and Kaik, J. PPG signal processing for pulse delay computing by using adaptive comb filter. *IFMBE Proc.*, 2009, **25**, 1653–1656.
13. Luster, E. A., Baumgartner, N., Adams, W. C. and Convertino, V. A. Effects of hypovolemia and posture on responses to the Valsalva maneuver. *Aviat. Space Environ. Med.*, 1996, **67**, 308–313.

Fotopletüsmograafilise signaali töötlus pulsi viiteaja mõõtmisel adaptiivse kammfiltriga

Kristjan Pilt, Kalju Meigas, Rain Ferenets ja Jüri Kaik

Ajalist viidet elektrokardiograafilise (EKG) signaali R-piigi ja fotopletüsmograafilise (PPG) signaali tõusva frondi vahel nimetatakse pulsi viiteajaks. Eelnevates uurimustes on täheldatud selle korreleeruvust vererõhuga. Liikuval inimesel registreeritud PPG-signaal võib olla mõjutatud liikumisest tingitud müradest. Antud töös töötati välja adaptiivne kammfilter mürade filtrimiseks, mis kasutab EKG-signaali referentsina, ja analüüsiti selle filtri mõju PPG-signaalile ning pulsilaine viiteajale.

Töös realiseeritud adaptiivse kammfiltri väljund arvutatakse korduvate signaalilõikude keskmistamise teel. EKG-signaali R-piigid tähistavad iga PPG-signaali korduse algust. Iga filtreeritava korduse jaoks interpoleeritakse eelnevad kordused sellega võrdseks. Väljundi arvutamisel võetakse igast perioodist vastava järjekorranumbriga hetkväärtus ja need keskmistatakse.

Suurendades keskmistatud korduste arvu, on võimalik saavutada suurem signaal/müra-suhe, kuid väikesed muutused signaalis võivad seetõttu ära kaduda. Selle vältimiseks kohandati kammfiltrit nii, et keskmise arvutamisel kaasatakse hetkväärtusi möödunud kordustest väiksema kaaluga.

Filtrit testiti genereeritud PPG-signaaliga, millele oli lisatud juhuslik müra. Tuginedes tehtud eksperimentidele, kasutas kohandatud filter eelnevatest perioodidest kaks korda vähem infot väljundi arvutamiseks kui kohandamata filter. Kohandatud kammfilter surus mürasid maha 7 dB vähem kui kohandamata filter sama korduste arvu juures.

Testimise tulemused kinnitasid, et kammfiltril on keskmistav efekt ka pulsilaine viiteaja arvutamisel. Tehtud katsetest selgus, et pulsilaine viiteaeg on nihutatud poole korduste arvu võrra. Pulsilaine viiteaja muutuse puhul rohkem kordusi kasutav filter reageerib aeglasemalt kui vähem kordusi kasutav filter.

Katsed reaalsete signaalidega näitasid, et kammfiltriga on võimalik eemaldada liikumisest tingitud mürad, mis asuvad PPG-signaali sagedusdiapasoonis, ja määrata PPG-signaali tõusev front.

PUBLICATIONS

Publication III

Pilt K, Ferenets R, Meigas K, Lindberg L-G, Temitski K, Viigimaa M (2013) "New photoplethysmographic signal analysis algorithm for arterial stiffness estimation", *The Scientific World Journal*, vol. 2013, Article ID 169035, 9 pages (DOI: 10.1155/2013/169035).

Hindawi Publishing Corporation
The Scientific World Journal
Volume 2013, Article ID 169035, 9 pages
http://dx.doi.org/10.1155/2013/169035

Research Article

New Photoplethysmographic Signal Analysis Algorithm for Arterial Stiffness Estimation

Kristjan Pilt,[1] Rain Ferenets,[1] Kalju Meigas,[1] Lars-Göran Lindberg,[2] Kristina Temitski,[1] and Margus Viigimaa[1]

[1] *Department of Biomedical Engineering, Technomedicum, Tallinn University of Technology, Ehitajate tee 5, 19086 Tallinn, Estonia*
[2] *Department of Biomedical Engineering, Linköping Univeristy, 581 85 Linköping, Sweden*

Correspondence should be addressed to Kristjan Pilt; kristjan.pilt@cb.ttu.ee

Received 10 May 2013; Accepted 1 July 2013

Academic Editors: N. Bouguila, M. Engin, and T. Yamasaki

The ability to identify premature arterial stiffening is of considerable value in the prevention of cardiovascular diseases. The "ageing index" (*AGI*), which is calculated from the second derivative photoplethysmographic (SDPPG) waveform, has been used as one method for arterial stiffness estimation and the evaluation of cardiovascular ageing. In this study, the new SDPPG analysis algorithm is proposed with optimal filtering and signal normalization in time. The filter parameters were optimized in order to achieve the minimal standard deviation of *AGI*, which gives more effective differentiation between the levels of arterial stiffness. As a result, the optimal low-pass filter edge frequency of 6 Hz and transitionband of 1 Hz were found, which facilitates *AGI* calculation with a standard deviation of 0.06. The study was carried out on 21 healthy subjects and 20 diabetes patients. The linear relationship ($r = 0.91$) between each subject's age and *AGI* was found, and a linear model with regression line was constructed. For diabetes patients, the mean *AGI* value difference from the proposed model y_{AGI} was found to be 0.359. The difference was found between healthy and diabetes patients groups with significance level of $P < 0.0005$.

1. Introduction

There has been an increased interest in the development of innovative noninvasive methods and devices for the diagnosis of cardiovascular diseases [1–3]. Photoplethysmographic (PPG) waveform analysis has been used as one method [4].

PPG is a noninvasive optical technique for measuring changes in blood circulation that is mainly used for monitoring blood perfusion in the skin. The PPG finger sensor consists of a light emitting diode (LED), which is often red or infrared, and a photodetector (PD) [5]. PD and LED are on the opposite side of the finger. The light is emitted from the LED to the skin and a small fraction of light intensity changes is received by the PD, which are related to blood flow, blood volume, blood vessel wall movement, and the orientation of red blood cells in the underlying tissue [6, 7]. The PPG signal consists of different components: DC and AC components and noise, which can be caused by the poor perfusion state and motion artifacts [5]. Noise can be eliminated by using different filtering techniques [8]. The AC component is synchronous with the heart rate and depends on changes in the pulsatile pressure and pulsatile blood volume.

It is apparent that the AC component of the PPG signal changes with age and the waveform transforms from a wavy into a triangular-shaped signal (Figure 1, upper part). Regarding time domain, different methods to analyze the waveform of the PPG signal, measured at the finger, can be used for arterial stiffness estimation and evaluation of cardiovascular aging [9–11].

One option is to use the second derivative of the PPG signal (SDPPG), which was first introduced by Takazawa et al. [12]. The SDPPG is analyzed by using the amplitudes of the distinctive waves "a", "b", "c", "d", and "e", which are situated in the systolic phase of the heart cycle (Figure 1, lower part). The amplitudes of the waves are normalized as follows: b/a, c/a, d/a, and e/a. They found that normalized amplitude b/a increases and c/a, d/a, and e/a decrease in proportion to the increase in the subject's age. As a result an "ageing index" (*AGI*) parameter was proposed according to

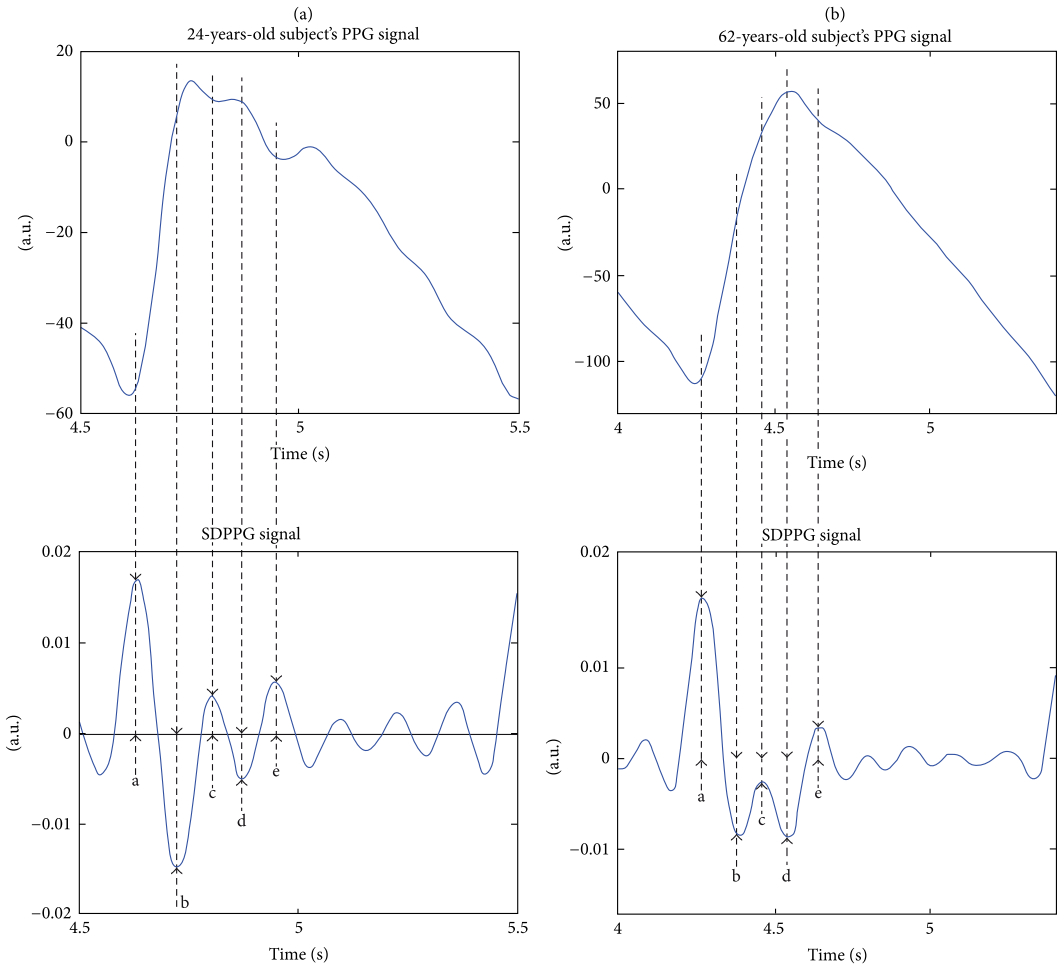

FIGURE 1: The finger PPG signal and its second derivative with distinct waves "a", "b", "c", "d", and "e" of 24-year (a) and 62-year-old (b) subjects.

$AGI = (b-c-d-e)/a$, where the a, b, c, d, and e are the amplitudes of the waves. The AGI is used to describe the cardiovascular age of the subject.

In recent publications, the correlation relationship between cardiovascular risk factors and the SDPPG normalized amplitudes values has been analyzed statistically [13–15]. Normalized amplitudes of SDPPG and AGI can be good parameters for a screening method to detect increases in the stiffness of the arteries [16].

The sample segment of PPG and SDPPG signal, which has been registered from a 37-year-old healthy subject, with AGI values, is shown in Figure 2. The SDPPG signal is processed, and the wave amplitudes are detected according to a study by Millasseau et al. [17]. The similar processing method has been also described in less detail in other studies [12–15]. It is assumed that the cardiovascular system does not change over short periods in cases of healthy subjects. It is visible from Figure 2 that the AGI values for the healthy subject are noticeably higher for the first and third periods. The difference between maximal and minimal AGI values is 0.47, which constitutes about 39% from the whole scale of AGI [12]. Furthermore, the detected peaks in the first and third periods are located to the beginning of systolic phase of the PPG signal compared to the second and fourth periods. As a result the amplitudes of detected peaks in the consecutive periods describe different phase of the PPG waveform and AGI values become noticeably different. This leads to higher standard deviation of AGI and to faulty interpretation of the results for a single subject. The detection of the peaks from different phases of PPG signal in case of consecutive periods is due to the insufficient suppression of PPG signal higher components and noise.

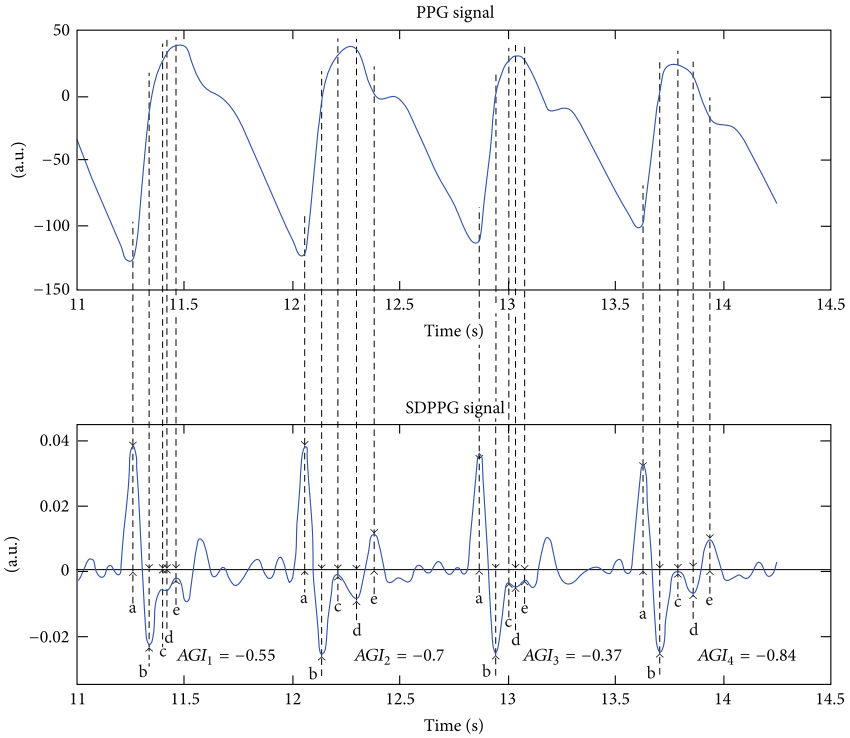

Figure 2: The sample segment of the PPG signal (upper part) from a 37-year-old healthy subject and its second derivative (lower part) with detected wave peaks and *AGI* values. The SDPPG signal is processed, and the wave amplitudes are detected according to a study by Millasseau et al. [17].

The *AGI* has to be calculated with low standard deviation in order to differentiate the subjects with increased stiffness from the healthy subjects. In this study, we have improved the SDPPG analysis method in order to obtain the *AGI* values with minimal standard deviation and to detect the waves at the same locations within one period of the PPG signal. The algorithm is tested on group of healthy subjects and a small group of diabetes patients as a pilot study.

2. Methods

2.1. SDPPG Analysis Algorithm. Normalization of the period's length, averaging, filtering, and detection of the waves from the SDPPG signal are illustrated in a block diagram in Figure 3. The PPG signal is filtered with low- and high-pass FIR filters in order to separate DC components and high frequency noise. The cutoff frequencies for the low- and high-pass filters are selected as 30 Hz and 0.5 Hz, respectively. Both filters are designed using the window method, with the Hamming window function where the corresponding filter orders are chosen as 500 for the low-pass after and 4000 for the high-pass filter.

Subsequently the PPG signal is differentiated two and four times (Figure 3). The simplest differentiator calculates the differences between two consecutive samples of the signal, which is also known as the first-difference differentiator. This kind of differentiator works as a high-pass filter, and the high frequencies are amplified as a result. However, the unwanted noise is located at higher frequencies for the PPG signal. Due to the reason outlined previously, the Smooth Noise Robust Differentiator (SNRD) is used.

The SNRD has been developed for different cases that are particularly beneficial for carrying out experiments with noisy data where differentiation is required [18]. This differentiation scheme possesses the following characteristics: precise at low frequencies, smooth and guaranteed suppression of high frequencies. The order of the differentiator determines the suppression of the high frequencies. In this algorithm, the fifth order of the differentiator is used, which is also the lowest possible one. At the lower frequencies (0–15 Hz), where the majority of the power of the PPG signal is located, the first-difference differentiator and SNRD frequency responses are practically equal.

In practice, biosignals such as PPG, which are related to heart activity, are recurring but not periodic. This means that the harmonic components of the two consecutive recurrences of the PPG signal and its derivatives can be at different frequencies. In this study, the low-pass filter is used with static

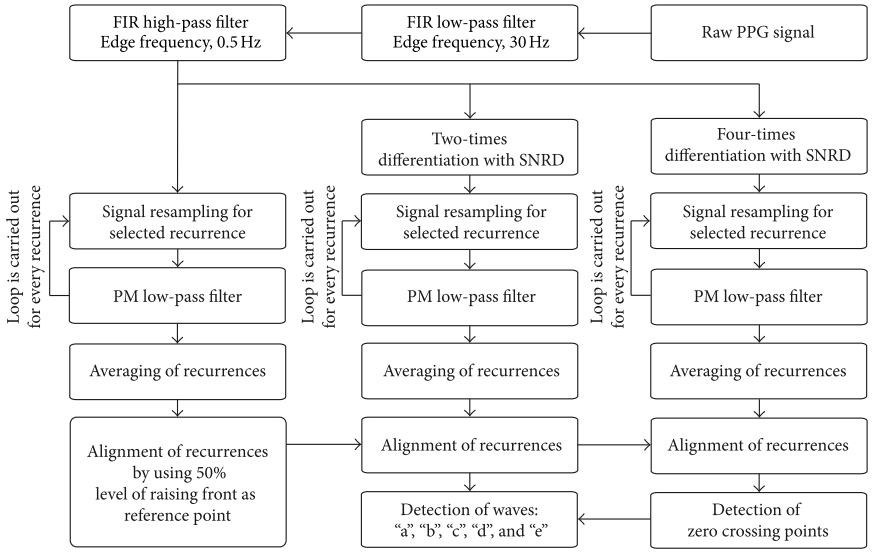

Figure 3: Block diagram of the signal processing for the second derivative analysis.

edge frequency. Accordingly, certain numbers of harmonic components are passed and all others are suppressed. The lengths of the PPG signal recurrences are then normalized to ensure that all the harmonic components are processed in the same way (Figure 3).

The PPG signal is resampled in such a way that one of the selected recurrence lengths is 1 s, which corresponds to the pulse frequency of 1 Hz. In this case, the fundamental frequency is situated at 1 Hz. All the other components lay at the frequency multiples of the fundamental frequency. In the next step, the signal is filtered with the 1 Hz wide transition-band PM filter [19]. The maximum allowable errors for the pass and stop bands are set at 0.001. The resampling and filtering are also carried out with the second and fourth derivatives of the PPG signal. After filtering, the copy of selected recurrence is aligned with other normalized and filtered recurrences from this PPG signal. The recurrences of PPG signals can be aligned by using different distinct points from the signal as reference, for example, the recurrence maximal or minimal point of the raising front. The recurrence minimal point can be difficult to determine, because of the wavy ending of the diastole phase. It is also difficult to determine the PPG signal maximal point as it depends on the state of the cardiovascular system [20]. The 50 percent level of the PPG signal raising front is used as the reference point for the alignment of the recurrences. Furthermore, the second and fourth derivatives are moved according to the movement of the PPG signal recurrences.

The resampling, filtering, and aligning processes outlined previously are carried out separately for every recurrence in PPG signals. The averaged waveform for one subject with its 9 recurrences is given in Figure 4.

Subsequently, the peaks of waves "a", "b", "c", "d", and "e" are found from the averaged SDPPG waveform. Firstly, the zero crossings of the averaged fourth derivative waveform are found. The peaks of waves "a", "b", "c", "d", and "e" are between zero crossings of the fourth derivative waveform as it is revealed in Figure 4. Secondly, the minimal and maximal points of the SDPPG waveform are located between the zero crossings of the fourth derivative waveform. There can be waveforms of the SDPPG, where the peaks of the "c" and "d" waves do not appear. In this case, the "c" and "d" waves are determined in the places of the SDPPG waveform, where the fourth derivative is maximal or minimal between zero crossings.

2.2. Optimization of PM Low-Pass Filter Edge Frequency. The recurrences and averaged waveform of the SDPPG are affected by the edge frequency of the PM low-pass filter. The optimal edge frequency of the PM low-pass filter was optimized in order to achieve the lowest standard deviation of the SDPPG wave amplitudes, which ultimately minimizes the standard deviation of *AGI*. In addition, the variation in the placement of waves "a", "b", "c", "d", and "e" on time domain has to be minimal throughout all the periods for one subject. Here, it is assumed that the cardiovascular system does not change over short periods in cases of healthy subjects. The optimization of the PM low-pass filter edge frequency was carried out on signals from a group of healthy subjects.

The width of the PM low-pass filter transition-band was 1 Hz and the edge frequency was changed between 4 and 14 Hz with a step of 1 Hz. The order of the corresponding PM filter was 3255 at sampling frequency 1 kHz. The 3–13 harmonic components in addition to the fundamental harmonic are passed through the filter as the recurrences of the SDPPG were normalized to the frequency of 1 Hz. In this way, the influence of each harmonic component to waves "a", "b", "c", "d", and "e" can be analyzed.

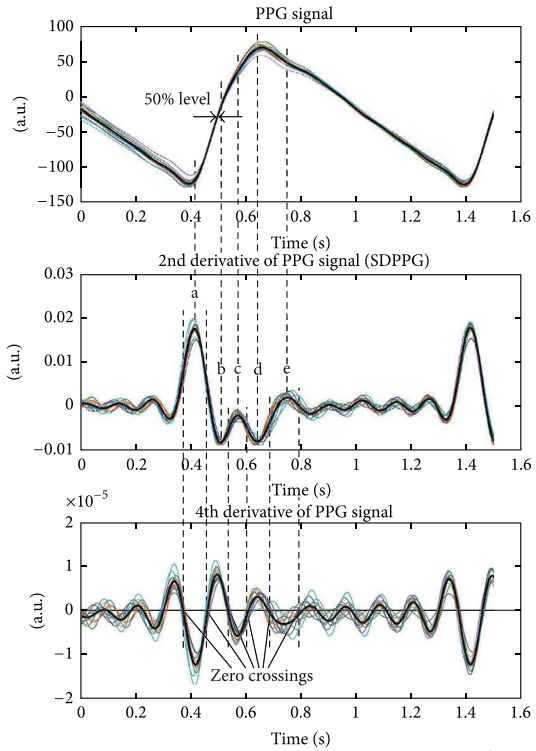

Figure 4: The averaged PPG and its second derivative and fourth derivative waveforms (black bold line) with filtered and normalized recurrences (thin lines). The recurrences are aligned according to 50% of the PPG signal raising front and the distinct waves "a", "b", "c", "d", and "e" are detected by using the zero crossings of the fourth derivative.

The standard deviations for the normalized amplitudes, *b*/*a*, *c*/*a*, *d*/*a*, *e*/*a*, and *AGI* were calculated for each edge frequency. For the standard deviation calculation, the normalized amplitudes, x_a, from normalized SDPPG recurrences and from the averaged SDPPG waveform were used. The normalized amplitudes from the averaged SDPPG waveform were taken as average values x_{avg}. The standard deviations were calculated for signals from each healthy subject, *k*, by using following equation:

$$SD(k) = \sqrt{\frac{\sum_{i=1}^{n} \left(x_a(i) - x_{avg}\right)^2}{n-1}}, \quad (1)$$

where *i* is the number of period and *n* is the total number of periods in the processed signal. Similarly, the standard deviation of the detected wave peaks on the time domain was calculated. The standard deviations were averaged over the group of subjects by using following equation:

$$SD_{avg} = \frac{1}{m} \cdot \sum_{k=1}^{m} SD(k), \quad (2)$$

where *m* is the total number of healthy subjects.

2.3. Pilot Study on Patients. The improved SDPPG signal analysis algorithm was tested on the signals from a group of healthy and diabetes patients. The optimal PM low-pass filter edge frequency was used for the analysis. The SDPPG waves were detected and *AGI* values were calculated with standard deviations.

2.4. Subjects. The study was performed after approval of the protocol by the Tallinn Ethics Committee on Medical Research at the National Institute for Health Development, Estonia. The PPG signals for the analysis were registered from healthy subjects and diabetes patients.

All the subjects in the healthy group were aged from 21 to 66 years. They were not on permanent medication and they were dealing with various levels of physical activity in their everyday lives. As the waveform of the PPG signal varies with age, the subjects were divided into the following age groups: 20–30, 30–40, 40–50, 50–60, and 60–70. Each age group, except the groups of 50–60 and 60–70, comprised five subjects. Those age groups comprised three subjects, because it was difficult to find healthy subjects to fulfill our criteria. In all, 21 healthy subjects ($m = 21$) participated in the study.

All subjects in the group of diabetes patients had received diagnosis from a medical doctor. In all, 20 diabetes patients participated in this pilot study. The patients were aged between 27 and 66 years. The diabetes patients may have increased arterial stiffness due to the sclerotic processes in the vessels.

2.5. Instrumentation. All signal processing was carried out in MATLAB. The high- and low-pass filter coefficients were calculated by using the "fir1" function. A separate function was written for calculating coefficients of the SNRD [18]. The coefficients of PM filter were calculated using functions "firpmord" and "firpm."

The PPG signals were registered from the index finger by using an experimental measurement complex [21], which included a Nellcor finger clip sensor and lab-built PPG module, among other devices. The PPG signal was digitized with a PCI MIO-16-1 data acquisition card and registered with LabVIEW environment. The sampling frequency was 1 kHz. The 1-minute long signal was recorded, and a 15-period long segment ($n = 15$) was selected for the SDPPG analysis. The signal registration was carried out, while the subject was in a resting position. The subject was in a resting position at least 10 minutes prior to the measurements. The room temperature was around 23 degrees during the experiments.

3. Results

The general change in standard deviation of the normalized amplitudes and *AGI* in cases of different edge frequencies is illustrated in Figures 5(a)–5(e). For each edge frequency, the given standard deviation is averaged over the group of healthy subjects. The minimal average standard deviation for *AGI*, *b*/*a*, *c*/*a*, *d*/*a*, and *e*/*a* is 0.06, 0.02, 0.04, 0.03, and 0.02 respectively. For all parameters, the minimal standard

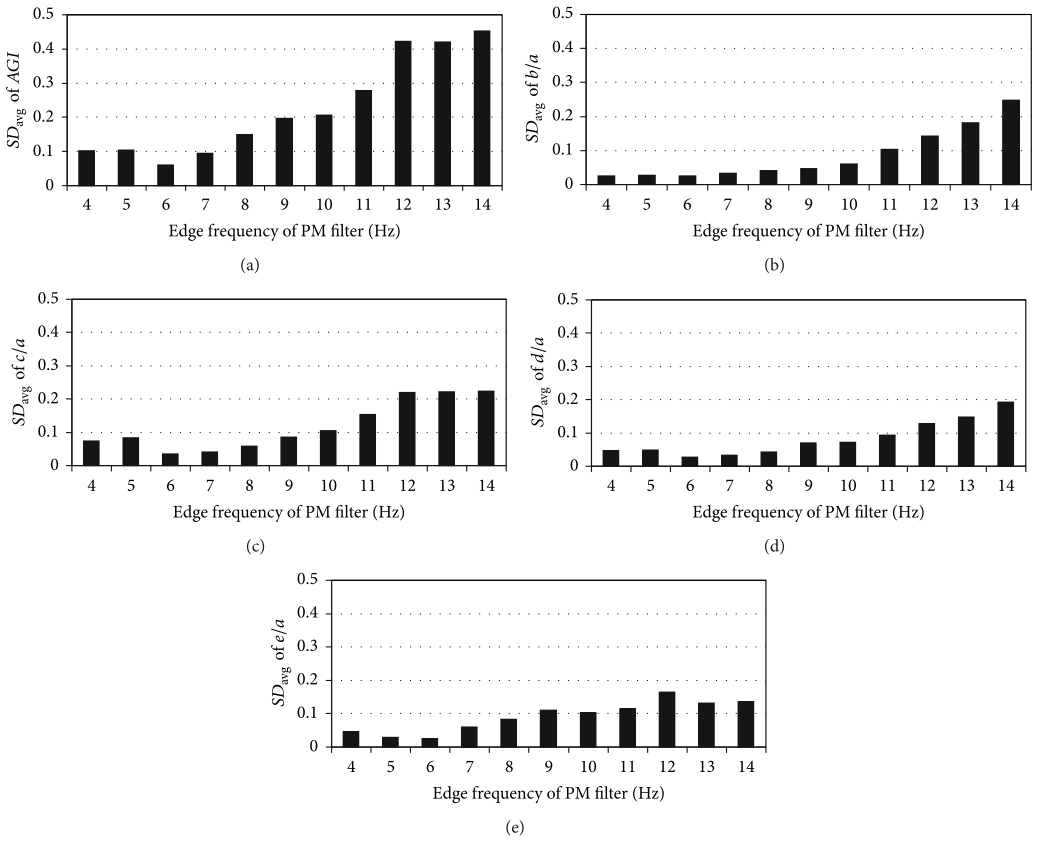

FIGURE 5: The average standard deviations (SD_{avg}) of *AGI* and normalized amplitudes at different edge frequencies for 21 healthy subjects. (a) *AGI*s at different edge frequencies; (b) normalized amplitudes b/a at different edge frequencies; (c) normalized amplitudes c/a at different edge frequencies; (d) normalized amplitudes d/a at different edge frequencies; (e) normalized amplitudes e/a at different edge frequencies.

deviation was found where the edge frequency of the PM filter is 6 Hz and transition band is 1 Hz.

Similarly, in Figures 6(a)–6(e), the standard deviations to characterize the dispersion of wave peaks "a", "b", "c", "d", and "e" in the time domain are given. The given standard deviations are averaged over the group of healthy subjects. The minimal average standard deviations for wave peaks "a", "b", "c", "d", and "e" in the time domain are 2.2 ms, 1.9 ms, 4.6 ms, 2.8 ms, and 5.0 ms, respectively. The minimal standard deviations can be found for the edge frequency of 6 Hz for all waves, except for wave "b". In the case of wave "b", the minimal standard deviation was at edge frequency of 4 Hz.

For the purpose of comparison, the same PPG signals were also processed with the algorithm described by Millasseau et al. [17]. The average standard deviation for *AGI* value is 0.12.

The *AGI* and age relationship for the healthy subjects and diabetes patients with standard deviation bars are illustrated in Figure 7(a). The PM filter edge frequency and transition-band were 6 Hz and 1 Hz, respectively, which according to the previously presented results seems to be optimal for the SDPPG analysis. In addition, regression analysis was carried out in order to estimate the relationship between *AGI* and age by using generalized linear model. As a first approach the general linear model was used, which is a case of the generalized linear model with identity link function. A following regression model was proposed: $y_{\mathrm{AGI}} = 0.019x - 1.556$. Despite of relatively simple model high correlation $r = 0.91$ was found between *AGI* and age for the healthy group, which shows the strong linear relationship between two variables.

In Figure 7(b) it can be seen the Bland-Altman plot for the proposed model y_{AGI}. The standard deviations for the model a $SD_{\mathrm{AGI}} = 0.126$. For diabetes patients the mean *AGI* value difference from the proposed model y_{AGI} is $mean_{\mathrm{Dia}} = 0.359$. The *AGI* differences from the proposed model y_{AGI} were compared between healthy and diabetes patients groups. Paired t-test (two-sample assuming unequal variances) was performed in MS Excel with $\alpha = 0.05$. The significance level of paired t-test was $P < 0.0005$, which shows the difference between two groups.

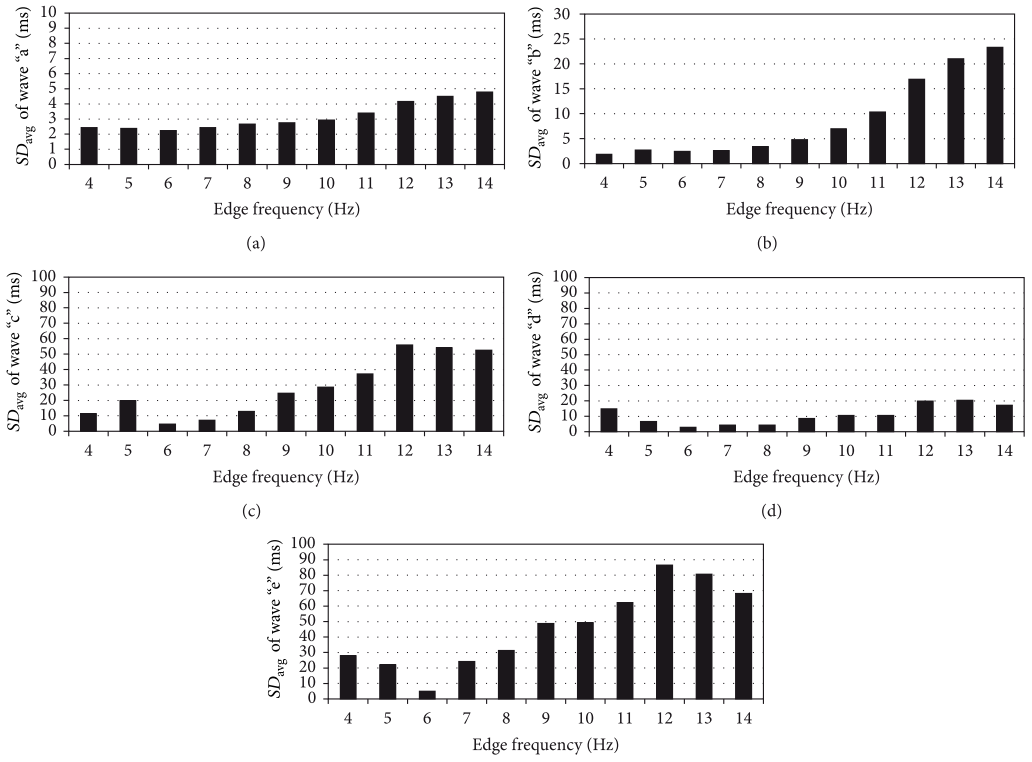

Figure 6: The average standard deviations (SD_{avg}) of the waves "a", "b", "c", "d", and "e" on the time domain at different edge frequencies for 21 healthy subjects. (a) standard deviation of wave "a" at different edge frequencies; (b) standard deviation of wave "b" at different edge frequencies; (c) standard deviation of wave "c" at different edge frequencies; (d) standard deviation of wave "d" at different edge frequencies; (e) standard deviation of wave "e" at different edge frequencies.

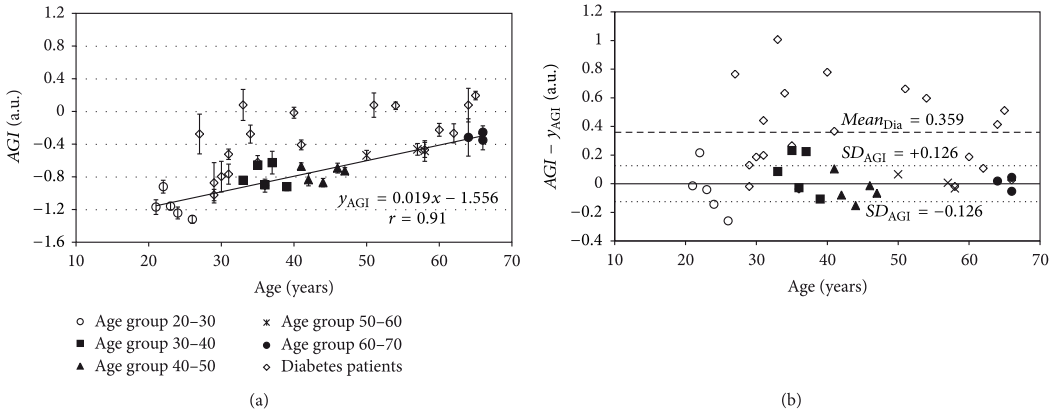

Figure 7: (a) The *AGI* data points with standard deviation (*SD*) bars for groups of healthy subjects and diabetes patients. The linear model line y_{AGI} is constructed for a group of healthy subjects. (b) Bland-Altman plot for constructed model. With dotted line the standard deviation levels for group of healthy subjects are given. With dashed line is given the mean *AGI* difference from linear model for diabetes patients.

4. Discussions

With an improved SDPPG analysis algorithm, the average standard deviation for the *AGI* value is 0.06, which constitutes about 5% of the whole scale of *AGI* [12]. Compared to the algorithm of Millasseau et al. [17], the average standard deviation is twice lower. As a result, subjects with increased arterial stiffness can be more easily differentiated from healthy subjects, and the prevention of cardiovascular disease can be improved.

The relatively high correlation relation was found between *AGI* and age by using the algorithm with optimal edge frequency (Figure 7(a)). This is in relation to previously published results by Takazawa et al. [12], in which a good correlation between *AGI* and age among healthy subjects was shown. There are still some deviations from the regression model line, y_{AGI}, which can be caused by the impact of cardiovascular deficiencies and the subject's biological age. In addition model can be more complex and dependent on additional variables, such as blood pressure. However, this should be considered in the scope of future studies.

The noticeably higher *AGI* values, compared to the healthy group of subjects, were found for diabetes patients (Figure 7(a)). The same behavior is also visible in Figure 7(b). Furthermore, the statistically significant difference was found between the healthy subjects and diabetes patients. The higher *AGI* values are caused by the increased arterial stiffness of diabetes patients. Nevertheless, some of the diabetes patients have similar *AGI* values compared to healthy subjects. It can be caused by the early diagnosis of diabetes mellitus, which is followed with efficient therapy, and as a result premature stiffening of the arteries has been stopped.

It can be seen from Figures 5(a)–5(e) that the lowest average standard deviation was achieved when the edge frequency of PM filter is 6 Hz. Close to 6 Hz, the normalized recurrences start to resemble. The larger standard deviations on higher edge frequencies are caused by the noise and unwanted frequency components of the PPG signal, which are situated at higher frequencies and amplified through differentiation. This causes the faulty detection of the waves from the single normalized recurrence and averaged SDPPG waveform. At lower edge frequencies, the harmonic components are suppressed, which form waves "a", "b", "c", "d", and "e", and the peaks of waves, "c" and "d", were missing in single normalized recurrences. As a result, the amplitude of the waves in single normalized recurrences and averaged SDPPG waveform are different, which caused the increase in standard deviation (Figures 5(a)–5(e)). This means that it is necessary to have a fundamental harmonic with 5 higher harmonic components in order to detect waves "a", "b", "c", "d", and "e" from the PPG signal.

The dispersion of wave peaks on time domain decreases, similar to the results seen in Figure 5, when the edge frequency of PM filter approaches 6 Hz (Figures 5(a)–6(e)). As in Figure 5, the detection of the waves from the single normalized recurrences and from the averaged SDPPG waveform can be different at higher frequencies, which increases the standard deviation. At frequencies lower than 6 Hz, the wave peaks can be missing in single normalized recurrence and the detection point is shifted compared with the averaged SDPPG waveform.

5. Conclusions

In conclusion, it can be said that the standard deviation of *AGI* values is minimized by using the improved SDPPG algorithm. Furthermore, the diabetes patients have noticeably higher *AGI* values, which are caused by an increase in the arterial stiffness. As a result, the subjects, with increased arterial stiffness can be more easily differentiated from healthy subjects and the prevention of cardiovascular disease can be improved. As a future study the more complex model should be considered in order to enhance the discrimination of the healthy subjects and patients with increased stiffness by taking into account additional physiological variables. In addition proposed algorithm should be compared with similar arterial stiffness estimation reference methods.

Acknowledgments

This work was supported by the Estonian Science Foundation Grant no. 7506, by the Estonian Targeted Financing Project SF0140027s07, and by the European Union through the European Regional Development Fund.

References

[1] M. W. Rajzer, W. Wojciechowska, M. Klocek, I. Palka, M. Brzozowska-Kiszka, and K. Kawecka-Jaszcz, "Comparison of aortic pulse wave velocity measured by three techniques: complior, sphygmocor and arteriograph," *Journal of Hypertension*, vol. 26, no. 10, pp. 2001–2007, 2008.

[2] S. S. Silvera, H. E. Aidi, J. H. F. Rudd et al., "Multimodality imaging of atherosclerotic plaque activity and composition using FDG-PET/CT and MRI in carotid and femoral arteries," *Atherosclerosis*, vol. 207, no. 1, pp. 139–143, 2009.

[3] M. R. Skilton, L. Boussel, F. Bonnet et al., "Carotid intima-media and adventitial thickening: comparison of new and established ultrasound and magnetic resonance imaging techniques," *Atherosclerosis*, vol. 215, no. 2, pp. 405–410, 2011.

[4] C. F. Clarenbach, A. Stoewhas, A. J. R. Van Gestel et al., "Comparison of photoplethysmographic and arterial tonometry-derived indices of arterial stiffness," *Hypertension Research*, vol. 35, no. 2, pp. 228–233, 2012.

[5] J. Allen, "Photoplethysmography and its application in clinical physiological measurement," *Physiological Measurement*, vol. 28, pp. R1–R39, 2007.

[6] A. A. R. Kamal, J. B. Harness, G. Irving, and A. J. Mearns, "Skin photoplethysmography—a review," *Computer Methods and Programs in Biomedicine*, vol. 28, no. 4, pp. 257–269, 1989.

[7] L. G. Lindberg and P. Å. Öberg, "Optical properties of blood in motion," *Optical Engineering*, vol. 32, pp. 253–257, 1993.

[8] K. Pilt, K. Meigas, R. Ferenets, and J. Kaik, "Photoplethysmographic signal processing using adaptive sum comb filter for pulse delay measurement," *Estonian Journal of Engineering*, vol. 16, no. 1, pp. 78–94, 2010.

[9] M. Huotari, N. Yliaska, V. Lantto, K. Määttä, and J. Kostamovaara, "Aortic and arterial stiffness determination by photoplethysmographic technique," *Procedia Chemistry*, vol. 1, no. 1, pp. 1243–1246, 2009.

[10] S. C. Millasseau, J. M. Ritter, K. Takazawa, and P. J. Chowienczyk, "Contour analysis of the photoplethysmographic pulse measured at the finger," *Journal of Hypertension*, vol. 24, no. 8, pp. 1449–1456, 2006.

[11] U. Rubins, "Finger and ear photoplethysmogram waveform analysis by fitting with Gaussians," *Medical and Biological Engineering and Computing*, vol. 46, no. 12, pp. 1271–1276, 2008.

[12] K. Takazawa, N. Tanaka, M. Fujita et al., "Assessment of vasoactive agents and vascular aging by the second derivative of photoplethysmogram waveform," *Hypertension*, vol. 32, no. 2, pp. 365–370, 1998.

[13] J. Hashimoto, D. Watabe, A. Kimura et al., "Determinants of the second derivative of the finger photoplethysmogram and brachial-ankle pulse-wave velocity: The Ohasama study," *American Journal of Hypertension*, vol. 18, no. 4, pp. 477–485, 2005.

[14] T. Otsuka, T. Kawada, M. Katsumata, and C. Ibuki, "Utility of second derivative of the finger photoplethysmogram for the estimation of the risk of coronary heart disease in the general population," *Circulation Journal*, vol. 70, no. 3, pp. 304–310, 2006.

[15] T. Otsuka, T. Kawada, M. Katsumata, C. Ibuki, and Y. Kusama, "Independent determinants of second derivative of the finger photoplethysmogram among various cardiovascular risk factors in middle-aged men," *Hypertension Research*, vol. 30, no. 12, pp. 1211–1218, 2007.

[16] A. Grabovskis, Z. Marcinkevics, Z. Lukstina et al., "Usability of photoplethysmography method in estimation of conduit artery stiffness," in *Novel Biophotonic Techniques and Applications*, vol. 8090 of *Proceedings of SPIE*, May 2011.

[17] S. C. Millasseau, R. P. Kelly, J. M. Ritter, and P. J. Chowienczyk, "The vascular impact of aging and vasoactive drugs: comparison of two digital volume pulse measurements," *American Journal of Hypertension*, vol. 16, no. 6, pp. 467–472, 2003.

[18] P. Holoborodko, "Smooth noise robust differentiators," http://www.holoborodko.com/pavel/numerical-methods/numerical-derivative/smooth-low-noise-differentiators/, 2008.

[19] T. W. Parks and J. H. McClellan, "Chebyshev approximation for nonrecursive digital filters with linear phase," *IEEE Transactions Circuit Theory*, vol. 19, no. 2, pp. 189–194, 1972.

[20] W. W. Nichols and M. F. O'Rourke, *McDonald's Blood Flow in Arteries: Theoretic, Experimental and Clinical Principles*, Hodder-Arnold, London, UK, 5th edition, 2005.

[21] K. Pilt, K. Meigas, M. Viigimaa, K. Temitski, and J. Kaik, "An experimental measurement complex for probable estimation of arterial stiffness," in *Proceedings of the 32nd International Conference of the IEEE Engineering in Medicine and Biology Society*, pp. 194–197, Buenos Aires, Argentina, 2010.

PUBLICATIONS

Publication IV

Pilt K, Meigas K, Temitski K, Viigimaa M (2012) "Second derivative analysis of forehead photoplethysmographic signal in healthy volunteers and diabetes patients", *In: IFMBE Proceedings of World Congress on Medical Physics and Biomedical Engineering, Beijing, China, May 26-31*, 410-413 (DOI: 10.1007/978-3-642-29305-4_109).

Second derivative analysis of forehead photoplethysmographic signal in healthy volunteers and diabetes patients

K. Pilt, K. Meigas, K. Temitski and M. Viigimaa

Tallinn University of Technology / Technomedicum / Department of Biomedical Engineering, Tallinn, Estonia

Abstract— **The second derivative analysis has been used to characterize the changes in forehead photoplethysmographic (PPG) signal, which are caused by the stiffness of blood vessels. Before the distinctive wave amplitudes were measured the forehead PPG signals from healthy volunteers and diabetes patients were filtered, two times differentiated, normalized in length, and averaged. The correlation relationships between normalized amplitudes and age were found. The values of normalized amplitudes b/a and d/a were found to be influenced by the stiffness of the blood vessels.**

Keywords— **Photoplethysmography, second derivative method, arterial stiffness.**

I. Introduction

There has been increasing interest in the non-invasive methods for screening and diagnosis of cardiovascular diseases [1]. The stiffening of the arteries has been considered to be an early sign of pathology in arteriosclerosis [2] and number of non-invasive devices has been developed for the screening and diagnosis (Arteriograph, Complior, Sphygmocor). It has been found that a decrease in small arterial compliance appears with the structural changes in the large arteries [3]. Photoplethysmographic (PPG) waveform analysis has been used as one method for the estimation of peripheral arterial stiffness [4].

PPG is an optical non-invasive technique for monitoring blood perfusion in the skin [5]. The light from the source, which is often red or infrared, is emitted to the skin. The light is absorbed, reflected and scattered in the tissue and blood. A small fraction of light intensity changes are received by a photodetector, which can be placed adjacent to the light source (reflection mode) or to the opposite side of the measured volume (transmission mode). Changes in the intensity of the received light are related to blood flow, blood volume, blood vessel wall movement and the orientation of red blood cells in the underlying tissue.

The DC component of the PPG signal varies slowly and reflects variations in the total blood volume of the examined tissue. The AC component is synchronous with the heart rate and depends on changes in the pulsatile pressure and pulsatile blood volume. Both components of the PPG signal can be influenced by respiration, regulatory features such as vasomotion, sympathetic nervous system activity and other factors that influence local perfusion.

The AC component waveform of the finger PPG signal has been analyzed by second derivative method. The method is used to quantify the changes in the signal, which can be caused, besides the other factors, also by the stiffness changes in the microvascular bed. The second derivative of the PPG signal (SDPPG) was firstly introduced by Takazawa et al [6]. They analyzed the SDPPG waveform amplitudes of the distinctive waves ‘a’, ‘b’, ‘c’, ‘d’, and ‘e’, which are situated in the systolic part of the heart cycle (Fig. 1). The amplitudes of the waves are normalized as follows: b/a, c/a, d/a, and e/a. They found that normalized amplitude b/a increases and c/a, d/a, and e/a decrease in proportion to the increase of the subject’s age.

The PPG signal can be obtained easily from forehead by using reflection mode sensor. This location has been used for the SpO_2, respiration [7] and heart [8] and respiration rate monitoring. Our interest is to use the forehead PPG signal second derivative analysis for the arterial stiffness estimation. The vascular bed of the forehead tissue differs from the finger and it may reveal new possibilities for the stiffness estimation. There is also lack of information about forehead SDPPG analysis from relevant literature unlike with finger signal.

II. Methods

The forehead signal has been registered by using commercially available MASIMO LNOP TF-I forehead sensor. It consists of LED and photodetector, which are placed adjacent to each other. The photodetector registers the back reflected light intensity changes. The distance between LED and photodetector centers is 7mm. The LED consists of two light sources with wavelengths of 880nm (infrared) and 660nm (red). In this study the infrared LED was used. The MASIMO sensor is connected to the lab-built PPG module. The output signal from PPG module is digitalized with National Instruments PCI MIO-16-E1 data acquisition card with sampling frequency of 1kHz. The PPG signal is monitored in online and recorded through program, which is written in LabVIEW environment [9].

M. Long (Ed.): World Congress on Medical Physics and Biomedical Engineering, IFMBE Proceedings 39, pp. 410–413, 2012.
www.springerlink.com

The registered signals are analyzed in MATLAB environment. The PPG signal was filtered with low- and high-pass FIR filters in order to separate DC components and high frequency noise. The cut-off frequencies for the low- and high-pass filters were selected as 30 Hz and 0.5 Hz, respectively. Both filters were designed using window method, with the Hamming window function where the corresponding filter orders were chosen as 500 for the low-pass and 4000 for the high-pass filter.

As follows, the PPG signal was differentiated two times. The differentiator works as a high-pass filter and as a result the higher frequency components are amplified. The higher frequencies have to be suppressed, because it consists of unwanted noise, which are amplified. The Smooth Noise Robust Differentiator (SNRD) was used, because this kind of differentiation suppresses also the higher frequencies. The SNRD has been developed for experiments with noisy data where differentiation is required [10]. In this study the fifth order of the SNRD was used.

Higher frequency components need to be suppressed with FIR filter even after the SNRD, because of the amplified noise. In practice, biosignals such as PPG, which are related to the heart activity, are recurring but not periodic. This means that the harmonic components of the two consecutive recurrences of the PPG signal and its derivatives can be situated at different frequencies. In this study the low-pass filter was used with static edge-frequency. By this follows that certain numbers of harmonic components are passed and all the others are suppressed. The lengths of the PPG signal recurrences are then normalized to ensure that all the harmonic components are processed in the same way.

All the recurrences of PPG signal was limited equally with six harmonical components, which has been found as optimal for the SDPPG signal analysis in the previous study. Firstly, the PPG signal was resampled in such a way that one of the selected recurrence length was 1s, which corresponds to the pulse frequency of 1 Hz. In this case the fundamental frequency is situated at 1 Hz. All the other components lay at the frequency multiples of the fundamental frequency. Secondly, the signal was filtered with Parks-McClellan optimal equiripple FIR (PM) filter with edge-frequency of 6Hz and width of transition-band was 1Hz. The maximum allowable errors, i.e. ripples, for the pass- and stop-band were set at 0.001. The resampling and filtering was also carried out with the second derivative of the PPG signal. Thirdly, the copy of selected recurrence was aligned with other normalized and filtered recurrences from this PPG signal. The 50 per cent level of the PPG signal raising front was used as the reference point for the alignment of the recurrences. Furthermore the second derivative was moved according to the movement of the PPG signal

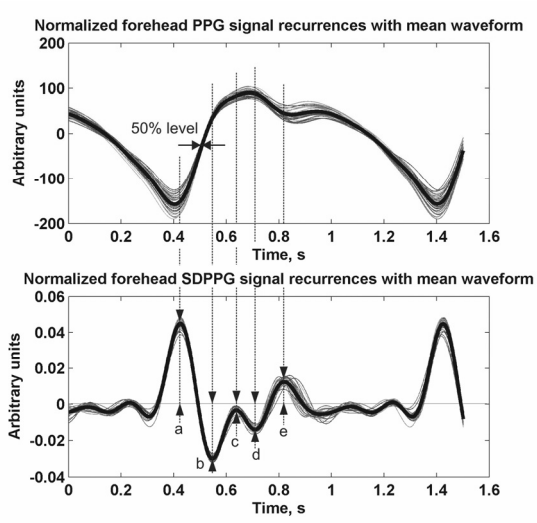

Fig. 1 Forehead PPG signal and second derivative of PPG signal with detected amplitudes ‘a’, ‘b’, ‘c’, ‘d’, and ‘e’. Normalized forehead PPG signal recurrences are given with thin gray lines and calculated mean waveform is given with bold line (upper figure). Normalized forehead SDPPG signal recurrences are given with thin gray lines and calculated mean waveform is given with bold line (lower figure).

recurrences. The resampling, filtering and aligning processes outlined above have been carried out separately for every recurrence in PPG signals. As a result the normalized and averaged PPG signal and its second derivative waveforms were calculated from processed recurrences. The amplitudes 'a', 'b', 'c', 'd', and 'e' were detected from normalized and averaged SDPPG signal (Fig. 1).

It is difficult to determine the stiffness of the blood vessels in the vascular bed of forehead. In this study we used the Arteriograph (TensioMed, Budapest, Hungary) measurements as reference to determine the pulse wave velocity (PWV) in aorta [11]. PWV is related to the stiffness of aorta through Moens-Korteweg equation [12]. With the increased PWV in aorta we can assume that also the stiffness of the blood vessels in forehead has been increased.

The PPG signal registration and measurements with Arteriograph were performed on 22 volunteers (18 males and 4 females with mean age of 36 year) and on 2 diabetic patients (one male and one female with mean age of 30). The subject was in the supine position for at least 20 minutes before the measurements and this position also remained constant during the registration of the signals. The room temperature was kept constant at around 23 degrees Celsius during the experiments. Firstly, the Arteriograph measurement was carried out. In all measurements the cuff size was

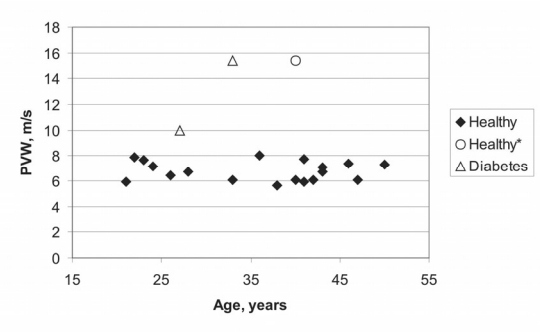

Fig. 2 The relationship between Arteriograph measured aortic PWV and age for healthy volunteers and diabetes patients.

set, in accordance with the manufacturer's recommendation, as small as possible and placed tightly around the left arm. The measurement with Arteriograph is carried out and the average aortic PWV is calculated automatically by the TensioClinic (TensioMed, Budapest, Hungary) program. Arteriograph measurement was followed by the 1 minute long PPG signal registration from forehead. For every registered signal the above described signal processing was carried out and the amplitudes were detected from the normalized and averaged SDPPG waveform.

III. Results

The Arteriograph measured aortic PWV and age relationship is shown in Fig. 2. The standard deviation for every measurement was below 1m/s. The measurement results are given for healthy volunteers (Healthy), volunteer, who had noticeably higher PWV (Healthy*) and diabetes patients (Diabetes). The 40 year old volunteer had abnormally high PWV – 15.4m/s. Later examination showed that the subject had hypertension. It is also visible from the figure that diabetes patients have higher PWV than healthy volunteers.

The normalized amplitudes of the SDPPG signal and age relationships are given in Fig. 3. The normalized amplitude b/a of SDPPG has the positive correlation relationship to the age $r = 0.60$. The normalized amplitudes c/a, d/a, and e/a of SDPPG have negative correlation relationship to the age $r = -0.24$, $r = -0.59$, and $r = -0.50$ respectively. For each relationship the regression model was proposed. The regres-

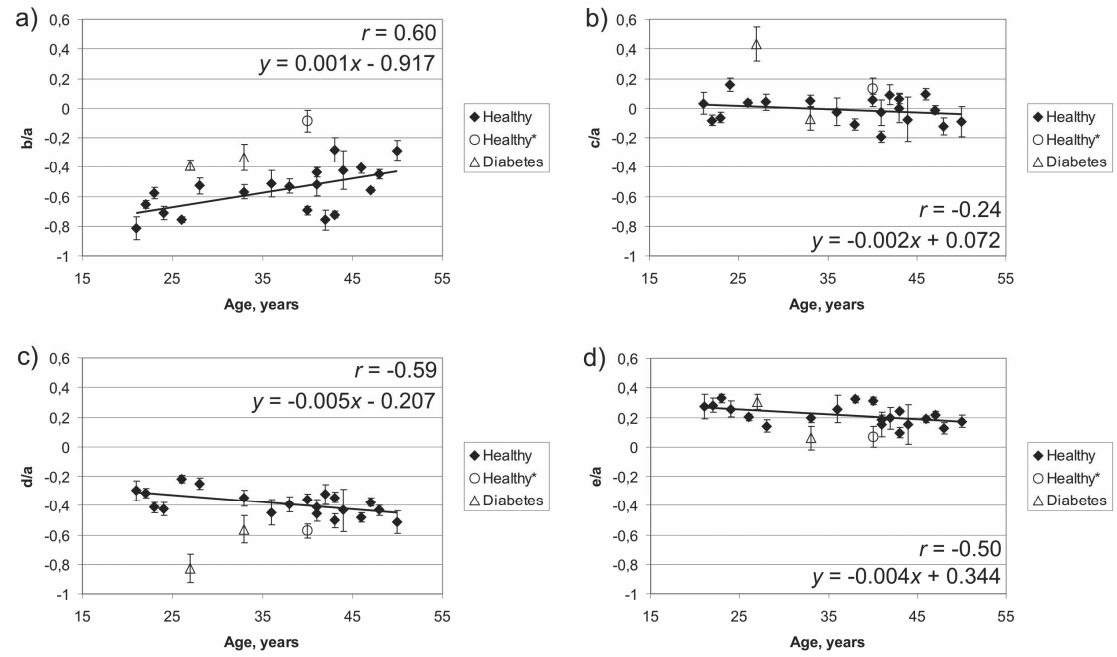

Fig. 3 The relationship between SDPPG normalized amplitudes a) b/a, b) c/a, c) d/a, d) e/a, and age with regression lines and correlation coefficients.

sion model was constructed by taking account only the healthy subjects. The standard deviations are given with bars for every subject.

IV. Discussion

The aortic PWV and normalized amplitudes of the SDPPG relationship to the age is given in Fig. 2 and 3, because the stiffness of the arteries should increase with age. High positive correlation between age and aortic PWV has also been reported before [13]. Still the positive correlation is not clearly visible in Fig. 2. It can be due to the number and narrow age range of the volunteers, who participated in the study. Healthy volunteers had aortic PWVs below 9m/s except one, who had PWV of 15.4m/s. The diabetes patients with age of 27 and 33 have high aortic PWVs of 10m/s and 15.4m/s respectively, which show the stiffening of the aorta.

The normalized amplitudes of finger SDPPG signal correlation relationship to the age was analyzed in the previous studies [6]. Here presented correlation relationships for the forehead SDPPG signal agrees with the finger. Normalized amplitudes b/a have positive and c/a, d/a, and e/a have negative correlation to the age. Still the absolute values of SDPPG normalized amplitudes differ between the forehead and finger. It can be due to the differences of the waveforms between the forehead and finger signal. In addition the number of subjects in this study is relatively low. The simultaneously registered forehead and finger PPG signals have to be analyzed to make the more precise comparisons.

Diabetes patients have higher normalized amplitude b/a and lower normalized amplitude d/a value than healthy volunteers (Fig. 3a and 3c). Similar behavior is visible for the volunteer, who had higher PWV in aorta. This kind of relationship is not visible for normalized amplitudes of c/a and e/a (Fig. 3b and 3d). It can be assumed that the changes in the forehead vascular bed, which are caused by the stiffening of the blood vessels, can be described with SDPPG signal normalized amplitudes b/a and d/a. However, the number of subjects with stiffer blood vessels has to be increased to make more general conclusions.

Acknowledgment

This work was supported by the Estonian Science Foundation Grant no. 7506, by the Estonian targeted financing project SF0140027s07, and by the European Union through the European Regional Development Fund.

References

1. Skilton M R, Boussel L, Bonnet F, Bernard S, Douek P C, Moulin P, Serusclat A (2011) Carotid intima-media and adventitial thickening: comparison of new and established ultrasound and magnetic resonance imaging techniques. Atherosclerosis 215:405-410
2. Cernes R, Zimlichman R, Shargorodsky M (2008) Arterial elasticity in cardiovascular disease: focus on hypertension, metabolic syndrome and diabetes. Adv Cardiol 45:65-81
3. Cohn J N, Duprez D A, Grandits G A (2005) Arterial elasticity as part of a comprehensive assessment of cardiovascular risk and drug treatment. Hypertension 46:217–220
4. Millasseau S C, Ritter J M, Takazawa K, Chowienczyk P J (2006) Contour analysis of the photoplethysmographic pulse measured at the finger. J Hypertens 24:1449-1456
5. Allen J (2007) Photoplethysmography and its applications in clinical physiological measurement. Physiol Meas 28:R1-R39
6. Takazawa K, Tanaka N, Fujita M, Matsuoka O, Saiki T, Aikawa M, Tamura S, Ibukiyama C (1998) Assessment of vasoactive agents and vascular aging by the second derivative of photoplethysmogram waveform. Hypertension 32:365-370
7. Johansson A (2003) Neural network for photoplethysmographic respiratory rate monitoring. Med Biol Eng Comput 41:242–248
8. Kim S H, Ryoo D W, Bae C (2008) U-healthcare system using smart headband, Conf. Proc. IEEE Eng. Med. Biol. Soc., Ann. Int. Conf. IEEE Eng. Med. and Biol. Soc., Vancouver, Canada, 2008, pp 1557-1560
9. Pilt K, Meigas K, Viigimaa M, Temitski K, Kaik J (2010) An experimental measurement complex for probable estimation of arterial stiffness, Conf. Proc. IEEE Eng. Med. Biol. Soc., Ann. Int. Conf. IEEE Eng. Med. and Biol. Soc., Buenos Aires, Argentina, 2010, pp 194-197
10. Holoborodko P (2008) Smooth noise robust differentiators at http://www.holoborodko.com/pavel/numerical-methods/numerical-derivative/smooth-low-noisedifferentiators/
11. Horváth I G, Németh A, Lenkey Z, Alessandri N, Tufano F, Kis P, Gaszner B, Cziráki A (2010) Invasive validation of a new oscillometric device (Arteriograph) for measuring augmentation index, central blood pressure and aortic pulse wave velocity. Hypertens 28:2068-2075
12. Nichols W W, O'Rourke M F (2005) McDonald's blood flow in arteries. Hodder-Arnold, London
13. Ohmori K, Emura S, Takashima T (2000) Risk factors of atherosclerosis and aortic pulse wave velocity. Angiology 51:53-60

Author: Kristjan Pilt
Institute: Department of Biomedical Engineering
Street: Ehitajate tee 5
City: Tallinn, 19086
Country: Estonia
Email: kristjan.pilt@cb.ttu.ee

PUBLICATIONS

Publication V

V **Pilt K**, Meigas K, Ferenets R, Temitski K and Viigimaa M (2013) "Photoplethysmographic signal waveform index for detection of increased arterial stiffness", *Manuscript submitted*

Photoplethysmographic signal waveform index for detection of increased arterial stiffness

K Pilt, K Meigas, R Ferenets, K Temitski and M Viigimaa

Department of Biomedical Engineering, Tallinn University of Technology, Ehitajate tee 5, 19086 Tallinn, Estonia

E-mail: kristjan.pilt@cb.ttu.ee

Abstract

The aim was to assess the validity of the photoplethysmographic (PPG) waveform index *PPGAI* for the detection of increased arterial stiffness. For this purpose, PPG signals were recorded from 24 healthy subjects and from 20 type II diabetes patients. Recorded PPG signals were processed with the analysis algorithm developed and the waveform index *PPGAI* similar to the augmentation index (AIx) was calculated. As a reference, the aortic AIx was assessed and normalized for a heart rate of 75 bpm (AIx@75) by a SphygmoCor device. A strong correlation (r=0.85) between the *PPGAI* and the aortic AIx@75 and a positive correlation of both indices with the age were found. Age corrections for the indices *PPGAI* and AIx@75 as regression models from the signals of healthy subjects were constructed. Both indices revealed a significant difference between the groups of diabetes patients and healthy controls. However, the *PPGAI* provided the best discrimination as the standard deviation of the regression model constituted 39% from the average difference of the diabetes patient group. The waveform index *PPGAI* based on the inexpensive PPG technology can be considered as a perspective measure of increased arterial stiffness estimation in clinical screenings.

Keywords: Arterial stiffness, photoplethysmography, diabetes mellitus, signal processing, augmentation index

1. Introduction

It is important to detect and diagnose the early signs of cardiovascular disease in order to apply effective prevention and treatment (Perk *et al* 2012). Premature increase in arterial stiffness has been considered a risk factor for cardiovascular disease. The arterial stiffness of a subject increases with age, hypertension, and diabetes mellitus in addition to other factors (Lee and Park 2013). Different methods and devices are used to estimate arterial stiffness (Laurent *et al* 2006, Woodman *et al* 2005).

Introduced by Murgo et al (Murgo *et al* 1980) the augmentation index (AIx) has been used as a surrogate parameter for arterial stiffness (Mitchell *et al* 2004, Schram *et al* 2004). Previous studies have shown that aortic AIx increases with age due to the increase in the stiffness of the arteries (Safar and London 2000). Among other devices (Laurent *et al* 2006, Woodman 2005), SphygmoCor can be used to estimate aortic AIx from a radial artery pulse waveform. The pulse waveform from radial artery is recorded by applanation tonometry. However, this method of pulse waveform recording is often time-consuming and requires a trained operator. To estimate arterial stiffness, we need a simple screening method, which is user independent, non-invasive, inexpensive, and rapidly performed. The photoplethysmographic (PPG) waveform analysis method may fulfill these criteria (Millasseau *et al* 2006).

PPG is an optical non-invasive method that can be used to detect blood flow and volume changes in peripheral vessels and smaller arteries at different body locations (Allen 2007). The PPG sensor consists of a light source, which is often a red or an infrared light emitting diode (LED), and a

photodetector. In the transmission mode, the photodetector is placed at the opposite side of the measured volume. In the reflection mode, the photodetector is adjacent to the light source. The light is emitted from the light source to the skin, where it is absorbed, reflected and scattered in the tissue and blood. A small fraction of back scattered (reflection mode) or transmitted (transmission mode) light intensity changes is received by the photodetector.

The PPG signal consists of a large and slowly varying DC component and about ten times smaller pulsating AC component. The pulsations in the AC component of the PPG signal are synchronous with the heart rate and depend on the changes in the pulsatile pressure and pulsatile blood volume. The AC component of the PPG signal is characterized by systolic and diastolic phases, which are separated by a notch or an inflection point (Chan *et al* 2007). Though origins of the pulsatile waveform components of the PPG signal have been studied; the phenomenon is still not fully understood (Allen 2007). Generally, it has been accepted that the AC component of the PPG signal can provide valuable information about the cardiovascular system.

It has been found that the PPG signal waveform depends on the location where the sensor is attached on the body (Allen and Murray 2003). In addition, the waveform changes are dependent on the biological age of the subject, which can be associated with the stiffness of blood vessels (Millasseau *et al* 2002, Hlimonenko *et al* 2003, Pilt *et al* 2012). The finger PPG signal waveform changes caused by aging have been studied on a frequency domain (Sherebrin and Sherebrin 1990).

Changes in the finger PPG signal waveform can be characterized through the amplitudes of distinctive points, which can be determined from period to period and subject to subject. As the PPG signal waveform is smooth compared to the pressure waveform, the early and late systolic inflection points cannot be easily detected. Within one period, a PPG signal has several convexes and concaves, visualized through the second derivative PPG (SDPPG) signal (Takazawa *et al* 1998). In our earlier study, an improved SDPPG waveform analysis algorithm was introduced for the arterial stiffness estimation (Pilt *et al* 2013a). Furthermore, in our pilot study, the normalized amplitudes at the locations of the SDPPG signal peaks were calculated and used as indices for cardiovascular aging (Pilt *et al* 2013b). In this study, the PPG waveform augmentation index (PPGAI) similar to the aortic augmentation index is calculated based on the normalized amplitudes for the discrimination of the subjects with higher arterial stiffness. The purpose is to compare the proposed PPG waveform PPGAI index with the SphygmoCor derived aortic AIx and to show that PPGAI index can be used for detection of premature cardiovascular ageing among diabetes patients. The study has been carried out on healthy subjects and diabetes patients with probable increase in arterial stiffness.

2. Methods

2.1 Subjects

We studied 24 healthy subjects between the age of 21 and 66 years (14 males and 10 females with a mean age of 41 years) and 20 type II diabetic patients (5 males and 15 females with a mean age of 44 years) between the age of 27 and 66 years. Nineteen healthy volunteers were engaged in some physical training or activity at least once a week. For healthy subjects, the blood pressure and body mass index had to be lower than 140/90mmHg and $<30 kg/m^2$, respectively. As different from healthy subjects, all the diabetes patients had glycohemoglobin above the normal level (5.9%).

The subject was in the supine position for at least 20 minutes before the blood pressure measurements. The supine position remained constant also during the radial artery waveform recording with a SphygmoCor device. After that during one minute the PPG and ECG signals were recorded. PPG signals were recorded from the index finger of the left hand. The room temperature was kept constant at around 23 ± 1 degrees Celsius.

This study has been approved by the Tallinn Ethics Committee on Medical Research at the National Institute for Health Development, Estonia. All the subjects gave written informed consent to participate in this study.

2.2 Determination of aortic AIx

The SphygmoCor device (AtCor Medical, Australia) was used to assess arterial stiffness. The peripheral pulse waveforms were recorded from the radial artery at the wrist by using applanation tonometry. The operator had passed SphygmoCor measurements training and had completed several hundred recordings. After the waveform was stabilized, the 10-second signal was recorded with a sampling rate of 128Hz. About 10 recurrences per subject were used in the analysis of the pulse

waveform. According to the recommendations from the manufacturer, only the recordings with an operator index above 85 (in the scale of 0 to 100) were used. The aortic waveform is generated from the radial artery waveform by using validated generalized transfer function (Chen *et al* 1997). AIx is derived from the aortic pulse waveform, as shown in figure 1. The AIx is expressed in percentages is calculated as follows:

$$AIx = \frac{P_1 - P_2}{PP} = \frac{AP}{PP}, \qquad (1)$$

where *PP* is the pulse pressure and *AP* is the augmentation pressure. As the AIx depends on the heart rate, the index has been normalized for the heart rate of 75bpm (Wilkinson *et al* 2000). The normalized AIx value is denoted as AIx@75. The AIx and AIx@75 values typically increase with age as the arteries turn out to be stiffer.

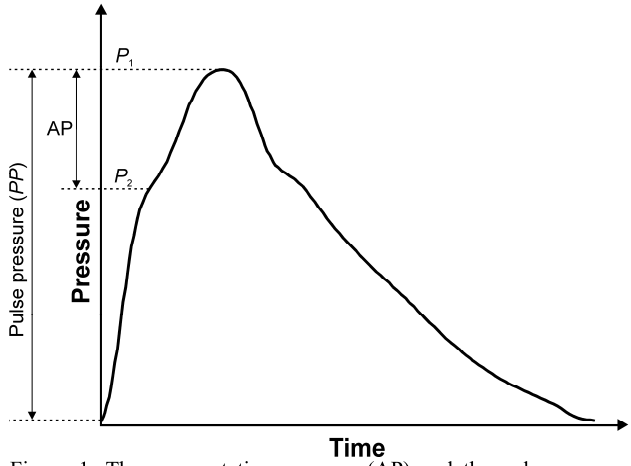

Figure 1. The augmentation pressure (AP) and the pulse pressure are determined from an average aortic pressure waveform and used for the AIx calculation.

2.3 Instrumentation

The PPG and ECG signals were registered by an experimental measurement complex described in our earlier paper (Pilt *et al* 2010). The commercially available Envitec F-3222-12 finger clip sensor (Honeywell, Germany) was connected to the lab-built PPG module. The PPG signal was recorded by the infrared LED of the sensor at the wavelength of 880nm. The single channel ECG signal was recorded synchronously with the PPG signal. The signals were digitized with a National Instruments PCI MIO-16-E1 data acquisition card (National Instruments, USA). The sampling frequency was set to 1kHz. The signals were monitored and recorded in the LabVIEW (National Instruments, USA) written program.

2.4 Analysis of PPG signal waveform and PPGAI

The PPG signal waveform was analyzed according to the algorithm described in our earlier studies (Pilt *et al* 2013a, Pilt *et al* 2013b). Briefly, a recorded PPG signal is filtered with a FIR high- and low-pass filter. Filters are designed using the window method, with the Hamming window function and the cut-off frequencies are selected 0.5Hz (filter order: 4000) and 30Hz (filter order: 500), respectively. The beginning and ending points of each recurrence in the PPG signal are detected by using R-peaks of the ECG signal. Thereafter, the PPG signal is differentiated for two and four times.

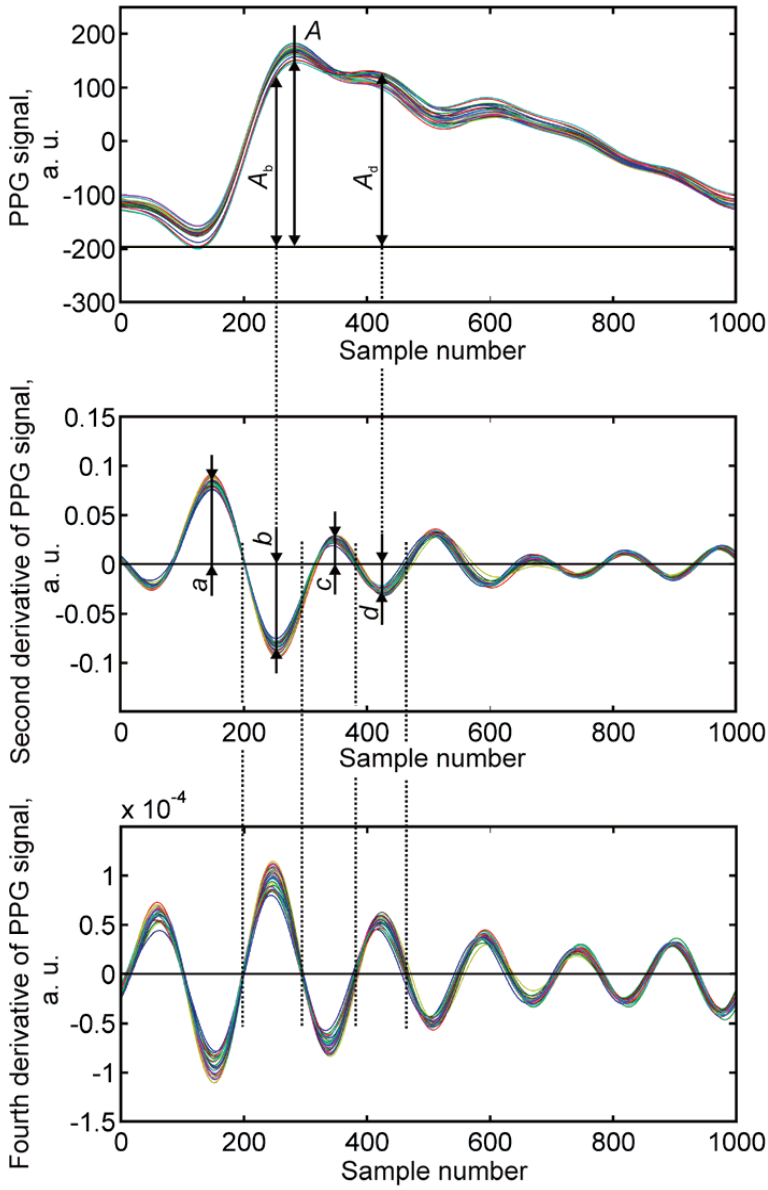

Figure 2. The resampled, filtered, and aligned waveforms from the constructed matrices with the detected wave peaks. Each colored line corresponds to one recurrence from the processed PPG signal.

As it follows here, all the recurrences of the PPG signal are limited equally with six harmonic components. For that purpose, the PPG signal is resampled such that one of the selected recurrence lengths is 1 s (1000 samples), which corresponds to the pulse frequency of 1 Hz. The resampled signal is filtered with a Parks-McClellan low-pass filter with an edge frequency of 6 Hz and a transition band of 1Hz. The maximum allowable errors, i.e. ripples, for the pass- and stop-band were set at 0.001. The

selected recurrence is now limited with six harmonic components and a copy of it is placed into the matrix. The copy of the selected recurrence is aligned in the matrix with other filtered recurrences from this PPG signal. The 50 per cent level of the PPG signal raising front is used as the reference point for the alignment of the recurrences in the matrix. The next recurrence is then selected from the PPG signal and the resampling, filtering and alignment process previously described is completed. Similarly, the recurrences are processed from the derivative signals and the matrices with recurrences are constructed. The constructed matrices for one PPG signal are illustrated in figure 2.

The fourth derivative waveform was used to detect the peaks from the SDPPG waveform. The SDPPG waveform peaks are looked up in the zones between two consecutive zero crossings from the fourth derivative PPG signal. The four wave peaks 'a', 'b', 'c', and 'd' are detected from each of the SDPPG waveform, as shown in figure 2. The amplitudes of the characteristic points A_b and A_d are measured from the PPG waveforms in the locations of the SDPPG waves 'b' and 'd', as indicated in figure 2. The characteristic amplitudes A_b and A_d are normalized with the PPG signal amplitude A, named as *PPGb* and *PPGd*, respectively. The PPG waveform PPGAI index is calculated as follows:

$$PPGAI = \frac{\frac{A_d}{A}}{\frac{A_b}{A}} = \frac{PPGd}{PPGb} \qquad (2)$$

The matrices are constructed for each recorded PPG signal separately. The wave peaks are detected and the *PPGAI* index is calculated for each waveform from the PPG signal. The *PPGAI* values are averaged and the standard deviations are calculated.

The waveform analysis algorithm described above was implemented in MATLAB (The MathWorks, USA). The function 'resample' was used in MATLAB to resample the signals. The one-minute long signals were processed offline after the experiments.

3. Results

Physiological parameters of the healthy subjects and diabetes patients are summarized in Table 1. The age, body mass index (BMI), systolic blood pressure (BP), diastolic BP, and heart rate are given as average values with a standard deviation (SD) for the controls and the diabetes patient group.

PPG signals were processed by using the waveform analysis algorithm described in the previous section. The linear relationship between *PPGAI* and AIx@75 investigated is illustrated in figure 3. In the analysis all the data points (44 altogether) from both subject groups were used and the Pearson's correlation coefficient was calculated. In addition, the regression model was calculated.

Table 1. Summary of the characteristic parameters of the subjects

	Healthy subjects	Diabetes patients
No. of subjects	24	20
Male/female	14/10	5/15
Age (years)	41 ± 13	44 ± 14
BMI ($kg \cdot m^{-2}$)	24.6 ± 2.4	27.9 ± 8.6
Systolic BP (mmHg)	124 ± 12	132 ± 20
Diastolic BP (mmHg)	82 ± 10	82 ± 13
Heart rate (bpm)	66 ± 6	78 ± 15

As the cardiovascular age of the subject can be associated with the stiffness of blood vessels, the relationship between the age and the *PPGAI* is illustrated in figure 4a. Each data point in figure 4a represents the average value of the index for one subject. In addition, figure 4b shows the relationship between the SphygmoCor calculated AIx@75 and the age. The linear model was constructed for both indices by using the data points from healthy subjects. The standard deviation SD_y was calculated for both models based on the data from healthy subjects. Pearson's correlation coefficient r was calculated in order to investigate the linear relationship between the indices and the *age*.

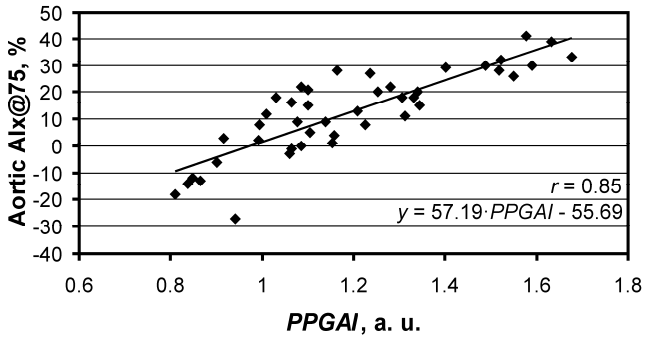

Figure 3. The relation between the *PPGAI* and the aortic AIx@75 with the regression line and the correlation coefficient.

The differences denoted as Δ between the data points and the constructed model were calculated for PPGAI and AIx@75 (eg. $\Delta_{\mathrm{PPGAI}} = y_{\mathrm{PPGAI}} - PPGAI$). The differences were averaged for data points from healthy subjects and diabetes patients and denoted as Δ_h and Δ_d, respectively. Δ_h=0 for PPGAI and AIx@75 as the models were constructed on the basis of data points from healthy subjects. For both indices, the data point differences from the proposed model were compared between the healthy and the diabetes patients groups. A paired t-test (Two-Sample Assuming Unequal Variances) was performed in MS Excel with α=0.05. The P-values from the t-test were P<0.0001 for both indices. Figure 5 shows averaged differences Δ_h and Δ_d as well as standard deviation bars of the model for both indices.

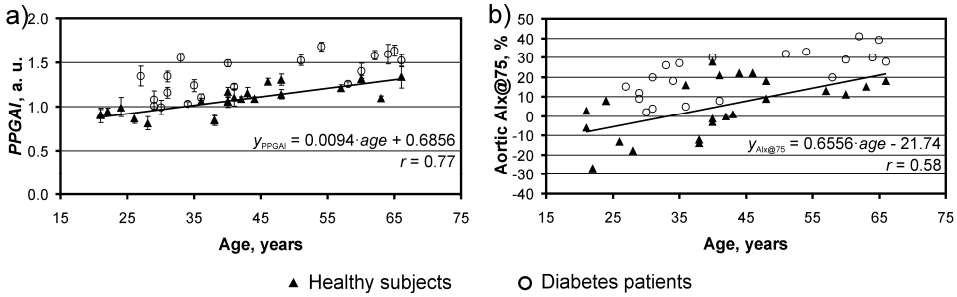

Figure 4. The relation between a) *PPGAI*, b) AIx@75, and age with regression lines and correlation coefficients.

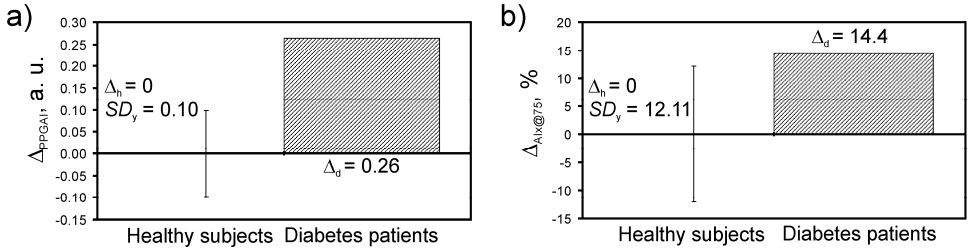

Figure 5. The averaged differences between data points and constructed models a) y_{PPGAI}, b) $y_{\mathrm{AIx@75}}$ for healthy subject Δ_h and diabetes patients Δ_d. For each index, the standard deviation bars SD_y of the model are given.

4. Discussion

The proposed *PPGAI* is strongly correlated (r=0.85) with aortic AIx@75 and it shows that the proposed PPG waveform index is related to the arterial stiffness. Similarly, Takazawa group found high correlation (r=0.86) between the invasive aortic pressure wave and the PPG signal augmentation indices. However, the PPG signal processing and the calculation of AIx in this study differ from the study by Takazawa group. Figure 3 reveals deviations from the regression line, which are mainly caused by the different origin of the signals. The PPG signal is related to the arterial pressure pulse, although the waveform is not the same (Millasseau *et al* 2000). In addition, the peripheral blood flow in finger depends on the activity of the sympathetic nervous system and the temperature, which may cause deviations in the PPG waveform (Nitzan *et al* 1998, Hertzman and Orth 1942, Pilt *et al* 2013c).

As the cardiovascular age of the subject can be associated with the stiffness of blood vessels (Millasseau *et al* 2002, Lee and Park 2013), the relations between the *PPGAI*, AIx@75 and the age are shown in figure 4. Relatively high correlation (r=0.77) was found between the *PPGAI* and the age. In addition, the data points from healthy subjects are situated close to the regression line. It is visible that data points from diabetes patients have noticeably higher values than those of healthy subjects. However, some data points from diabetes patients are situated close to the regression line. It can be assumed that the stiffness of the arteries has not increased for some of the diabetes patients due to the short duration of the disease or their active life styles. The SphygmoCor assessed AIx@75 data points from healthy subjects are more dispersed around the regression line. However, all the data points from diabetes patients are with higher values compared to the regression line.

In order to discriminate the subjects with increased arterial stiffness from healthy persons, the regression model was constructed for the age correction. For both indices the group differences were significant (P<0.0001). Figure 5 reveals that the average differences in the diabetes patient group from the constructed models are larger than the standard deviation of the given models. However, the standard deviation of the model $y_{\mathrm{AIx@75}}$ constitutes 84% from the average difference of the diabetes patient group Δ_{d}. The same ratio for the *PPGAI* is 39%, which is more than two times lower. As a result, the subject can be discriminated better by using the index *PPGAI*.

5. Conclusions

This study has shown that the PPG waveform index *PPGAI* calculated by the analysis algorithm developed earlier can be applied to discriminate the subjects with raised arterial stiffness from healthy persons. The *PPGAI* was compared with the recognized stiffness index AIx@75, which was obtained with a SphygmoCor device. Strong linear relation was found between the two indices. To discriminate the subjects, the age correction model was constructed for both indices. The largest difference between the standard deviation of the model and the average difference of the diabetes patient group was achieved with the *PPGAI* index. It can be assumed that the changes in the index finger PPG signal caused by the stiffening of the arteries can be detected with the waveform index *PPGAI*.

Acknowledgments

This work was supported by the European Union through the European Regional Development Fund.

References

Allen J and Murray A 2003 Age-related changes in the characteristics of the photoplethysmographic pulse shape at various body sites *Physiol. Meas.* **24** 297–307

Allen J 2007 Photoplethysmography and its applications in clinical physiological measurement *Physiol. Meas.* **28** R1-39

Brillante D G, O'Sullivan A J and Howes L G 2008 Arterial stiffness indices in healthy volunteers using non-invasive digital photoplethysmography *Blood. Press.* **17** 116-23

Chan G S H, Middleton P M, Branko G C, Wang L and Lovell N H 2007 Automatic detection of left ventricular ejection time from a finger photoplethysmographic pulse oximetry waveform: comparison with Doppler aortic measurement *Physiol. Meas.* **28** 439–52

Chen C H, Nevo E, Fetics B, Pak P H, Yin F C, Maughan W L, Kass D A 1997 Estimation of central aortic pressure waveform by mathematical transformation of radial tonometry pressure: validation of generalized transfer function *Circulation* **95** 1827–36

Hertzman A B and Orth L W 1942 The vasomotor components in the vascular reactions in the finger to cold *Am. J. Physiol.* **136** 669–79

Hlimonenko I, Meigas K and Vahisalu R 2003 Waveform analysis of peripheral pulse wave detected in the fingertip with photoplethysmograph *Measure. Sci. Rev.* **3** 49–52

Laurent S, Cockcroft J, Van Bortel L, Boutouyrie P, Giannattasio C, Hayoz D, Pannier B, Vlachopoulos C, Wilkinson I and Struijker-Boudier H 2006 Expert consensus document on arterial stiffness: methodological issues and clinical applications *Eur. Heart. J.* **27** 2588–605

Lee S J and Park S H 2013 Arterial Ageing *Korean Circ. J.* **43** 73–9

Millasseau S C, Guigui F G, Kelly R P, Prasad K, Cockcroft J R, Ritter J M and Chowienczyk P J 2000 Noninvasive assessment of the digital volume pulse. Comparison with the peripheral pressure pulse *Hypertension* **36** 952-6

Millasseau S C, Kelly R P, Ritter J M and Chowienczyk P J 2002 Determination of age-related increases in large artery stiffness by digital pulse contour analysis *Clin. Sci. (Lond)* **103** 371-7

Millasseau S C, Kelly R P, Ritter J M and Chowienczyk P J 2003 The vascular impact of aging and vasoactive drugs: comparison of two digital volume pulse measurements *Am. J. Hypertens.* **16** 467-72

Millasseau S C, Ritter J M, Takazawa K and Chowienczyk P J 2006 Contour analysis of the photoplethysmographic pulse measured at the finger *J. Hypertens.* **24** 1449-56

Mitchell G F, Parise H, Benjamin E J, et al 2004 Changes in arterial stiffness and wave reflection with advancing age in healthy men and women: the Framingham Heart Study *Hypertension* **43** 1239-45

Murgo J P, Westerhof N, Giolma J P, Altobelli S A 1980 Aortic input impedance in normal man: relationship to pressure wave forms *Circulation* **62** 105-16

Nitzan M, Babchenko A, Khanokh B and Landau D 1998 The variability of the photoplethysmographic signal—a potential method for the evaluation of the autonomic nervous system *Physiol. Meas.* **19** 93–102

Perk J et al 2012 European Guidelines on cardiovascular disease prevention in clinical practice *European Heart Journal* **33** 1635–701

Pilt K, Meigas K, Viigimaa M, Temitski K and Kaik J 2010 An experimental measurement complex for probable estimation of arterial stiffness *Proc. 32nd Annual International Conf. of the IEEE EMBC* **1** 194–7

Pilt K, Meigas K, Temitski K and Viigimaa M 2012 Second derivative analysis of forehead photoplethysmographic signal in healthy volunteers and diabetes patients *IFMBE Proceedings* **39** 410–3

Pilt K, Ferenets R, Meigas K, Lindberg L-G, Temitski K, Viigimaa M 2013a New Photoplethysmographic Signal Analysis Algorithm for Arterial Stiffness Estimation *The Scientific World Journal* 2013, Article ID 169035, 9 pages

Pilt K, Meigas K, Temitski K and Viigimaa M 2013b The analysis of finger photoplethysmographic waveform in healthy volunteers and diabetes patients *IFMBE Proceedings* **38** 55-8

Pilt K, Meigas K, Temitski K and Viigimaa M 2013c The effect of local cold and warm exposure on index finger photoplethysmographic signal waveform *Proc. 35th Annual International Conf. of the IEEE EMBC* **1** 2300–3

Safar M E and London G M 2000 Therapeutic studies and arterial stiffness in hypertension: recommendations of the European Society of Hypertension *Journal of Hypertension* **18** 1527-35

Schram M T, Henry R M, van Dijk R A, et al 2004 Increased central artery stiffness in impaired glucose metabolism and type 2 diabetes: the Hoorn Study *Hypertension* **43** 176-81

Sherebrin M H and Sherebrin R Z 1990 Frequency Analysis of the Peripheral Pulse Wave Detected in the Finger with a Photoplethysmograph *IEEE Trans. Biomed. Eng.* **37** 313-7

Takazawa K, Tanaka N, Fujita M, Matsuoka O, Saiki T, Aikawa M, Tamura S and Ibukiyama C 1998 Assessment of vasoactive agents and vascular aging by the second derivative of photoplethysmogram waveform *Hypertension* **32** 365-70

Wilkinson I B, MacCallum H, Flint L, Cockcroft J R, Newby D E, Webb D J 2000 The influence of heart rate on augmentation index and central arterial pressure in humans *J Physiol.* **525** 263–70

Woodman R J, Kingwell B A, Beilin L J, Hamilton S E, Dart A M and Watts G F 2005 Assessment of central and peripheral arterial stiffness: studies indicating the need to use a combination of techniques *Am. J. Hypertens.* **18** 249–60

ELULOOKIRJELDUS

1. Isikuandmed

Ees- ja perekonnanimi	Kristjan Pilt
Sünniaeg ja -koht	10.11.1981, Tallinn, Eesti
Kodakondsus	eestlane

2. Kontaktandmed

Aadress	Sõpruse pst. 255-36, 13414 Tallinn, Eesti
Telefon	+372 620 22 10
E-posti aadress	kristjan.pilt@cb.ttu.ee

3. Hariduskäik

Õppeasutus (nimetus lõpetamise ajal)	Lõpetamise aeg	Haridus (eriala/kraad)
Tallinna Saksa Gümnaasium	2000	Keskharidus
Tallinna Tehnikaülikool	2005	Elektroonika ja biomeditsiinitehnika, bakalaureusekraad
Tallinna Tehnikaülikool	2008	Elektroonika, magistrikraad

4. Keelteoskus (alg-, kesk- või kõrgtase)

Keel	Tase
Eesti	Emakeel, kõrgtase
Inglise	Kõrgtase
Vene	Algtase
Soome	Algtase
Jaapani	Algtase

5. Täiendusõpe

Õppimise aeg	Täiendusõppe läbiviija nimetus
10.2003-09.2004	*University of Electro-Communications*, Tokyo, Japan
17-18.10.2011	Dr Richard M. Felderi koolitus „Mõjusa õpetamise õpituba“, Tallinna Tehnikaülikool
09.2011-02.2012	Linköpingi Ülikool, Rootsi
03.2007-09.2012	4 Rahvusvahelise doktorikooli iBioMEP täiendkursust
04.05.2012	Täienduskoolitus „Biooptika meditsiinitehnikas“, Tallinna Tehnikaülikool

6. Teenistuskäik

Töötamise aeg	Tööandja nimetus	Ametikoht
06.2003-07.2003	AS Ecomatic	Automaatika kilpide komplekteerija
2005-2006	SA Põhja-Eesti Regionaalhaigla	Klienditeenindaja
2009-k.a.	Tallinna Tehnikaülikool	Teadur

7. Teadustegevus

Optiliste meetodite kasutamine ateroskleroosi varajasel diagnoosil

8. Loometöö

Loengumaterjalid aines “Mikrolaine- ja optiline tehnika”, koostanud Kristjan Pilt ja Kalju Meigas, TTÜ, 2012, ISBN 978-9949-23-305-2

9. Tunnustused

Aasta Tehnikaüliõpilane 2008 - Eesti Inseneride Liidu aunimetus

10. Juhendatud lõputööd

- Sandra Silluta, MSc. Arterite elastsusmooduli määramine Moens-Korteweg'i valemi põhjal ning seoste leidmine ühise unearteri intima-media paksusega, TTÜ, 2013
- Jaana Lauri, MSc. Samafaasipunktide detekteerimise meetodite võrdlus pulsilaine viiteaegade määramiseks, TTÜ, 2012
- Argo Veide, MSc. Kunstlikult tekitatud peegelduste uurimine perifeerselt arterilt registreeritud rõhulaines, TTÜ, 2012
- Annika Mikola, BSc. Difuusse peegelduse uurimine tugevalt hajutavas ja neelavas keskkonnas ning võrdlus Monte Carlo meetodiga, TTÜ, 2012
- Mikk Viidebaum, MSc. Moens-Kortewegi võrrandi põhjal pulsilaine levikiiruse ja vererõhu vahelise seose eksperimentaalne uurimine käsivarrel, TTÜ, 2011
- Ester Jürgenson, MSc. Pulsilaine levikiiruse määramise võrdlus seadmetega Arteriograph ja SphygmoCor, TTÜ, 2011

11. Teadustöö põhisuunad

SF0140027s07, Biosignaalide interpreteerimine meditsiinitehnikas, 2007-2012
ETF5888, Koherentse fotodetekteerimise kasutamine kardiovaskulaarses diagnostikas - vererõhu ja arteri viskoelastsete parameetrite mitteinvasiivne monitoring, 2004-2007
AR13061, Kõrgtasemelisel signaalitöötlustehnoloogial põhinevad EEG algoritmid ajuhäirete automaatseks tuvastamiseks, 2013-2015
ETF6173, Mikrolainekiirguse mõju kognitiivsetele funktsioonidele, 2005-2008
ETF7506, Optilise koherentse fotodetekteerimise kasutamine ateroskleroosi varajasel diagnoosil, 2008-2011
ETF8621, Uudne optiline meetod ureemiliste toksiinide - alatoitumuse ja kroonilise põletiku ning SVH riski potentsiaalsete markerite, monitooringuks, 2011-2014
ETF6936, Uudne optiline multikomponent monitor neerupuudulikkusega patsientide ravi kvaliteedi hindamiseks, 2007-2010
VIR523, Töövõime ja sotsiaalne kaasatus, 2011-2013

APPENDIX 3

CURRICULUM VITAE

1. Personal data

Name	Kristjan Pilt
Date and place of birth	10.11.1981, Tallinn, Estonia

2. Contact information

Address	Sõpruse pst. 255-36, 13414 Tallinn, Eesti
Phone	+372 620 22 10
E-mail	kristjan.pilt@cb.ttu.ee

3. Education

Educational institution	Graduation year	Education (field of study/degree)
Tallinn German Gymnasium	2000	Secondary education
Tallinna University of Technology	2005	Electronics and biomedical technology, bachelor degree
Tallinna University of Technology	2008	Electronics, master degree

4. Language competence/skills (fluent, average, basic skills)

Language	Level
Estonian	Mother-tongue, fluent
English	Fluent
Russian	Basic skills
Finnish	Basic skills
Japanese	Basic skills

5. Special courses

Period	Educational or other organization
10.2003-09.2004	*University of Electro-Communications*, Tokyo, Japan
03.2007-09.2012	4 graduate courses in International Doctoral Programme – iBioMEP
17-18.10.2011	Dr Richard M. Felder's course "Effective College Teaching Workshop", Tallinn University of Technology
09.2011-02.2012	Linköping University, Sweden
04.05.2012	Complementary training "Bio-optics in medical technology", Tallinn University of Technology

6. Professional Employment

Period	Organization	Position
06.2003-07.2003	Ecomatic Ltd.	Automation control system replenisher
2005-2006	North Estonia Medical Centre	Client service
2009-	Tallinn University of Technology	Research scientist

7. Scientific work

Application of optical methods in early diagnosis of atherosclerosis

8. Creative work

Lecture materials in "Microwave and optical technics", compiled by Kristjan Pilt and Kalju Meigas, TUT, 2012, ISBN 978-9949-23-305-2

9. Honours and awards

Technical Student of the Year 2008 - Estonian Association of Engineers Title of Honor

10. Supervised theses

- Sandra Silluta, MSc. Assessment of elastic modulus of arteries using Moens-Korteweg equation and finding connections with intima-media thickness of common carotid artery, TUT, 2013
- Jaana Lauri, MSc. The comparison of the detection methods of the same phase points for the calculation of the pulse transit time, TUT, 2012
- Argo Veide, MSc. Investigation of artificially induced reflections in registered pressure wave from peripheral artery, TUT, 2012
- Annika Mikola, BSc. Study of diffuse reflectance in highly scattering and absorbing medium and comparison with Monte Carlo method, TUT, 2012
- Mikk Viidebaum, MSc. Experimental investigation of the relationship between pulse wave velocity and blood pressure on human arm based on Moens-Korteweg equation, TUT, 2011
- Ester Jürgenson, MSc. Comparison of pulse wave velocity measurement using Arteriograph and SphygmoCor devices, TUT, 2011

11. Main areas of scientific work/Current research topics

ETF6936, A novel optical multicomponent monitor estimating ESRD patients' treatment quality, 2007-2010
ETF8621, A novel optical technology for monitoring of uremic toxins - potential markers for malnutrition–inflammation syndrome and CVD risk, 2011-2014
AR13061, Algorithms for automatic detection of brain disorders based on advanced EEG signal processing techniques, 2013-2015
ETF7506, Application of Coherent Photodetection in Early Diagnosis of Atherosclerosis, 2008-2011
ETF5888, Application of Method for Coherent Photodetection in Cardiovascular Diagnostics - Non-Invasive Monitoring of the Blood Pressure and the Viscoelastic Parameters of Arteries, 2004-2007
SF0140027s07, Interpretation of Biosignals in Biomedical Engineering, 2007-2012
ETF6173, Microwave effects on cognitive functions, 2005-2008
VIR523, Work Ability and Social Inclusion, 2011-2013

DISSERTATIONS DEFENDED AT
TALLINN UNIVERSITY OF TECHNOLOGY ON
NATURAL AND EXACT SCIENCES

1. **Olav Kongas**. Nonlinear Dynamics in Modeling Cardiac Arrhytmias. 1998.

2. **Kalju Vanatalu**. Optimization of Processes of Microbial Biosynthesis of Isotopically Labeled Biomolecules and Their Complexes. 1999.

3. **Ahto Buldas**. An Algebraic Approach to the Structure of Graphs. 1999.

4. **Monika Drews**. A Metabolic Study of Insect Cells in Batch and Continuous Culture: Application of Chemostat and Turbidostat to the Production of Recombinant Proteins. 1999.

5. **Eola Valdre**. Endothelial-Specific Regulation of Vessel Formation: Role of Receptor Tyrosine Kinases. 2000.

6. **Kalju Lott**. Doping and Defect Thermodynamic Equilibrium in ZnS. 2000.

7. **Reet Koljak**. Novel Fatty Acid Dioxygenases from the Corals *Plexaura homomalla* and *Gersemia fruticosa.* 2001.

8. **Anne Paju**. Asymmetric oxidation of Prochiral and Racemic Ketones by Using Sharpless Catalyst. 2001.

9. **Marko Vendelin**. Cardiac Mechanoenergetics *in silico*. 2001.

10. **Pearu Peterson**. Multi-Soliton Interactions and the Inverse Problem of Wave Crest. 2001.

11. **Anne Menert**. Microcalorimetry of Anaerobic Digestion. 2001.

12. **Toomas Tiivel**. The Role of the Mitochondrial Outer Membrane in *in vivo* Regulation of Respiration in Normal Heart and Skeletal Muscle Cell. 2002.

13. **Olle Hints**. Ordovician Scolecodonts of Estonia and Neighbouring Areas: Taxonomy, Distribution, Palaeoecology, and Application. 2002.

14. **Jaak Nõlvak**. Chitinozoan Biostratigrapy in the Ordovician of Baltoscandia. 2002.

15. **Liivi Kluge**. On Algebraic Structure of Pre-Operad. 2002.

16. **Jaanus Lass**. Biosignal Interpretation: Study of Cardiac Arrhytmias and Electromagnetic Field Effects on Human Nervous System. 2002.

17. **Janek Peterson**. Synthesis, Structural Characterization and Modification of PAMAM Dendrimers. 2002.

18. **Merike Vaher**. Room Temperature Ionic Liquids as Background Electrolyte Additives in Capillary Electrophoresis. 2002.

19. **Valdek Mikli**. Electron Microscopy and Image Analysis Study of Powdered Hardmetal Materials and Optoelectronic Thin Films. 2003.

20. **Mart Viljus**. The Microstructure and Properties of Fine-Grained Cermets. 2003.

21. **Signe Kask**. Identification and Characterization of Dairy-Related *Lactobacillus.* 2003

22. **Tiiu-Mai Laht**. Influence of Microstructure of the Curd on Enzymatic and Microbiological Processes in Swiss-Type Cheese. 2003.

23. **Anne Kuusksalu**. 2–5A Synthetase in the Marine Sponge *Geodia cydonium*. 2003.

24. **Sergei Bereznev**. Solar Cells Based on Polycristalline Copper-Indium Chalcogenides and Conductive Polymers. 2003.

25. **Kadri Kriis**. Asymmetric Synthesis of C_2-Symmetric Bimorpholines and Their Application as Chiral Ligands in the Transfer Hydrogenation of Aromatic Ketones. 2004.

26. **Jekaterina Reut**. Polypyrrole Coatings on Conducting and Insulating Substracts. 2004.

27. **Sven Nõmm**. Realization and Identification of Discrete-Time Nonlinear Systems. 2004.

28. **Olga Kijatkina**. Deposition of Copper Indium Disulphide Films by Chemical Spray Pyrolysis. 2004.

29. **Gert Tamberg**. On Sampling Operators Defined by Rogosinski, Hann and Blackman Windows. 2004.

30. **Monika Übner**. Interaction of Humic Substances with Metal Cations. 2004.

31. **Kaarel Adamberg**. Growth Characteristics of Non-Starter Lactic Acid Bacteria from Cheese. 2004.

32. **Imre Vallikivi**. Lipase-Catalysed Reactions of Prostaglandins. 2004.

33. **Merike Peld**. Substituted Apatites as Sorbents for Heavy Metals. 2005.

34. **Vitali Syritski**. Study of Synthesis and Redox Switching of Polypyrrole and Poly(3,4-ethylenedioxythiophene) by Using *in-situ* Techniques. 2004.

35. **Lee Põllumaa**. Evaluation of Ecotoxicological Effects Related to Oil Shale Industry. 2004.

36. **Riina Aav**. Synthesis of 9,11-Secosterols Intermediates. 2005.

37. **Andres Braunbrück**. Wave Interaction in Weakly Inhomogeneous Materials. 2005.

38. **Robert Kitt**. Generalised Scale-Invariance in Financial Time Series. 2005.

39. **Juss Pavelson**. Mesoscale Physical Processes and the Related Impact on the Summer Nutrient Fields and Phytoplankton Blooms in the Western Gulf of Finland. 2005.

40. **Olari Ilison**. Solitons and Solitary Waves in Media with Higher Order Dispersive and Nonlinear Effects. 2005.

41. **Maksim Säkki**. Intermittency and Long-Range Structurization of Heart Rate. 2005.

42. **Enli Kiipli**. Modelling Seawater Chemistry of the East Baltic Basin in the Late Ordovician–Early Silurian. 2005.

43. **Igor Golovtsov**. Modification of Conductive Properties and Processability of Polyparaphenylene, Polypyrrole and polyaniline. 2005.

44. **Katrin Laos**. Interaction Between Furcellaran and the Globular Proteins (Bovine Serum Albumin β-Lactoglobulin). 2005.

45. **Arvo Mere**. Structural and Electrical Properties of Spray Deposited Copper Indium Disulphide Films for Solar Cells. 2006.

46. **Sille Ehala**. Development and Application of Various On- and Off-Line Analytical Methods for the Analysis of Bioactive Compounds. 2006.

47. **Maria Kulp**. Capillary Electrophoretic Monitoring of Biochemical Reaction Kinetics. 2006.

48. **Anu Aaspõllu.** Proteinases from *Vipera lebetina* Snake Venom Affecting Hemostasis. 2006.

49. **Lyudmila Chekulayeva**. Photosensitized Inactivation of Tumor Cells by Porphyrins and Chlorins. 2006.

50. **Merle Uudsemaa**. Quantum-Chemical Modeling of Solvated First Row Transition Metal Ions. 2006.

51. **Tagli Pitsi**. Nutrition Situation of Pre-School Children in Estonia from 1995 to 2004. 2006.

52. **Angela Ivask**. Luminescent Recombinant Sensor Bacteria for the Analysis of Bioavailable Heavy Metals. 2006.

53. **Tiina Lõugas**. Study on Physico-Chemical Properties and Some Bioactive Compounds of Sea Buckthorn (*Hippophae rhamnoides* L.). 2006.

54. **Kaja Kasemets**. Effect of Changing Environmental Conditions on the Fermentative Growth of *Saccharomyces cerevisae* S288C: Auxo-accelerostat Study. 2006.

55. **Ildar Nisamedtinov**. Application of ^{13}C and Fluorescence Labeling in Metabolic Studies of *Saccharomyces* spp. 2006.

56. **Alar Leibak**. On Additive Generalisation of Voronoï's Theory of Perfect Forms over Algebraic Number Fields. 2006.

57. **Andri Jagomägi**. Photoluminescence of Chalcopyrite Tellurides. 2006.

58. **Tõnu Martma**. Application of Carbon Isotopes to the Study of the Ordovician and Silurian of the Baltic. 2006.

59. **Marit Kauk**. Chemical Composition of $CuInSe_2$ Monograin Powders for Solar Cell Application. 2006.

60. **Julia Kois**. Electrochemical Deposition of $CuInSe_2$ Thin Films for Photovoltaic Applications. 2006.

61. **Ilona Oja Açik**. Sol-Gel Deposition of Titanium Dioxide Films. 2007.

62. **Tiia Anmann**. Integrated and Organized Cellular Bioenergetic Systems in Heart and Brain. 2007.

63. **Katrin Trummal**. Purification, Characterization and Specificity Studies of Metalloproteinases from *Vipera lebetina* Snake Venom. 2007.

64. **Gennadi Lessin**. Biochemical Definition of Coastal Zone Using Numerical Modeling and Measurement Data. 2007.

65. **Enno Pais**. Inverse problems to determine non-homogeneous degenerate memory kernels in heat flow. 2007.

66. **Maria Borissova**. Capillary Electrophoresis on Alkylimidazolium Salts. 2007.

67. **Karin Valmsen**. Prostaglandin Synthesis in the Coral *Plexaura homomalla*: Control of Prostaglandin Stereochemistry at Carbon 15 by Cyclooxygenases. 2007.

68. **Kristjan Piirimäe**. Long-Term Changes of Nutrient Fluxes in the Drainage Basin of the Gulf of Finland – Application of the PolFlow Model. 2007.

69. **Tatjana Dedova**. Chemical Spray Pyrolysis Deposition of Zinc Sulfide Thin Films and Zinc Oxide Nanostructured Layers. 2007.

70. **Katrin Tomson**. Production of Labelled Recombinant Proteins in Fed-Batch Systems in *Escherichia coli*. 2007.

71. **Cecilia Sarmiento**. Suppressors of RNA Silencing in Plants. 2008.

72. **Vilja Mardla**. Inhibition of Platelet Aggregation with Combination of Antiplatelet Agents. 2008.

73. **Maie Bachmann**. Effect of Modulated Microwave Radiation on Human Resting Electroencephalographic Signal. 2008.

74. **Dan Hüvonen**. Terahertz Spectroscopy of Low-Dimensional Spin Systems. 2008.

75. **Ly Villo**. Stereoselective Chemoenzymatic Synthesis of Deoxy Sugar Esters Involving *Candida antarctica* Lipase B. 2008.

76. **Johan Anton**. Technology of Integrated Photoelasticity for Residual Stress Measurement in Glass Articles of Axisymmetric Shape. 2008.

77. **Olga Volobujeva**. SEM Study of Selenization of Different Thin Metallic Films. 2008.

78. **Artur Jõgi**. Synthesis of 4'-Substituted 2,3'-dideoxynucleoside Analogues. 2008.

79. **Mario Kadastik**. Doubly Charged Higgs Boson Decays and Implications on Neutrino Physics. 2008.

80. **Fernando Pérez-Caballero**. Carbon Aerogels from 5-Methylresorcinol-Formaldehyde Gels. 2008.

81. **Sirje Vaask**. The Comparability, Reproducibility and Validity of Estonian Food Consumption Surveys. 2008.

82. **Anna Menaker**. Electrosynthesized Conducting Polymers, Polypyrrole and Poly(3,4-ethylenedioxythiophene), for Molecular Imprinting. 2009.

83. **Lauri Ilison**. Solitons and Solitary Waves in Hierarchical Korteweg-de Vries Type Systems. 2009.

84. **Kaia Ernits**. Study of In_2S_3 and ZnS Thin Films Deposited by Ultrasonic Spray Pyrolysis and Chemical Deposition. 2009.

85. **Veljo Sinivee**. Portable Spectrometer for Ionizing Radiation "Gammamapper". 2009.

86. **Jüri Virkepu**. On Lagrange Formalism for Lie Theory and Operadic Harmonic Oscillator in Low Dimensions. 2009.

87. **Marko Piirsoo**. Deciphering Molecular Basis of Schwann Cell Development. 2009.

88. **Kati Helmja**. Determination of Phenolic Compounds and Their Antioxidative Capability in Plant Extracts. 2010.

89. **Merike Sõmera**. Sobemoviruses: Genomic Organization, Potential for Recombination and Necessity of P1 in Systemic Infection. 2010.

90. **Kristjan Laes**. Preparation and Impedance Spectroscopy of Hybrid Structures Based on $CuIn_3Se_5$ Photoabsorber. 2010.

91. **Kristin Lippur**. Asymmetric Synthesis of 2,2'-Bimorpholine and its 5,5'-Substituted Derivatives. 2010.

92. **Merike Luman**. Dialysis Dose and Nutrition Assessment by an Optical Method. 2010.

93. **Mihhail Berezovski**. Numerical Simulation of Wave Propagation in Heterogeneous and Microstructured Materials. 2010.

94. **Tamara Aid-Pavlidis**. Structure and Regulation of BDNF Gene. 2010.

95. **Olga Bragina**. The Role of Sonic Hedgehog Pathway in Neuro- and Tumorigenesis. 2010.

96. **Merle Randrüüt**. Wave Propagation in Microstructured Solids: Solitary and Periodic Waves. 2010.

97. **Marju Laars**. Asymmetric Organocatalytic Michael and Aldol Reactions Mediated by Cyclic Amines. 2010.

98. **Maarja Grossberg**. Optical Properties of Multinary Semiconductor Compounds for Photovoltaic Applications. 2010.

99. **Alla Maloverjan**. Vertebrate Homologues of Drosophila Fused Kinase and Their Role in Sonic Hedgehog Signalling Pathway. 2010.

100. **Priit Pruunsild**. Neuronal Activity-Dependent Transcription Factors and Regulation of Human *BDNF* Gene. 2010.

101. **Tatjana Knjazeva**. New Approaches in Capillary Electrophoresis for Separation and Study of Proteins. 2011.

102. **Atanas Katerski**. Chemical Composition of Sprayed Copper Indium Disulfide Films for Nanostructured Solar Cells. 2011.

103. **Kristi Timmo.** Formation of Properties of $CuInSe_2$ and $Cu_2ZnSn(S,Se)_4$ Monograin Powders Synthesized in Molten KI. 2011.

104. **Kert Tamm**. Wave Propagation and Interaction in Mindlin-Type Microstructured Solids: Numerical Simulation. 2011.

105. **Adrian Popp**. Ordovician Proetid Trilobites in Baltoscandia and Germany. 2011.

106. **Ove Pärn**. Sea Ice Deformation Events in the Gulf of Finland and This Impact on Shipping. 2011.

107. **Germo Väli**. Numerical Experiments on Matter Transport in the Baltic Sea. 2011.

108. **Andrus Seiman**. Point-of-Care Analyser Based on Capillary Electrophoresis. 2011.

109. **Olga Katargina**. Tick-Borne Pathogens Circulating in Estonia (Tick-Borne Encephalitis Virus, *Anaplasma phagocytophilum*, *Babesia* Species): Their Prevalence and Genetic Characterization. 2011.

110. **Ingrid Sumeri**. The Study of Probiotic Bacteria in Human Gastrointestinal Tract Simulator. 2011.

111. **Kairit Zovo**. Functional Characterization of Cellular Copper Proteome. 2011.

112. **Natalja Makarytsheva**. Analysis of Organic Species in Sediments and Soil by High Performance Separation Methods. 2011.

113. **Monika Mortimer**. Evaluation of the Biological Effects of Engineered Nanoparticles on Unicellular Pro- and Eukaryotic Organisms. 2011.

114. **Kersti Tepp**. Molecular System Bioenergetics of Cardiac Cells: Quantitative Analysis of Structure-Function Relationship. 2011.

115. **Anna-Liisa Peikolainen**. Organic Aerogels Based on 5-Methylresorcinol. 2011.

116. **Leeli Amon**. Palaeoecological Reconstruction of Late-Glacial Vegetation Dynamics in Eastern Baltic Area: A View Based on Plant Macrofossil Analysis. 2011.

117. **Tanel Peets**. Dispersion Analysis of Wave Motion in Microstructured Solids. 2011.

118. **Liina Kaupmees**. Selenization of Molybdenum as Contact Material in Solar Cells. 2011.

119. **Allan Olspert**. Properties of VPg and Coat Protein of Sobemoviruses. 2011.

120. **Kadri Koppel**. Food Category Appraisal Using Sensory Methods. 2011.

121. **Jelena Gorbatšova**. Development of Methods for CE Analysis of Plant Phenolics and Vitamins. 2011.

122. **Karin Viipsi**. Impact of EDTA and Humic Substances on the Removal of Cd and Zn from Aqueous Solutions by Apatite. 2012.

123. **David Schryer**. Metabolic Flux Analysis of Compartmentalized Systems Using Dynamic Isotopologue Modeling. 2012.

124. **Ardo Illaste**. Analysis of Molecular Movements in Cardiac Myocytes. 2012.

125. **Indrek Reile**. 3-Alkylcyclopentane-1,2-Diones in Asymmetric Oxidation and Alkylation Reactions. 2012.

126. **Tatjana Tamberg**. Some Classes of Finite 2-Groups and Their Endomorphism Semigroups. 2012.

127. **Taavi Liblik**. Variability of Thermohaline Structure in the Gulf of Finland in Summer. 2012.

128. **Priidik Lagemaa**. Operational Forecasting in Estonian Marine Waters. 2012.

129. **Andrei Errapart**. Photoelastic Tomography in Linear and Non-linear Approximation. 2012.

130. **Külliki Krabbi**. Biochemical Diagnosis of Classical Galactosemia and Mucopolysaccharidoses in Estonia. 2012.

131. **Kristel Kaseleht**. Identification of Aroma Compounds in Food using SPME-GC/MS and GC-Olfactometry. 2012.

132. **Kristel Kodar**. Immunoglobulin G Glycosylation Profiling in Patients with Gastric Cancer. 2012.

133. **Kai Rosin**. Solar Radiation and Wind as Agents of the Formation of the Radiation Regime in Water Bodies. 2012.

134. **Ann Tiiman**. Interactions of Alzheimer's Amyloid-Beta Peptides with Zn(II) and Cu(II) Ions. 2012.

135. **Olga Gavrilova**. Application and Elaboration of Accounting Approaches for Sustainable Development. 2012.

136. **Olesja Bondarenko**. Development of Bacterial Biosensors and Human Stem Cell-Based *In Vitro* Assays for the Toxicological Profiling of Synthetic Nanoparticles. 2012.

137. **Katri Muska**. Study of Composition and Thermal Treatments of Quaternary Compounds for Monograin Layer Solar Cells. 2012.

138. **Ranno Nahku**. Validation of Critical Factors for the Quantitative Characterization of Bacterial Physiology in Accelerostat Cultures. 2012.

139. **Petri-Jaan Lahtvee**. Quantitative Omics-level Analysis of Growth Rate Dependent Energy Metabolism in *Lactococcus lactis*. 2012.

140. **Kerti Orumets**. Molecular Mechanisms Controlling Intracellular Glutathione Levels in Baker's Yeast *Saccharomyces cerevisiae* and its Random Mutagenized Gluthatione Over-Accumulating Isolate. 2012.

141. **Loreida Timberg**. Spice-Cured Sprats Ripening, Sensory Parameters Development, and Quality Indicators. 2012.

142. **Anna Mihhalevski**. Rye Sourdough Fermentation and Bread Stability. 2012.

143. **Liisa Arike**. Quantitative Proteomics of *Escherichia coli*: From Relative to Absolute Scale. 2012.

144. **Kairi Otto**. Deposition of In_2S_3 Thin Films by Chemical Spray Pyrolysis. 2012.

145. **Mari Sepp**. Functions of the Basic Helix-Loop-Helix Transcription Factor TCF4 in Health and Disease. 2012.

146. **Anna Suhhova**. Detection of the Effect of Weak Stressors on Human Resting Electroencephalographic Signal. 2012.

147. **Aram Kazarjan**. Development and Production of Extruded Food and Feed Products Containing Probiotic Microorganisms. 2012.

148. **Rivo Uiboupin**. Application of Remote Sensing Methods for the Investigation of Spatio-Temporal Variability of Sea Surface Temperature and Chlorophyll Fields in the Gulf of Finland. 2013.

149. **Tiina Kriščiunaite**. A Study of Milk Coagulability. 2013.

150. **Tuuli Levandi**. Comparative Study of Cereal Varieties by Analytical Separation Methods and Chemometrics. 2013.

151. **Natalja Kabanova**. Development of a Microcalorimetric Method for the Study of Fermentation Processes. 2013.

152. **Himani Khanduri**. Magnetic Properties of Functional Oxides. 2013.

153. **Julia Smirnova**. Investigation of Properties and Reaction Mechanisms of Redox-Active Proteins by ESI MS. 2013.

154. **Mervi Sepp**. Estimation of Diffusion Restrictions in Cardiomyocytes Using Kinetic Measurements. 2013.

155. **Kersti Jääger**. Differentiation and Heterogeneity of Mesenchymal Stem Cells. 2013.

156. **Victor Alari**. Multi-Scale Wind Wave Modeling in the Baltic Sea. 2013.

157. **Taavi Päll**. Studies of SD44 Hyaluronan Binding Domain as Novel Angiogenesis Inhibitor. 2013.

158. **Allan Niidu**. Synthesis of Cyclopentane and Tetrahydrofuran Derivatives. 2013.

159. **Julia Geller**. Detection and Genetic Characterization of *Borrelia* Species Circulating in Tick Population in Estonia. 2013.

160. **Irina Stulova**. The Effects of Milk Composition and Treatment on the Growth of Lactic Acid Bacteria. 2013.

161. **Jana Holmar**. Optical Method for Uric Acid Removal Assessment During Dialysis. 2013.

162. **Kerti Ausmees**. Synthesis of Heterobicyclo[3.2.0]heptane Derivatives *via* Multicomponent Cascade Reaction. 2013.

163. **Minna Varikmaa**. Structural and Functional Studies of Mitochondrial Respiration Regulation in Muscle Cells. 2013.

164. **Indrek Koppel**. Transcriptional Mechanisms of BDNF Gene Regulation. 2014.